

Contract Report 2002-08

**Spatial Distribution, Variation, and Trends
in Storm Precipitation Characteristics Associated
with Soil Erosion in the United States**

by
Steven E. Hollinger, James R. Angel, and Michael A. Palecki

**Prepared for the
United State Department of Agriculture**

November 2002



Illinois State Water Survey
Atmospheric Environment Section
Champaign, Illinois

A Division of the Illinois Department of Natural Resources

**Spatial Distribution, Variation, and Trends
in Storm Precipitation Characteristics Associated
with Soil Erosion in the United States**

Steven E. Hollinger, James R. Angel, and Michael A. Palecki

Final Contract Report
AG 68-7482-7-306

United States Department of Agriculture
Natural Resources Conservation Service
Water and Climate Center
Portland, Oregon

Atmospheric Environment Section
Illinois State Water Survey
2204 Griffith Drive
Champaign, Illinois 61820-7495

November 2002

Abstract

Soil erosion and nonpoint source pollution runoff rates are estimated using output from the Revised Universal Soil Loss Equation (RUSLE). The underlying influence of climate on surface transport processes as represented in the RUSLE is carried within one constant, the R-factor. It has been assumed that the R-factor is temporally stationary; that is, it does not change with time. The purpose of this study was to process climate information from the most recent decades to update the R-factor, to examine the nature of precipitation variation and change and their impacts on the R-factor over space and time, and, specifically, to test the hypothesis that storm erosivity and the R-factor are temporally stationary. This was addressed by developing a database of precipitation data and related information needed to calculate single-storm erosivity and cumulative R-factor for each half-month of the year and for the total year. In addition the 10-year, single-storm erosive index for each station is provided.

The R-factor, a nonlinear, cumulative measure of the erosive energy contained in storm precipitation, was calculated directly from 15-minute rainfall data. However, because of some undocumented quality difficulties with the 15-minute data, single-storm erosivity index statistics for accumulation into R-factors were calculated from more reliable daily data through the use of a power law transfer function. These new R-factors were tested for spatial covariation, which was found to be minimal in even terrain, and related to the limited amount of station R-factor data from past studies. Comparison with past R-factor studies indicated strongly that the methodologies used adequately duplicated old R-factors based on data from the 1930s to the 1950s. General increases observed in R-factors in this study were related to increasing amounts of precipitation and storms with rainfall greater than 12.7 millimeters, especially in the western United States. Mean seasonal patterns of storm precipitation total, duration, intensity, 30-minute and 15-minute maximum intensity, kinetic energy, erosivity, and the numbers of storms also were mapped for the conterminous United States. These analyses showed distinct patterns of precipitation change with seasons and identified regions of strong gradients where climate change first may be noticed.

Trend analyses of storm precipitation variables over the 1971-1999 period indicated the lack of temporal stationarity of storm characteristics. Storm duration changes were especially an important cause of the observed changes in storm precipitation totals. However, storm trends in 30-minute maximum intensity seemed to be more important in changing the patterns of storm erosivity. Examination of storm characteristic response to interannual and interdecadal variations also indicated that storm characteristics were responding at these time scales to large-scale climate system forcings. In the winter season, atmospheric teleconnections such as the Pacific/North American Pattern and the North Atlantic Oscillation were shown to influence not only storm track positions and the number of storms at a location, but also the characteristics of individual storms. El Niño and La Niña events of the Southern Oscillation (ENSO events) had distinctive impacts on storm variables in every season of the year. Even the Pacific Decadal Oscillation showed a clear effect on storm characteristics, especially in the western United States.

The results of R-factors derived from modern data compared to previous R-factors combined with storm characteristic trend and variability studies indicate conclusively that storm precipitation characteristics change sufficiently over time to warrant an evaluation of the necessity to recalculate R-factors on a regular basis.

Table of Contents

	<i>Page</i>
Introduction	1
Objectives	2
R-factor Computation	2
R-factor Equations	3
30-Minute Maximum Rainfall Intensity Adjustment	5
Data Quality Assurance	8
Missing Data Identification and Adjustment	10
Prorating Missing Data	10
Filling Data Gaps by Regression	12
R-factor Computation from Higher Quality Daily Data	15
R-factor Computation Results	16
Omission of 100-Year Storms	16
Uncertainty of R-factor Values	17
Old and New R-factor Value Comparison	18
Changes in Precipitation Climatology Since Previous R-factor Studies	27
Comparison of 1936-1957, 1971-1999, and Wischmeier and Smith Data	31
Possible Nonclimate Causes for Differences between R-factors	34
10-Year EI Return Interval EI Levels	36
Geographical Distribution and Temporal Variability of Storm Characteristics	38
Seasonal Variations	38
Storm Total Precipitation	38
Storm Duration	40
Storm Precipitation Intensity	40
Storm Kinetic Energy (E)	45
Storm Maximum 30-Minute Precipitation Intensity (I_{30})	45
Storm Erosivity (EI_{30})	50
Number of Storms	50
Storm Maximum 15-Minute Precipitation Intensity	56
Maximum 15-Minute Precipitation Intensity and Storm Intensity Ratio	56
Trends in Storm Characteristics	56
Annual Trend Maps	61
Winter Trend Maps	61
Spring Trend Maps	64
Summer Trend Maps	64
Fall Trend Maps	67
Conclusion	67
Interannual and Interdecadal Variations	67
Winter Teleconnections	69
El Niño and La Niña Events of the Southern Oscillation	70
The Pacific Decadal Oscillation	79
Summary	85
Acknowledgments	87
References	87

List of Tables

	<i>Page</i>
Table 1. The 23 USDA Breakpoint Stations and Their Average Ratio of $(I_{30})_B$ to $(I_{30})_{15}$	7
Table 2. R-factor Values ($\text{MJ mm ha}^{-1} \text{ h}^{-1} \text{ yr}^{-1}$) Generated by Not Accounting for Missing Data (Case 1) and by Prorating Missing Data during Each 24 Half-month Period (Case 2)	12
Table 3. Preparation and Testing of Regression Relationships between 2-Week Precipitation Totals and 2-Week EI Values ($\text{MJ mm ha}^{-1} \text{ h}^{-1} \text{ yr}^{-1}$)	13
Table 4. R-factor Values ($\text{MJ mm ha}^{-1} \text{ h}^{-1} \text{ yr}^{-1}$) Generated Using Regression Equations from Table 1 to Fill Gaps Caused by Missing 2-Week EI Values	14
Table 5. R-Factor Values ($\text{MJ mm ha}^{-1} \text{ h}^{-1} \text{ yr}^{-1}$) for All Stations Included in the New Computation and in Table 17 of Agriculture Handbook 573 (Stations in Italics Below Station are Daily Substitutes for 15-Minute Stations)	20
Table 6. Minimum and Maximum Values of R-factor ($\text{MJ mm ha}^{-1} \text{ h}^{-1} \text{ yr}^{-1}$) for the Brown-Foster Equation with Coefficients (-0.72, 0.082) and the Wischmeier-Smith Values in Table 17 in Agricultural Handbook 537 (Stations in Italics Below a Station are Daily Substitutes for 15-Minute Stations)	22
Table 7. Values of R-factor ($\text{MJ mm ha}^{-1} \text{ h}^{-1} \text{ yr}^{-1}$) for the 50, 20, and 5 Percent Probability Levels with the Brown-Foster Equation Coefficients (-0.72, 0.082) and the Wischmeier-Smith Values in Table 17 in Agricultural Handbook 537 (Stations in Italics Below a Station are Daily Substitutes for 15-Minute Stations)	24
Table 8. Percent of United States Showing Increased or Decreased Precipitation between 1971-1999 and 1936-1957 (Wischmeier, 1962), and between 1971-1999 and 1948-1983 (Istok, 1989)	28
Table 9. Minimum, Maximum, and Median Values of Erosion Index (EI, $\text{MJ mm ha}^{-1} \text{ h}^{-1} \text{ yr}^{-1}$) for the Brown-Foster Equation Coefficients (-0.72, 0.082) for 1971-1999 Data, the Brown-Foster Equation for 1936-1957 Data, and the Wischmeier-Smith Values in Table 17 in Agricultural Handbook 537 (Stations in Italic Below a Station are Daily Substitutes for 15-Minute Stations)	33

List of Figures

	<i>Page</i>
Figure 1. Comparison of EI values computed using the Wischmeier-Smith equation, the Brown-Foster equation with coefficients of 0.050, and 0.082, and the McGregor- Mutchler equation	4
Figure 2. Fractional differences between the Wischmeier-Smith equation and the Brown-Foster equation with the b coefficient equal to 0.050 and 0.082, and the difference between the EI computed with the two coefficients in the Brown-Foster equation	4
Figure 3. Schematic of a 30-minute storm with fixed 30-minute time intervals	6
Figure 4. Conversion factor based on the number of fixed-interval observational units	6
Figure 5. Schematic of a 30-minute storm with fixed 30-minute time intervals	8
Figure 6. Number of stations in each 2 degree longitude by 2 degree latitude grid cell	18
Figure 7. Coefficient of variation of R-factor for each 2 degree longitude by 2 degree latitude grid cell	19
Figure 8. An R-factor map created from 1971-1999 daily data with regression equations developed using 15-minute station data	19
Figure 9. Ratio of climate division average annual precipitation for 1971-1999/1936-1957, expressed as a percentage. Values above 100 percent indicate an increase in precipitation over time	28
Figure 10. Annual precipitation (mm) for the Trans Pecos region of western Texas. Darker line segments represent average precipitation amounts for 1936-1957 and 1971-1999, respectively	29
Figure 11. Annual precipitation (mm) for the south-central region of Iowa. Darker line segments represent average precipitation amounts for 1936-1957 and 1971-1999, respectively	30
Figure 12. Ratio of climate division average a) winter, b) spring, c) summer, and d) fall precipitation for 1971-1999/1936-1957, expressed as a percentage. Values above 100 percent indicate an increase in precipitation over time	31
Figure 13. Ratio of climate division average a) winter, b) spring, c) summer, and d) fall, and e) annual precipitation for 1971-1999/1948-1983, expressed as a percentage. Values above 100 percent indicate an increase in precipitation over time	32

Figure 14. Relationship between R-factor calculated using the Brown-Foster equation and the 1971-1999 and 1936-1957 daily precipitation data. Dotted line indicates the 1:1 relationship	35
Figure 15. Relationship between R-factor computed from 1936-1957 data by Wischmeier and Smith and the Brown-Foster equation and daily regression equations. Dotted line indicates the 1:1 relationship	35
Figure 16. Value of erosivity index for a single-storm 10-year return frequency (MJ mm ha ⁻¹ hr ⁻¹)	37
Figure 17. Mean total storm precipitation (mm) for all storms during a) winter, b) spring, c) summer, d) fall, and e) the entire year	39
Figure 18. Mean storm total precipitation (mm) for all storms with greater than 12.7 mm of rainfall or a 15-minute rainfall intensity greater than 24 mm hr ⁻¹ during a) winter, b) spring, c) summer, d) fall, and e) the entire year	41
Figure 19. Mean storm duration (hr) for all storms during a) winter, b) spring, c) summer, d) fall, and e) the entire year	42
Figure 20. Mean storm duration (hr) for all storms with greater than 12.7 mm of rainfall or a 15-minute rainfall intensity greater than 24 mm hr ⁻¹ during a) winter, b) spring, c) summer, d) fall, and e) the entire year	43
Figure 21. Mean storm intensity (mm hr ⁻¹) for all storms during a) winter, b) spring, c) summer, d) fall, and e) the entire year	44
Figure 22. Mean storm intensity (mm hr ⁻¹) for all storms with greater than 12.7 mm of rainfall or a 15-minute rainfall intensity greater than 24 mm hr ⁻¹ during a) winter, b) spring, c) summer, d) fall, and e) the entire year	46
Figure 23. Mean storm kinetic energy (E, MJ ha ⁻¹) for all storms during a) winter, b) spring, c) summer, d) fall, and e) the entire year	47
Figure 24. Mean storm kinetic energy (E, MJ ha ⁻¹) for all storms with greater than 12.7 mm of rainfall or a 15-minute rainfall intensity greater than 24 mm hr ⁻¹ during a) winter, b) spring, c) summer, d) fall, and e) the entire year	48
Figure 25. Mean maximum 30-minute rainfall intensity (mm hr ⁻¹) for all storms during a) winter, b) spring, c) summer, d) fall, and e) the entire year	49

Figure 26. Mean maximum 30-minute rainfall intensity (mm hr ⁻¹) for all storms with rainfall greater than 12.7 mm or a 15-minute intensity greater than 24 mm hr ⁻¹ during a) winter, b) spring, c) summer, d) fall, and e) the entire year.	51
Figure 27. Mean storm erosivity (EI ₃₀ , MJ mm ha ⁻¹ hr ⁻¹) value for all storms during a) winter, b) spring, c) summer, d) fall, and e) the entire year.	52
Figure 28. Mean storm erosivity (EI ₃₀ , MJ mm ha ⁻¹ hr ⁻¹) value for all storms with rainfall greater than 12.7 mm or a 15-minute intensity greater than 24 mm hr ⁻¹ during a) winter, b) spring, c) summer, d) fall, and e) the entire year.	53
Figure 29. Mean number of storms during a) winter, b) spring, c) summer, d) fall, and e) the entire year.	54
Figure 30. Mean number of storms for all storms with rainfall greater than 12.7 mm or a 15-minute intensity greater than 24 mm hr ⁻¹ during a) winter, b) spring, c) summer, d) fall, and e) the entire year.	55
Figure 31. Mean maximum 15-minute intensity (mm hr ⁻¹) for all storms during a) winter, b) spring, c) summer, d) fall, and e) the entire year.	57
Figure 32. Mean maximum 15-minute intensity (mm hr ⁻¹) for all storms with rainfall greater than 12.7 mm or a 15-minute intensity greater than 24 mm hr ⁻¹ during a) winter, b) spring, c) summer, d) fall, and e) the entire year.	58
Figure 33. Mean ratio of 15-minute maximum intensity to total storm intensity for all storms during a) winter, b) spring, c) summer, d) fall, and e) the entire year.	59
Figure 34. Mean ratio of 15-minute maximum intensity to total storm intensity for all storms with rainfall greater than 12.7 mm or a 15-minute intensity greater than 24 mm hr ⁻¹ during a) winter, b) spring, c) summer, d) fall, and e) the entire year.	60
Figure 35. Annual 1971-1999 trends in storm characteristics for a) storm totals, b) storm duration, c) storm intensity, d) maximum 30-minute precipitation, e) storm EI, and f) number of storms. Trends are expressed as percent change per decade where negative trends are cross-hatched, positive trends are gray, and no trend is white. Black dots represent stations.	62
Figure 36. Winter 1971-1999 trends in storm characteristics for a) storm totals, b) storm duration, c) storm intensity, d) maximum 30-minute precipitation, e) storm EI, and f) number of storms. Trends are expressed as percent change per decade where negative trends are cross-hatched, positive trends are gray, and no trend is white. Black dots represent stations.	63

- Figure 37. Spring 1971-1999 trends in storm characteristics for a) storm totals, b) storm duration, c) storm intensity, d) maximum 30-minute precipitation, e) storm EI, and f) number of storms. Trends are expressed as percent change per decade where negative trends are cross-hatched, positive trends are gray, and no trend is white. Black dots represent stations 65
- Figure 38. Summer 1971-1999 trends in storm characteristics for a) storm totals, b) storm duration, c) storm intensity, d) maximum 30-minute precipitation, e) storm EI, and f) number of storms. Trends are expressed as percent change per decade where negative trends are cross-hatched, positive trends are gray, and no trend is white. Black dots represent stations 66
- Figure 39. Fall 1971-1999 trends in storm characteristics for a) storm totals, b) storm duration, c) storm intensity, d) maximum 30-minute precipitation, e) storm EI, and f) number of storms. Trends are expressed as percent change per decade where negative trends are cross-hatched, positive trends are gray, and no trend is white. Black dots represent stations 68
- Figure 40. Percentage differences between storm statistics for positive PNA and negative PNA winter seasons for the period 1971-1999: a) number of storms, b) storm precipitation total, c) storm duration, d) storm precipitation intensity, e) storm 30-minute maximum precipitation intensity, and f) storm erosivity. Positive differences are gray, negative differences are cross-hatched. Dots represent stations that have at least one valid storm for each event mode. A valid storm must have a precipitation total greater than 12.7 mm or a precipitation maximum intensity greater than 25.4 mm hr⁻¹. 71
- Figure 41. Percentage differences between storm statistics for positive NAO and negative NAO winter seasons for the period 1971-1999: a) number of storms, b) storm precipitation total, c) storm duration, d) storm precipitation intensity, e) storm 30-minute maximum precipitation intensity, and f) storm erosivity. Positive differences are gray, negative differences are cross-hatched. Dots represent stations that have at least one valid storm for each event mode. A valid storm must have a precipitation total greater than 12.7 mm or a precipitation maximum intensity greater than 25.4 mm hr⁻¹. 72

- Figure 42. Percentage differences between storm statistics for El Niño and La Niña events during winter months for the period 1971-1999: a) number of storms, b) storm precipitation total, c) storm duration, d) storm precipitation intensity, e) storm 30-minute maximum precipitation intensity, and f) storm erosivity. Positive differences are gray, negative differences are cross-hatched. Dots represent stations that have at least one valid storm for each event mode. A valid storm must have a precipitation total greater than 12.7 mm or a precipitation maximum intensity greater than 25.4 mm hr⁻¹. 74
- Figure 43. Percentage differences between storm statistics for El Niño and La Niña events during spring months for the period 1971-1999: a) number of storms, b) storm precipitation total, c) storm duration, d) storm precipitation intensity, e) storm 30-minute maximum precipitation intensity, and f) storm erosivity. Positive differences are gray, negative differences are cross-hatched. Dots represent stations that have at least one valid storm for each event mode. A valid storm must have a precipitation total greater than 12.7 mm or a precipitation maximum intensity greater than 25.4 mm hr⁻¹. 75
- Figure 44. Percentage differences between storm statistics for El Niño and La Niña events during summer months for the period 1971-1999: a) number of storms, b) storm precipitation total, c) storm duration, d) storm precipitation intensity, e) storm 30-minute maximum precipitation intensity, and f) storm erosivity. Positive differences are gray, negative differences are cross-hatched. Dots represent stations that have at least one valid storm for each event mode. A valid storm must have a precipitation total greater than 12.7 mm or a precipitation maximum intensity greater than 25.4 mm hr⁻¹. 77
- Figure 45. Percentage differences between storm statistics for El Niño and La Niña events during fall months for the period 1971-1999: a) number of storms, b) storm precipitation total, c) storm duration, d) storm precipitation intensity, e) storm 30-minute maximum precipitation intensity, and f) storm erosivity. Positive differences are gray, negative differences are cross-hatched. Dots represent stations that have at least one valid storm for each event mode. A valid storm must have a precipitation total greater than 12.7 mm or a precipitation maximum intensity greater than 25.4 mm hr⁻¹. 78

Figure 46. Percentage differences between storm statistics for positive PDO and negative PDO time periods during winter months for the period 1971-1999: a) number of storms, b) storm precipitation total, c) storm duration, d) storm precipitation intensity, e) storm 30-minute maximum precipitation intensity, and f) storm erosivity. Positive differences are gray, negative differences are cross-hatched. Dots represent stations that have at least one valid storm for each event mode. A valid storm must have a precipitation total greater than 12.7 mm or a precipitation maximum intensity greater than 25.4 mm hr⁻¹. 80

Figure 47. Percentage differences between storm statistics for positive PDO and negative PDO time periods during spring months for the period 1971-1999: a) number of storms, b) storm precipitation total, c) storm duration, d) storm precipitation intensity, e) storm 30-minute maximum precipitation intensity, and f) storm erosivity. Positive differences are gray, negative differences are cross-hatched. Dots represent stations that have at least one valid storm for each event mode. A valid storm must have a precipitation total greater than 12.7 mm or a precipitation maximum intensity greater than 25.4 mm hr⁻¹. 81

Figure 48. Percentage differences between storm statistics for positive PDO and negative PDO time periods during summer months for the period 1971-1999: a) number of storms, b) storm precipitation total, c) storm duration, d) storm precipitation intensity, e) storm 30-minute maximum precipitation intensity, and f) storm erosivity. Positive differences are gray, negative differences are cross-hatched. Dots represent stations that have at least one valid storm for each event mode. A valid storm must have a precipitation total greater than 12.7 mm or a precipitation maximum intensity greater than 25.4 mm hr⁻¹. 83

Figure 49. Percentage differences between storm statistics for positive PDO and negative PDO time periods during fall months for the period 1971-1999: a) number of storms, b) storm precipitation total, c) storm duration, d) storm precipitation intensity, e) storm 30-minute maximum precipitation intensity, and f) storm erosivity. Positive differences are gray, negative differences are cross-hatched. Dots represent stations that have at least one valid storm for each event mode. A valid storm must have a precipitation total greater than 12.7 mm or a precipitation maximum intensity greater than 25.4 mm hr⁻¹. 84

Spatial Distribution, Variation, and Trends in Storm Precipitation Characteristics Associated with Soil Erosion in the United States

Introduction

Nonpoint source pollution and soil erosion by water from agricultural lands have been major environmental concerns for many years. Estimation of potential erosion requires the use of either the Universal Soil Loss Equation or USLE (Wischmeier and Smith, 1978) or the Revised Universal Soil Loss Equation RUSLE (Renard and Ferreira, 1993). Both the USLE and RUSLE use data about the landscape (soil texture, and slope steepness and length) and the climate (the R-factor), along with cropping and erosion prevention practices, to compute erosion runoff from both agricultural and rangelands.

The R-factor, the only climate variable in RUSLE, is a measure of the erosive force of precipitation events measured in megajoule millimeter per hour per hectare per year ($\text{MJ mm h}^{-1} \text{ha}^{-1} \text{yr}^{-1}$). The R-factor values east of the Rocky Mountains were computed from 22 years of rainfall data (1936-1957) for 181 stations supplemented by information from an additional 1,700 daily rainfall stations (Wischmeier and Smith, 1978). The R-factor maps for the eastern United States were redrawn to more closely fit the existing data (Renard and Freimund, 1994) as part of the RUSLE development. The R-factor values for the western United States were computed using 1971-1983 data for 713 stations. Upon completion of the development of RUSLE, an east-west discontinuity in the R-factor isolines existed in the transition between the High Plains states (North and South Dakota, Nebraska, Kansas, Oklahoma, and Texas) and the Front Range states (Montana, Wyoming, Colorado, and New Mexico). A change in the rainfall regimes of the two different periods may have caused this discontinuity.

An unpublished pilot study conducted by Hollinger, Angel, Waltman, and Svoboda demonstrated significant differences in North Central U.S. R-factor values when computed with the 1961-1990 climate record and compared to the original R-factor values. The R-factor values increased by an average of 10 percent when computed using the 1961-1990 2-year, 6-hour rainfall return frequency (Wischmeier and Smith, 1978) for 55 stations in the North Central region. Huff and Angel (1992) found that the frequency of rain events of all magnitudes has increased in this same region.

Differences in R-factor values computed using different time periods point to the need to evaluate the temporal stationarity of R-factor values. By definition, stationarity means that the R-factor values do not change with time. A testable null hypothesis is that storm precipitation characteristics and R-factor values are temporally stationary. Because R-factor differences were observed using two different time periods, and rainfall studies have shown an increase in large rain events, an alternative hypothesis is that storm rainfall characteristics and thus R-factor values are not temporally stationary. Even if storm precipitation characteristics and R-factor values are stationary, interannual and interdecadal variations are observed in the climate record. These variations across the United States need to be studied to determine their effects on the R-factor and its components.

Objectives

The objectives of this research were to 1) test the null hypothesis that storm precipitation characteristics and R-factor values are temporally stationary, 2) create a database that provides the precipitation data necessary to compute the single-storm erosivity index (EI) and R-factor, 3) compute 10-year EI return frequencies for use in erosion control structure design and operations, 4) evaluate the spatial difference of rainstorm characteristics across the United States, and 5) evaluate the effect of oceanic-atmospheric teleconnections on R-factor interannual and interdecadal variations. This work was conducted cooperatively by the Illinois State Water Survey/Midwestern Regional Climate Center (ISWS/MRCC) and the United States Department of Agriculture (USDA) Natural Resources Conservation Services (NRCS) National Water and Climate Center (NWCC).

R-factor Computation

A major difficulty in computing EIs and the R-factor is obtaining representative data for different storm increments. The original EIs were computed using “breakpoint” data obtained by analyzing charts from recording rain gauges. This is very labor intensive, and most chart-recording rain gauges have been replaced by rain gauges that record rainfall at 15-minute intervals. In an ideal situation, EIs and the R-factor would be computed from rainfall data recorded at an interval of 5 minutes or less (5-minute rainfall data). However, such data are not generally available from stations that record rainfall.

From the 1970s to the present, recording rain gauges have used punch tape to record rainfall in 15-minute intervals. Records for 15-minute data are available for 3,700 stations in the United States (National Climate Data Center, NCDC TD-3260). These stations have varying lengths of record with varying amounts of missing data. There are approximately 6,400 hourly rainfall stations (NCDC TD-3240) and 12,800 daily rainfall stations (NCDC TD-3200). The majority of the hourly stations are 15-minute stations where the 15-minute rainfall data are totaled to hourly values. Daily rainfall stations include all first order and National Weather Service Cooperative Observer Program stations.

Storm erosivity values initially were calculated using 15-minute rainfall data. However, concerns regarding data quality, specifically the accuracy of flags indicating data presence or absence, made it necessary to calculate the R-factor with a procedure that used daily precipitation data. Missing or flagged data within almost all the 15-minute station data time series underestimated the true R-factor for different years, and thus an underestimation of the mean R-factor over the period of record for each station. Further, the length of record for the 15-minute stations varied from station to station, resulting in highly variable R-factor values for neighboring stations. Daily rainfall data are more complete and provide a more coherent picture of the spatial variation of the R-factor.

A description follows of the equations used for computing the R-factor, the development of the coefficient to convert the 30-minute maximum precipitation intensity to its breakpoint equivalent, procedures used to perform data quality assurance, approaches used to adjust for missing data, comparisons of the new R-factor map and values to previous versions, computation of the 10-year return interval EI level, and analyses of storm structure variables.

R-factor Equations

The R-factor has units of MJ mm ha⁻¹ h⁻¹ yr⁻¹ and is defined as:

$$R = \frac{1}{n} \sum_{j=1}^n \left[\sum_{k=1}^m E_k (I_{30})_k \right]_j \quad (1)$$

where E is the total storm kinetic energy (MJ ha⁻¹), I₃₀ is the maximum 30-minute rainfall intensity (mm h⁻¹), j is an index of the number of years (n) used to produce the mean, and k is an index of the number of storms (m) each year (Renard and Freimund, 1994). The definition for E is given by

$$E_k = \sum_{r=1}^s e_r \Delta V_r \quad (2)$$

where e_r is the rainfall energy in MJ ha⁻¹ mm⁻¹, and V_r is the depth of rainfall in mm for the rth increment of the storm. The number of increments (s) is determined by storm length and data resolution. If a storm lasts 2 hours and hourly data are used, s = 2; if 15-minute data are used, as in this study, s = 8. The rainfall energy of the storm (e_r) is calculated from Renard and Freimund, (1994):

$$e_r = 0.29[1 - 0.72 \exp(-0.05i_r)] \quad (3)$$

where i_r is the rainfall intensity (mm hr⁻¹) for a particular storm increment. Equation 3, the unit energy equation, will be referred to as the Brown-Foster equation (Brown and Foster, 1987).

A second form of the unit energy equation was proposed by McGregor and Mutchler (1976). Both the Brown-Foster equation and the McGregor-Mutchler equation have a finite unit energy value at zero rainfall. These equations are compared to the equation developed by Wischmeier and Smith (1958) in Figure 1. Two different b coefficients are shown for the Brown-Foster equation: the b coefficient of 0.05 is the original value used in the Brown-Foster equation, while b equal to 0.082 is a more recent estimation of the coefficient. Results from the Brown-Foster equation with a b coefficient of 0.082 (McGregor et al., 1995) almost duplicate results from the McGregor-Mutchler equation.

The differences expressed as a fractional deviation from the Wischmeier-Smith equation are shown (Figure 2). Differences between the e_r values computed using the Brown-Foster equation, with b coefficients of 0.050 and 0.082, and the Wischmeier-Smith equation were computed as: Δ = (BF - WS)/WS, where WS is the e_r value computed from the Wischmeier-Smith equation and BF is the e_r value computed from the Brown-Foster equation. Rainfall energy computed using the Brown-Foster equation with a b coefficient of 0.05 is more than 5 percent less than energy computed using the Wischmeier-Smith equation with rainfall intensities ranging from 1 to 25 mm hr⁻¹. With the Brown-Foster b coefficient equal to 0.082, computed rainfall

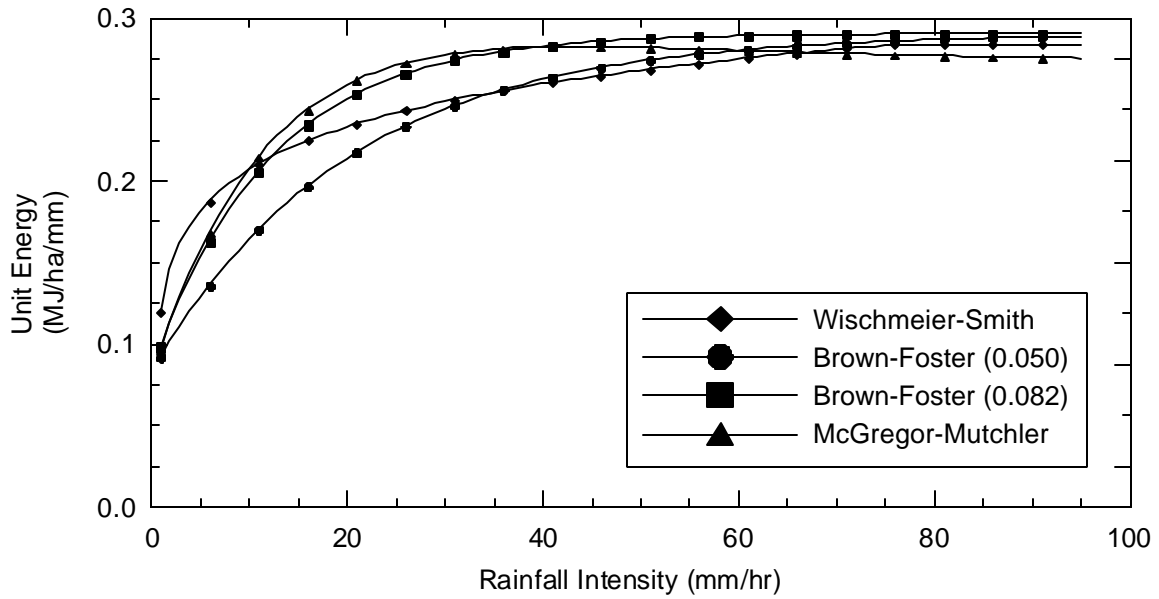


Figure 1. Comparison of EI values computed using the Wischmeier-Smith equation, the Brown-Foster equation with coefficients of 0.050, and 0.082, and the McGregor-Mutchler equation.

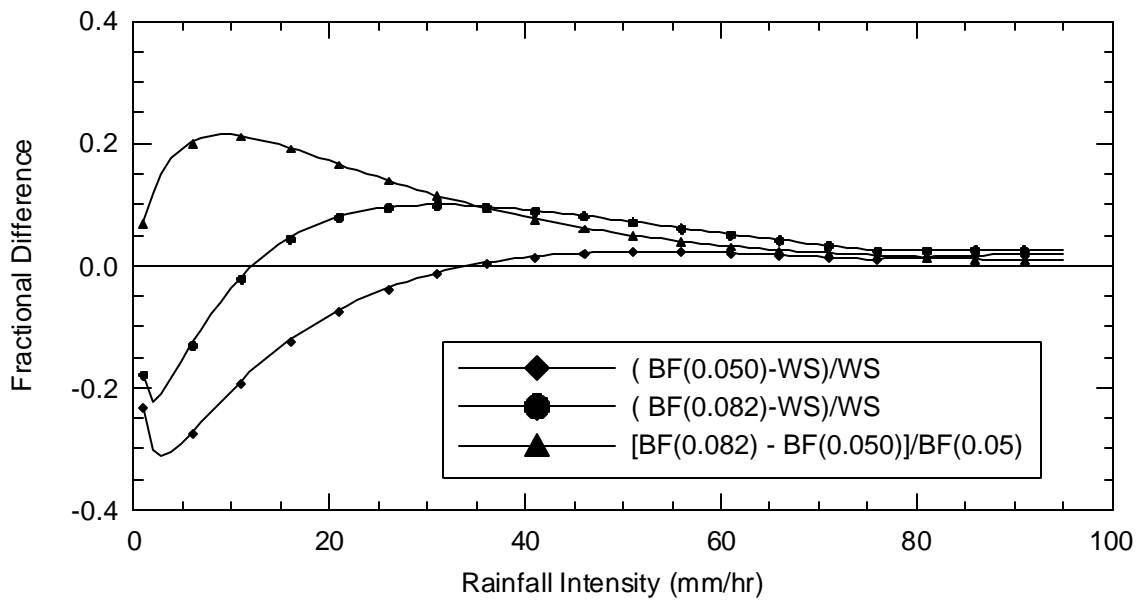


Figure 2. Fractional differences between the Wischmeier-Smith equation and the Brown-Foster equation with the b coefficient equal to 0.050 and 0.082, and the difference between the EI computed with the two coefficients in the Brown-Foster equation.

energy deviations greater than 5 percent occur from 1 to 9 mm hr⁻¹ (less rainfall energy) and from 17 to 60 mm hr⁻¹ (greater rainfall energy).

The difference between the e_r derived with the Brown-Foster equation using the two different coefficients was computed as: $\Delta = (BF_{0.082} - BF_{0.050})/BF_{0.050}$. Deviations greater than 5 percent occur between 1 and 49 mm hr⁻¹, with the values computed using the coefficient of 0.082 being greater than the values computed using the coefficient of 0.05.

The Brown-Foster equation with a b coefficient of 0.082 is the preferred unit energy equation (George Foster, personnel communication, 2000) and was used in computing the R-factor in this work. The equation was applied directly to the 15-minute precipitation data to yield individual storm EI values; these were then combined into R-factors by proration or used to create regression relationships to daily precipitation.

30-Minute Maximum Rainfall Intensity Adjustment

Wischmeier and Smith (1978) used the 30-minute maximum rainfall rate, derived from breakpoint precipitation data $[(I_{30})_B]$, in the calculation of the R-factor. Breakpoint precipitation data from recording rain gauges were reported at intervals of fixed rainfall rates instead of intervals of fixed time. All rain gauges used to obtain the breakpoint data were equipped with strip charts that were manually digitized by selecting points where the rainfall rate changed slope. Breakpoint data were obtained by recording the times of changes in the slope of the rain trace on the strip chart, recording the total rainfall received, and computing the rainfall intensity for that period. While the number of sites with suitable modern breakpoint data is very limited, more than 1,800 stations across the United States have adequate 15-minute rainfall data. Unfortunately, the temporal resolution of 15-minute data was not adequate for fully specifying the $(I_{30})_B$. It is highly unlikely that the $(I_{30})_B$ of a storm, assumed to be the true 30-minute maximum rainfall intensity (I_{30}) , would be captured in two consecutive 15-minute periods fixed by the clock (e.g., 2:00, 2:15, 2:30, and 2:45). The more likely case was that the two consecutive 15-minute periods (Figure 3) would miss part of the true I_{30} .

In order to allow the use of the more numerous 15-minute observations in the R-factor calculation, an equation was introduced to relate the 30-minute maximum rainfall derived from 15-minute data $[(I_{30})_{15}]$ to the $(I_{30})_B$ through a ratio:

$$(I_{30})_B = (I_{30})_{15}k \quad (4)$$

where k is the adjustment factor. Weiss (1964) approached the general problem from a theoretical sense. He found that when the duration of the event and the fixed observational time interval were the same length (e.g., true 24-hour total from 1-day fixed periods, true 60-minute total from fixed 1-hour periods, etc.), the conversion factor was always 1.14. The relationship for up to 24 observational units is shown (Figure 4). For a true 30-minute rainfall from two fixed 15-minute observational units, Weiss (1964) calculated a conversion factor of 1.0667, assuming that the true 30-minute maximum is independent of clock time. As part of this project, breakpoint data from sites across the United States were used to test this hypothesis by directly calculating the ratio between the two types of 30-minute maxima.

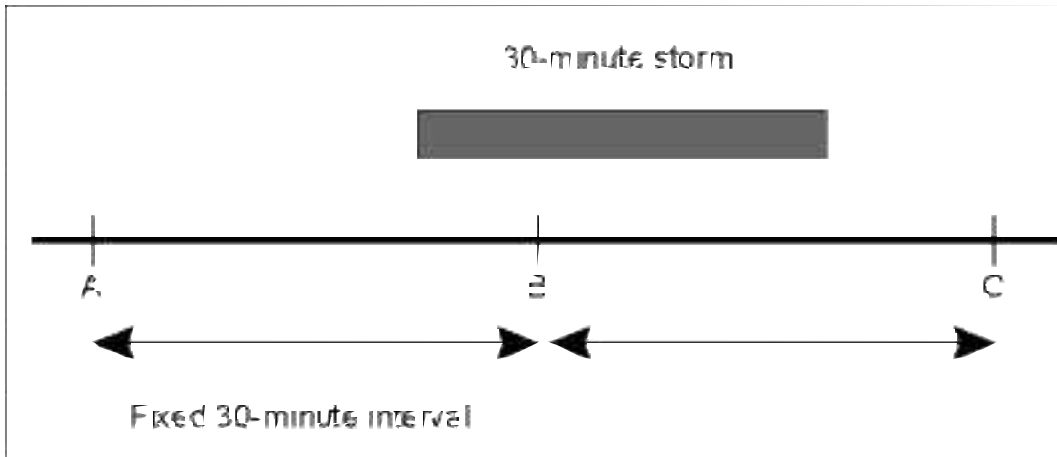


Figure 3. Schematic of a 30-minute storm with fixed 30-minute time intervals.

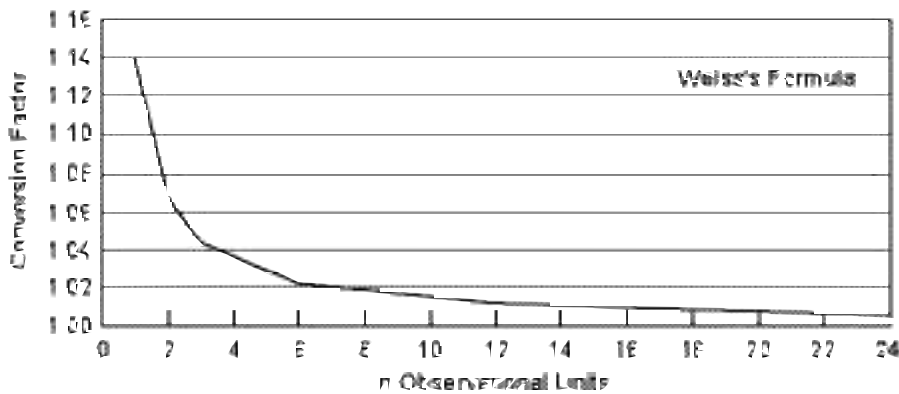


Figure 4. Conversion factor based on the number of fixed-interval observational units.

Breakpoint precipitation data from 23 USDA sites across the United States (Table 1) were used to calculate the difference between the $(I_{30})_{15}$ data and the $(I_{30})_B$ data for several hundred storms. The overall mean ratio of $(I_{30})_B$ to $(I_{30})_{15}$ for all storms at the 23 sites was 1.034, which was statistically significantly different ($p = 0.05$) than Weiss's theoretically derived value of 1.0667. It is also statistically significantly different than 1.0 at $p = 0.05$. The results show no statistically significant differences in this ratio among the 23 sites. Storms with durations of 15 minutes or less would be completely captured by two 15-minute intervals, leading to more cases of the ratio being exactly 1. Approximately 6.5 percent of the storms from the breakpoint data had durations of 15 minutes or less. However, excluding these events only increased the ratio from 1.034 to 1.035, a nonsignificant difference.

Using a theoretical approach, Weiss assumed that the start time of the event within a specified time period was randomly distributed and that precipitation fell within discrete events. Examination of the start time of $(I_{30})_B$ for the 23 USDA sites showed that the assumption of

Table 1. The 23 USDA Breakpoint Stations and Their Average Ratio of $(I_{30})_B$ to $(I_{30})_{15}$

<i>Station ID</i>	<i>Station name</i>	<i>Years of data</i>	<i>Average ratio</i>
<i>Southeast</i>			
L08	Vero Beach, FL	1974-1975	1.032
L10	Watkinsville, GA	1945-1979	1.036
L62	Oxford, MS	1957-1972	1.033
L83	Goodwin Creek, MS	1970-1974	1.045
<i>Northeast</i>			
L16	Mahantango Creek, PA	1968-1990	1.036
L67	N. Danville, VT	1958-1979	1.021
<i>North Central</i>			
L17	Edwardsville, IL	1938-1955	1.040
L19	Lafayette, IN	1940-1953	1.021
L22	Ames, IA	1968-1980	1.054
L26	Coshocton, OH	1937-1992	1.041
L31	Fennimore, WI	1939-1969	1.032
L61	Monticello, IL	1949-1982	1.040
L71	Treynor, IA	1941-1990	1.037
<i>Southern Great Plains</i>			
L34	Cherokee, OK	1942-1960	1.044
L42	Reisel, TX	1939-1981	1.045
L70	Sonora, TX	1968-1972	1.039
<i>Northern Great Plains</i>			
L44	Hastings, NE	1938-1967	1.028
<i>Southwest</i>			
L45	Safford, AZ	1937-1975	1.023
L47	Albuquerque, NM	1939-1972	1.023
L63	Walnut Gulch, AZ	1954-1990	1.033
<i>Northwest</i>			
L56	Moscow, ID	1937-1942	1.011
L68	Reynolds Creek, ID	1962-1981	1.024
<i>Hawaii</i>			
L77	Kunia, HI	1972-1978	1.036
Mean			1.034
Standard Deviation			0.010

random start time was valid. The most likely explanation for the differences in the observed and theoretical approach to estimating the ratio was the assumption that precipitation fell during discrete events (e.g., capture of a 30-minute storm in two fixed time periods). However, in the R-factor application, the 30-minute rainfall event is usually embedded in some longer rainfall event. With the $(I_{30})_B$ beginning at 3:07 a.m. and ending at 3:36 a.m. and embedded in some larger storm (Figure 5), the 15-minute period ending at 3:30 a.m. would miss the last 6 minutes of the end of the $(I_{30})_B$. However, as illustrated, the 15-minute period ending at 3:15 a.m. would pick up

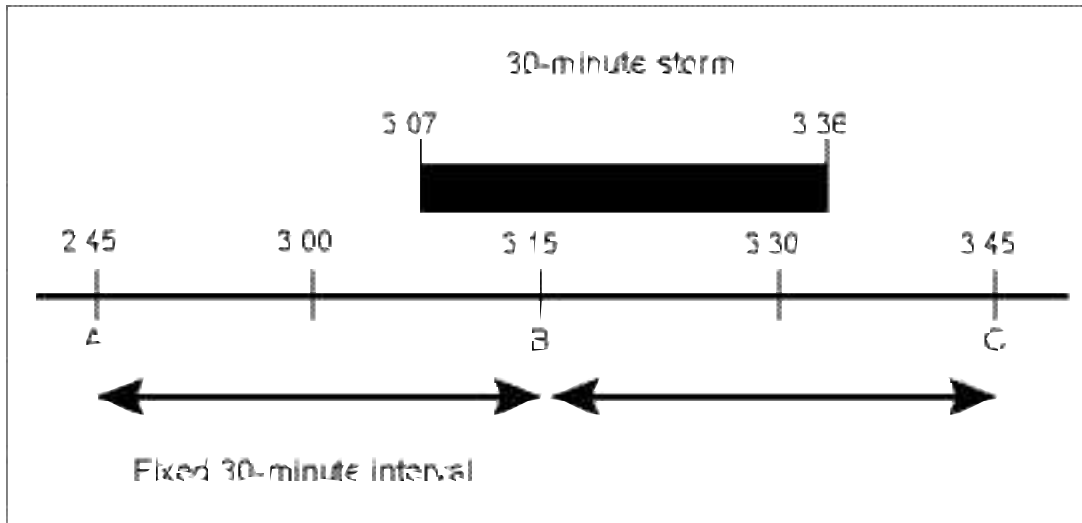


Figure 5. Schematic of a 30-minute storm with fixed 30-minute time intervals.

rainfall falling at a lower rain rate from 3:00 a.m. to 3:06 a.m. Therefore, extra rainfall at the beginning of the first 15-minute measurement partially compensates for the missed rainfall at the end of $(I_{30})_B$. This situation, not accounted for in Weiss's calculations, has the effect of reducing the ratio needed to adjust $(I_{30})_{15}$ to $(I_{30})_B$ from 1.0667 to approximately 1.034. The empirical ratio derived in this study was used when calculating the EI for a storm.

Data Quality Assurance

A total of 2,375 15-minute stations with known latitudes, longitudes, and elevations were identified with more than seven years of data. These station records were screened to determine the start and end of the rainfall record and the percentage of missing data based on monthly records. This simple screening provided an initial indication of the quality of the data available. Final quality assurance involved screening each record for quality control flags, using the computer programs developed to compute the EI, R-factor, and storm structure variables.

Each record of a 15-minute data file (NCDC TD-3260) contains 15-minute period precipitation for a single day on days when precipitation occurred. Each record includes quality control flags indicating missing data, accumulated data, and data flagged for various reasons (Hammer, 1998) by the National Climate Data Center (NCDC). In computing the EI, only storms used had no flags present and were separated from flagged or missing data by more than six hours. Adjacent days also were examined to ensure the existence of a 6-hour gap between storms and flagged or missing data, and to identify multi-day storms. Examination of adjacent days was necessary to establish the beginning and end times of storms, because the present study defined storms as those periods with precipitation that were separated by six complete hours with no precipitation before or after the storm (Renard et al., 1997). With this definition, individual days can have multiple storms, and storms can occur over periods of time involving more than one calendar day. This storm definition and data requirement ensured that individual storm statistics

were not invalidated by incorporating missing or flagged data influences. However, this practice increased the percentage of data classified as missing. Even with the highest quality stations, the percentages of missing data were sufficient to require accounting for these periods in calculating cumulative variables, such as the R-factor, and monthly and annual rainfall. A total of 1,409 of the initial 2,375 15-minute stations were used in the following 15-minute station analysis.

One problem that contributed to missing data and proved to be highly intractable was the use of the “g” flag in the NCDC TD-3260 data set to indicate the presence of an operational instrument at the beginning of a month. This flag was located in the first record of every month for which the 15-minute station was measuring precipitation. If a month started with this flag and then was followed directly by another “g” flag on the first day of the next month, it was assumed that no rainfall was detected during the month of the first “g” flag because a lack of data flags is an indication that the gauge was operational. Unfortunately, this proved to be an invalid assumption, as some stations in obviously humid climates displayed series of “g” flag records. For instance, a station at Ashland, Alabama, reported the following series of records while nearby reports showed about 20 inches of rain in the area during the period:

```
15M01036900QPCPHT19790600010020015 00000g 2500 00000
15M01036900QPCPHT19790700010020015 00000g 2500 00000
15M01036900QPCPHT19790800010020015 00000g 2500 00000
15M01036900QPCPHT19790900010020015 00000g 2500 00000
15M01036900QPCPHT19791000010020015 00000g 2500 00000
```

The above records indicated that it did not rain for four consecutive months (June 1979 - September 1979). In fact, the collocated daily precipitation data were missing, indicating that all of these 15-minute precipitation data also should have been flagged as missing. Instead, a program reading the records above would assume that the station was active and received no rain. This problem was first identified when trying to reconcile the very low R-factor value calculated for the St. Louis Science Center, Missouri, which was only about 50-60 percent as large as surrounding station values. The problem at St. Louis was only slightly more subtle, in that valid records followed the “g” flag; however, these records consisted only of flagged values that were removed from consideration. For instance, the following example for November 1976 displays a “g” flag, despite the lack of valid data for the month.

```
15M23745200QPCPHT19761100010020015 00000g 2500 00000
15M23745200QPCPHT19761100250022015 99999[ 2500 00000I
15M23745200QPCPHT19761100270020815 99999] 2500 00000I
15M23745200QPCPHT19761200010020015 00000g 2500 00000
```

In this case, the month was dry, with only 0.76 inches of rain at the collocated daily precipitation station, including one R-factor qualifying storm of more than 0.5 inches. The 15-minute data would be processed as perfectly dry, however. This occurred many times in the record of this station, resulting in a greatly suppressed precipitation value despite the seeming lack of missing data. A further analysis in which TD-3260 months with zero precipitation were compared to an alternate data source led to the conclusion that tens of thousands of inadvertent “g” flags existed in the TD-3260 data set.

Missing Data Identification and Adjustment

Climatological series of any length almost always have some missing data. As the number of data points increases, the probability of a serially complete data record decreases. Because the NCDC TD 3260 15-minute precipitation data involve 96 measurements each day, the odds of having missing or defective data are greatly increased. Therefore, any analysis that requires a serially complete record, such as computing the total annual precipitation or the R-factor, will have gaps in the data record that will introduce errors and uncertainty into the final results. Several approaches were developed and tested for dealing with missing 15-minute data impacts on R-factor calculations: 1) prorating missing data periods, 2) using regression relationships to fill the gaps of missing data periods with estimated values, and 3) using regression relationships to directly relate daily precipitation data to storm EI to generate the R-factor from higher quality daily data. Each approach has advantages and drawbacks.

A gridded precipitation data set was made available by the Midwestern Regional Climate Center (MRCC) for independent checking of ambiguous missing data/zero precipitation periods. The MRCC produces and uses these data for real-time quality control of daily data (Kunkel et al., 1998). Daily gridded precipitation data have a spatial resolution of 1° longitude by 0.66° latitude. While daily gridded precipitation data were coarse compared to station data, the gridded data were quite sensitive indicators of any precipitation that fell within the grid cell. This sensitivity is due to the distance-weighted approach used to interpolate the gridded data from daily station data. These gridded precipitation data were used in several of the methods used to detect missing data and fill the gaps.

Prorating Missing Data

This approach to making missing data adjustments started with totaling individual storm EI totals into 24 half-month EI values for each year, and computing 24 mean half-month EI values. Missing data are not always randomly distributed within the 15-minute data time series for a given station, but often occur in lengthy consecutive periods due to equipment difficulties. This nonrandom time distribution of missing data leads to seasonal biases in annual R-factor calculations if the available data simply were added with no regard to the time of year. The seasonal biases are due to the tendency of rain gauges to fail during seasonally heavy rainstorms. Therefore, it is better to compute the R-factor for a station by summing the 24 individual half-month EI averages and then calculating the annual R-factor value as the sum of these means.

The key to this method was to identify half months with valid EI totals not affected by missing data and to adjust for missing data. The most straightforward method tested was to assume that the half month was valid if its EI exceeded zero. If it was zero and the MRCC gridded precipitation data for the two-week period was also zero, then the zero value was assumed to be valid. If these two conditions were met, then the half-month EI in question was given full weight in calculating the mean for that half month. If an individual half-month EI was found to be zero, even though precipitation was detected in the gridded data, the half month was deleted from the computation, reducing the magnitude of the denominator.

Each valid half-month period was checked for partial missing data by prorating the effect of that half-month EI on the mean for that period by the percentage of available data. For example, if 30 percent of the 15-minute data were missing in a half-month period, the yearly weight for that year's half-month period would be set to 0.7 and added to the total number of years used

to set the denominator in calculating the half-month mean EI. Thus, in a 20-year record, where there was no missing data for 19 of the half-month periods and 30 percent were missing in one year, the number of years used to compute the mean would be 19.7 rather than 20. This method seemed quite effective, except that it proved to be sensitive to the “g” flag inconsistencies of the 15-minute precipitation data set.

The presence of inaccurate “g” flags, as described in the last section, would lead to an underestimate of the R-factor by inflating the denominator while decreasing the EI sum. To correct the problem, a method was developed to evaluate the correctness of the half-month missing data percentage determined using all data and flags. The procedure involved comparing both the half-month EI and missing data percentage with appropriate daily gridded rainfall. To make the comparison, the gridpoint closest to the station was used. In the first attempt, if the rainfall at the gridpoint closest to the station exceeded zero and the half-month percent missing was zero, the percent missing data was changed to 100 percent. If the indicated rainfall at the gridpoint was zero and the percent missing data was zero, then the period was assumed to be correct. When the missing data percent was changed to 100, that half-month period was no longer included in the time period’s EI mean calculation. For example, if a station had a 30-year record, and all data for the 30-year half-month periods were in the record, the mean EI for the half-month period was computed by dividing the sum of the half-month EI by 30. If the analysis of the “g” flag identified two years in which the half-month periods were invalid (i.e., the percent missing data was zero, but rainfall was observed at the nearest gridpoint), the sum of the EI was divided by 28. In both cases, the EI for the two years identified was zero; therefore, the mean half-month EI value for the time period was increased because the sum of the EI was divided by a smaller number. Using this method at all 1,409 stations, 346,455 half-month periods (34 percent of the potential half-month periods) were identified in which the “g” flag and gridpoint rainfall were inconsistent. The assumptions used in the test highly inflated R-factors.

The second, more restrictive method used to compute the half-month EI was to create a new set of gridded data that counted the number of days when daily rainfall was greater than or equal to 12.7 mm, the normal storm inclusion threshold for computing the EI. If one or more days in a half-month period had a daily rainfall greater than 12.7 mm and the percent missing data for the half-month was zero, then the percent missing data for that half-month period was set to 100 percent, and that half-month period was not used in computing the mean EI value. With this method, only 46,938 problematic half-month periods (5 percent of the potential half-month periods) were identified for the 1,409 stations. The R-values were still inflated above calculations not taking the “g” flag into account, but less than the first method. Further, the R-values were more accurate than when the “g” flag was not taken into account.

The second method was superior to the first method for this application. Gridpoint data values were computed from several surrounding stations. Therefore, the number of storms or events observed at a gridpoint may have been greater than would have been observed at a specific station. The difference was due to the heterogeneity of rainfall and the spatial averaging used to compute the gridpoint value. By increasing the threshold for including an event, some of this overestimate was removed. For example, if rain were to have occurred in the northwest quadrant surrounding the gridpoint, but no rain occurred in the southeast quadrant, the gridpoint would report a rain event and amount, while the station in the southeast quadrant actually would not have received rain. The reverse situation, a gridpoint showing no event or rainfall amount while a station near the gridpoint showed a rainfall amount, would occur only in rare instances

**Table 2. R-factor Values (MJ mm ha⁻¹ h⁻¹yr⁻¹)
Generated by Not Accounting for Missing
Data (Case 1) and by Prorating Missing
Data during Each 24 Half-
month Period (Case 2)**

<i>Station name</i>	<i>Case 1</i>	<i>Case 2</i>
Dauphin Island, AL	8972	11881
Chicago, IL	2382	2796
Artesia, NM	1003	1381
Franklinton, NC	3700	4177
Richardton, ND	671	958
O'Donnell, TX	1585	1991
Mazama, WA	48	364

and then only if there was a very small amount of rain; in this case, the storm would be unlikely to qualify for the R-factor calculation if it were recorded at a single station.

While the validity of a suspicious “g” flag will never be known with 100 percent certainty, this method increases the certainty that a valid “g” flag was not eliminated. If the null hypothesis was that all original “g” flags were valid, a type I error occurs when a flag is rejected that should not have been rejected. A type II error occurs when a flag is accepted as valid when it should have been rejected. The first method, using a gridpoint rainfall value greater than zero, increases the type I error and decreases the type II error. The second method greatly reduces the type I error, but somewhat increases the type II error. In balance, the second “g” flag correction method combined with prorating resulted in the most robust direct R-factor calculations from the 15-minute data.

Prorating the missing data results in a significant increase in the R-factor over a simple summing of the available 15-minute EIs (Table 2). The seven stations selected for this analysis were high quality stations (less than 5 percent missing data) spread over the United States so that different climate regimes could be evaluated. Prorating missing data by half-month intervals resulted in an increase of the R-factor from 13 percent (Franklinton, North Carolina) to 658 percent (Mazama, Washington). Increases were 17 percent (Chicago, Illinois), 26 percent (O’Donnell, Texas), 32 percent (Dauphin Island, Alabama), 38 percent (Artesia, New Mexico), and 42 percent (Richardton, North Dakota). With this small sampling of stations, it is clear that the majority of the 15-minute station R-factor values would be underestimated by 30 to 40 percent if corrections for missing data were not made.

Filling Data Gaps by Regression

This approach filled data gaps by using regression equations between half-month EI values and half-month gridded precipitation totals to estimate the missing half-month EI values. The relationship between EI and precipitation was best characterized as a power law of the form:

$$EI = aP^b + e \quad (5)$$

where the first term on the right-hand side of the equation is deterministic and is composed of the precipitation amount (P) and the best-fit constants a and b. The second term, ϵ , is a random term (Richardson et al., 1983). Coefficients a and b were computed using linear regression and the linearized natural logarithm form of Equation (5): $\ln EI = \ln a + b \ln P$.

For seven selected stations with good records, half-month periods with less than 5 percent missing data and the serially complete gridded precipitation data set from the MRCC were used to calibrate the regression relationship. In computing the regression coefficients, 25 percent of the good data periods were withheld to test the accuracy of EI reconstructions based on the regression equations. The goodness of fit of the regression equations was tested using a paired t-test that compared the estimated EI from the regression equation to good data withheld from the regression computation. This method was generally effective, but there also were impacts from the “g” flag inconsistency problem that allowed missing data periods to be registered as valid. In a few cases, false zero half-month EIs were paired with large precipitation amounts from the gridded data, creating outliers that distorted the resulting regression equations.

The regression method of filling missing data resulted in all stations showing statistically significant regressions at the $p < 0.0001$ level (Table 3), explaining from 21.8 percent to 44.2 percent of the data variance (R^2) in each case. When regression equations were used to estimate 2-week EI values for the withheld data, only one of the seven stations failed to meet the null hypothesis of zero difference.

Regression equations were used to fill gaps in the 2-week EI records for each station, and the resulting R-factors were calculated. Case 1 (Table 4) was the standard approach to calculate the R-factor using only valid EI data and prorating the missing 15-minute data as indicated in the previous section. This was the baseline for comparison to the other three cases. Case 2 (Table 4) replaces 2-week EI values with regression estimates when more than 5 percent of the 15-minute

Table 3. Preparation and Testing of Regression Relationships between 2-Week Precipitation Totals and 2-Week EI Values ($\text{MJ mm ha}^{-1} \text{ h}^{-1} \text{ yr}^{-1}$)^{*}

Station ID	Station name	Period of record	$EI = aP^b$			Paired t-test
			a	b	R^2	
012172	Dauphin Is., AL	07/1975-12/1999	3.8168	1.1470	0.442	-0.923
111577	Chicago, IL	07/1980-12/1999	0.1009	1.8127	0.377	-0.978
290600	Artesia, NM	10/1973-12/1999	3.3351	1.0119	0.231	-1.188
313232	Franklinton, NC	05/1971-12/1999	0.9477	1.3257	0.218	0.494
327530	Richardton, ND	06/1977-12/1999	0.1259	1.8088	0.390	1.488**
416504	O'Donnell, TX	05/1971-12/1999	4.4125	1.0141	0.262	-0.156
455133	Mazama, WA	04/1971-12/1999	0.1516	1.4742	0.407	-0.283

Notes:

^{*}A power equation of the form $EI = aP^b$ was fit, where EI is a 2-week EI derived from a period with less than 5 percent missing 15-minute precipitation data, and P is a 2-week precipitation total from a serially complete gridded precipitation data set produced at MRCC. All regressions are statistically significant at $p < 0.0001$. The paired t-test statistic compares the regression estimates of EI with actual observed EI values for a 25 percent portion of cases randomly selected and set aside prior to the computation of the regression.

^{**}Failed to meet the null hypothesis of zero difference between estimated and observed values at the $p=0.10$ level.

Table 4. R-factor Values (MJ mm ha⁻¹ h⁻¹yr⁻¹) Generated Using Regression Equations from Table 1 to Fill Gaps Caused by Missing 2-Week EI Values*

Station name	Case 1		Case 2		Case 3		Case 4	
	R-factor	Gap %						
Dauphin Is., AL	11881	0.00	12115	8.50	11738	22.70	12164	31.46
Chicago, IL	2796	0.00	2864	10.68	2733	39.94	2697	33.12
Artesia, NM	1381	0.00	1455	6.67	1440	15.52	1189	30.00
Franklinton, NC	4177	0.00	4295	7.12	4324	8.19	4364	30.38
Richardton, ND	958	0.00	994	6.27	1014	27.01	1077	29.70
O'Donnell, TX	1991	0.00	2111	12.79	2109	13.79	2097	34.59
Mazama, WA	364	0.00	363	10.87	364	11.64	359	33.19

***Note:** Case 1, the baseline, is the R-factor determined using the proration procedure; Case 2 is the R-factor determined using the regression equations for the station's length of record; Case 3 is the same as Case 2 except data were gap filled to extend the record to include all years between 1971 and 1999; Case 4 is the R-factor computed from existing station record with all half-month periods with more than 5 percent missing data, and 25 percent of the valid cases randomly removed gap filled by regression.

data were missing. Gap filling was limited to the period of record of the station. The results show a tendency for the R-factor derived using gap-filled EI data to be 0 to 6 percent larger than the baseline calculation (Table 4). Because 15-minute precipitation values present but flagged were rejected in the baseline calculation method, it is not surprising that these periods correspond to slightly above average rain rates that, when filled by regression with independent precipitation records, result in a slightly larger R-factor.

Case 3 (Table 4) illustrates some interesting properties of the R-factor in regard to the station period of record. In addition to the missing 2-week EI values estimated in Case 2, additional estimates were made for any gaps between January 1971 and the beginning of the station period of record. Including the extra time altered the R-factor considerably for Dauphin Island and Chicago, and both went from a positive difference compared to the baseline in Case 2 to a negative difference of 1-2 percent in Case 3 (Table 4). By adding years from the drier 1970s to the R-factor period of record for these two stations, the result indicates the R-factor may have changed several percent in response to recent climate variations, rather than in response to far more extensive changes since the 1930s. Little change over Case 2 was seen in the other five stations. Richardton, North Dakota, showed the largest increase (2 percent) over Case 2. Both O'Donnell, Texas, and Mazama, Washington, showed no response to the additional data from 1971 to the start of the station records.

While Cases 2 and 3 showed the potential benefit of gap filling with regression methods, Case 4 illustrates the potential weakness of this approach. In this example, the same 25 percent of valid 2-week EI values that were withheld from the regression fitting also were withheld from the R-factor calculation. These periods, and remaining periods exceeding 5 percent missing 15-minute precipitation data, were gap filled with regression-estimated EI values. The resulting R-factors vary widely from the baseline in some cases, with differences ranging from -14 percent to +12 percent (Table 4). While gap filling by regression works reasonably well when stations have a small percentage of missing values, the method breaks down when stations have 25-30 percent missing data. This also confirms that the decision to select stations having less than 25 percent missing data for this project was a good one.

The experiment with gap filling by regression techniques indicated very limited benefit from its widespread application. For instance, the changes between the baseline, Case 1, and Case 2 were quite subtle. Case 2 illustrates the best practice with gap filling, and were all stations of this same high quality, gap filling may have been applicable. Unfortunately, most stations available for this study had a greater percentage of individual half-month EI values derived from periods missing more than 5 percent of their 15-minute precipitation data. Therefore, regression equations would explain lesser proportions of variance and would be less successful than with the stations used here. It was also clear that for the baseline, Case 1, R-factors generated directly from the available data were more conservative, with less likelihood of overinflating R-factor values in comparison to gap filling. The benefit from using regression-based gap filling did not appear to outweigh the potential costs, so it was not used in calculating R-factor values generated by this project.

R-factor Computation from Higher Quality Daily Data

The final approach to account for missing data was based on regression relationships (Richardson et al., 1983) between storm EI values and daily precipitation totals derived from 15-minute precipitation data using the power law approach as illustrated by Equation (5). For this work, EI, the dependent variable in Equation (5), was computed from the 15-minute rainfall data for each day, and P, the independent variable in Equation (5), was the total daily rainfall from the 15-minute rain gauge. Coefficients were computed for each 15-minute station regardless of station record length or missing data. This approach assumes that any missing storms have the same erosivity relationship with total daily precipitation as the available storms.

Regression coefficients relating daily rainfall totals to daily EIs were computed for three different time periods. First, all storm days in each half-month period were used to generate 24 sets of coefficients. Second, all storm days in each season were used to generate four sets of coefficients. Finally, all storm days were used to generate a coefficient set valid for the entire year. Although it would be preferable to use a regression relationship set that had the capability to vary with the annual cycle, this proved to be impractical. In drier regions of the country, it was impossible to compute valid coefficients for the half-month periods and seasons because of the small number of observations. Even in the wetter regions, half-month period and seasonal coefficients were not computed for some periods because missing data resulted in too few observations for computation of valid coefficients. Therefore, in the final analysis, only coefficients based on all storms throughout the year were consistently available, and these were used in the computation of the half-month EIs and the annual R-factor.

Daily data for the period 1971-1999 were used to compute final R-factor values. The choice of a uniform period avoided the spatial inconsistencies caused by the differing periods for 15-minute precipitation data stations. Daily stations used were those collocated with the 15-minute stations or the closest stations to the 15-minute station used to compute the regression equation coefficients. This approach reduced the effect of precipitation heterogeneity on R-factor results. Daily stations associated with the 15-minute stations were identified by computing the distance between the stations using the published station latitudes and longitudes. The R-factor values computed from daily station data were plotted at the location of the daily station. When a single daily station was associated with more than one 15-minute station, the equation associated with the 15-minute station closest to the daily station was used in calculating the R-factor value.

R-factor Computation Results

The R-factor was computed by applying one set of coefficients and Equation (5) for each daily station paired with a 15-minute station to calculate the daily EI values from daily precipitation data. Daily EI values then were summed to obtain both half-month EI totals and annual R-factor values. A limitation to this procedure is the inability to account for multi-day storms. With 15-minute data, it is possible to track storms over consecutive days because the true start and end of a storm can be determined. However, daily rainfall is recorded only once a day, providing a 24-hour total, but not the exact time of the start and end of a storm. The assumption is that all the storms occur during a single 24-hour period, or that multi-day storms are adequately represented by dividing them into one-day storms. A further assumption is that all storms possess storm characteristics that directly related to precipitation total. Storm energy and 30-minute maximum rainfall intensity characteristics are incorporated in the a and b coefficients of Equation (5).

Detailed results of this work, not included in the printed copy of this report, are available in digital form from either the Illinois State Water Survey (ISWS) in Champaign, Illinois, or the Natural Resource Conservation Service-Water and Climate Center (NRCS-WCC) in Portland, Oregon ([ftp.wcc.nrcs.usda.gov/support/climate/rusle/R Calculation/Documentation](ftp:wcc.nrcs.usda.gov/support/climate/rusle/R%20Calculation/Documentation)). The available results include:

1) *A table of the 15-minute stations used in computing the regression equations using Equation (5), and the corresponding daily station associated with the 15-minute station.* The elevation, latitude, and longitude of both the 15-minute and daily stations are given along with the distance in kilometers (km) between stations.

2) *A table of regression coefficients and coefficient of determination (R^2) for the regression equations based on Equation (5) for each 15-minute station.* Storm precipitation totals that exceeded the 100-year storm value were excluded from the regression computation. The intercept value in the table represents the multiplicative constant a in Equation (5), and the slope is the power coefficient, b. The a coefficient was derived from the intercept value and the b coefficient from the slope value in the linearized regression form of Equation (5).

3) *A table of the R-factor for each daily station based on the regression equation from the listed 15-minute station.* Also included in the table are the longitude and latitude of the 15-minute and corresponding daily station, distance between stations, number of years of record for the daily station, percentage of data missing from the daily record, number of rain days included in computing the R-factor, and the size of the 100-year storms for the 15-minute and daily stations.

4) *A table containing the names of the 15-minute and corresponding daily rainfall stations, minimum and maximum R-factor for the period of record, return frequency of an annual R-factor (annual EI value) for 2, 5, 10, and 20 years, and the 50, 20, and 5 percent annual R-factor probability.* The Gumbel distribution was used to compute return frequencies and R-factor probabilities. The 10-year return frequencies used to create the 10-year EI return frequency map were computed using the daily EI values and the L-moments method. Therefore, the 10-year EI return frequencies in the table will differ slightly from those in the 10-year EI return frequency map. The results may be downloaded from the NRCS-WCC ftp site.

Omission of 100-Year Storms

In the final computation, all storms that exceeded the 100-year return frequency were omitted from the database. The old R-factor included all storms with a total storm value greater

than 12.7 mm, including storms with 100-year or greater return periods. The decision to omit storms greater than or equal to a 100-year storm was made in conjunction with project advisors. This decision was based on the fact that many 100-year storms are very localized and result in increased variability of the R-factor across small regions. Furthermore, the R-factor was designed to estimate the erosion losses for a period of approximately 20 years, and erosion prevention structures are designed for a 10-year EI return frequency. The effect of omitting these large storms was introduced into the R-factor at two points. First, 100-year storms were not entered into the computation of the 15-minute EI vs. daily rainfall regression equations. Second, the large storms were omitted when the equations were applied to the daily rainfall data to obtain the storm EI values.

The effect of excluding the 100-year storms from the R-factor computation was examined by generating the R-factor with a) the 15-minute 100-year storm values included in the regression equation and the daily 100-year storm values included in the R-factor computation, b) the 15-minute 100-year storm values included in the regression equation and the daily 100-year storms excluded from the R-factor computation, c) the 15-minute 100-year storms excluded from the regression equation and the daily 100-year storms included in the R-factor computation, and d) both the 15-minute and daily 100-year storms excluded from the computation. A total of 39 stations were examined to determine the effect. These stations were the same ones used in both the current computation and in the work of Wischeimer and Smith (1978).

Comparison of the slope and intercept of the regression equations computed by including and excluding the 100-year storms for the 39 stations revealed that only eight of the 39 stations (21 percent) had equations with a different slope and intercept. The average difference of the slopes was -0.0002. As expected, the equations with 100-year or greater storms included had larger slopes than the equations with large storms excluded. Intercepts were identical out to four decimal points. Differences in the individual slopes were generally less than 3 percent, and differences in the individual intercepts were generally less than 0.5 percent.

The effect of omitting the 100-year or greater storms from daily rainfall records results in a greater difference. However, for the same 39 stations, the average change was a 3 percent increase when the 100-year or greater storms were included in the computation of the R-factor. The maximum difference is a 15.9 percent increase between Alexandria, Minnesota, and Long Prairie, Minnesota. An analysis of all the available stations shows an average increase in the R-factors of approximately 3.3 percent, with the greatest differences in the drier regions of the country where one or more large storms were excluded from the daily record.

This analysis shows that omitting the 100-year or greater storms had a small impact on the R-factor. However, it had the desirable effect of reducing the variability of the R-factor between neighboring stations in the dry western regions of the country.

Uncertainty of R-factor Values

To evaluate the uncertainty associated with R-factor values, local means, standard deviations, and the local coefficients of variation (CVs) were computed for stations within 2 degree longitude by 2 degree latitude (2x2) sliding grids, moved one degree at a time. This resulted in a local mean, standard deviation, and CV being computed for the 2x2 degree area around each whole degree latitude and longitude in the conterminous United States. A map (Figure 6) clearly showed the data-sparse areas in the western part of the country. States with 2x2 grid data voids

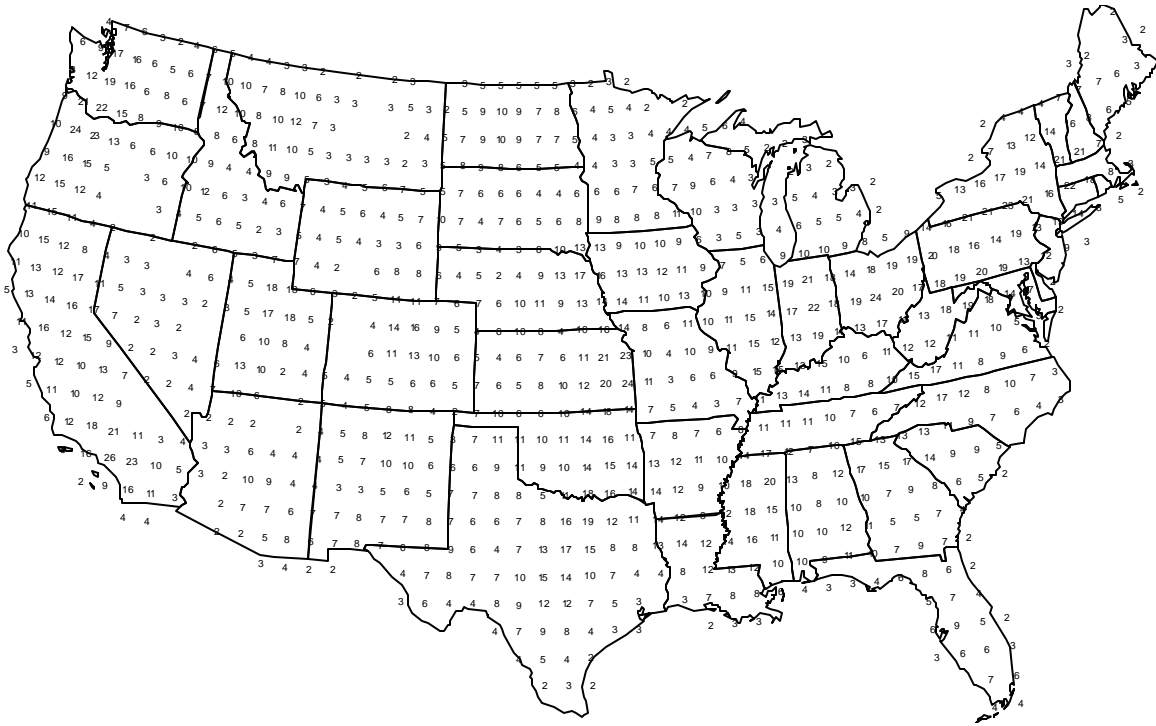


Figure 6. Number of stations in each 2 degree longitude by 2 degree latitude grid cell.

include Arizona, California, Colorado, Montana, Utah, Oregon, and Wyoming. With the exception of Montana, these data voids all occur in the desert regions of the West.

The CV map (Figure 7) showed the greatest local variability in the R-factor occurs in the low rainfall areas and in areas with large topographic variations (i.e., mountain ranges). Most of the country east of the Rocky Mountains showed a CV < 30 percent except for the Appalachian Mountains in North Carolina and Virginia, the Cape Cod region, and south-central Texas. The largest CVs occurred along the Sierra Nevada Mountain Range in California and Oregon where both topographic and precipitation gradients were substantial. The large CV in the Great Basin region was due to low rainfall in the deserts.

Old and New R-factor Value Comparison

Ideally, a comparison of the old and new R-factor maps should be made. This comparison was extremely problematic because the first maps were hand drawn, and files of the R-factor values with latitude and longitude coordinates were not available. Had these files existed, modern mapping software could have been used to compare the different maps. Consequently, only the modern map of the R-factor (Figure 8) was created.

Comparisons of the old and new R-factor values were made using tabular data from Wischmeier and Smith (1978) and R-factor values computed using modern rainfall data (1971-1999). The data and stations used in this comparison (Tables 5-7) were those in common with Wischmeier and Smith's (1978) Table 17. Comparisons between the old and new R-factors were

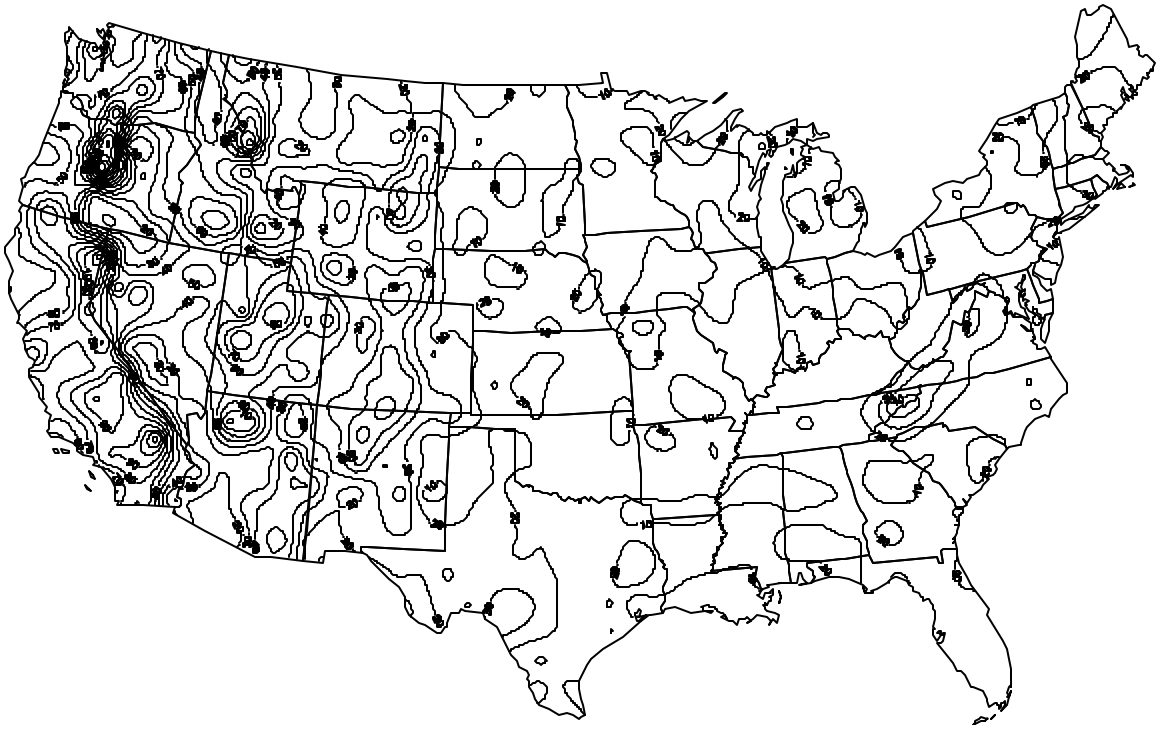


Figure 7. Coefficient of variation of the R-factor computed for each 2 degree longitude by 2 degree latitude grid cell.

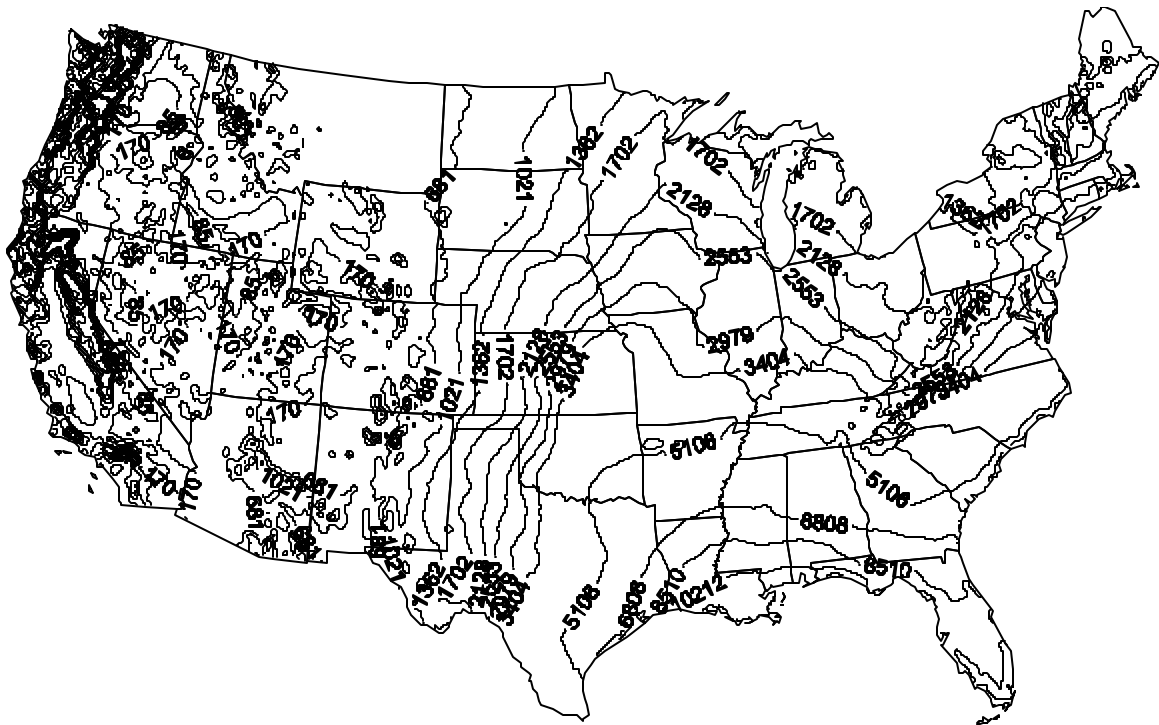


Figure 8. An R-factor map created from 1971-1999 daily data with regression equations developed using 15-minute station data.

Table 5. R-Factor Values (MJ mm ha⁻¹ h⁻¹yr⁻¹) for All Stations Included in the New Computation and in Table 17 of Agriculture Handbook 573 (Stations in Italics Below a Station are Daily Substitutes for 15-Minute Stations)

Station #	Station name	Longitude	Latitude	Elevation (m)	Number of years	Percent missing	R-factor Brown-Foster (-0.72,0.082)
Alabama							
10831	BIRMINGHAM_FAA_ARPT	-86.75	33.57	189	28.9	0.5	5463
California							
47851	SAN_LUIS_OBISPO_POLYTEC	-120.67	35.30	96	27.0	7.1	1430
Colorado							
50109	AKRON_4_E	-103.15	40.15	1284	27.7	4.8	783
Connecticut							
63449	HARTFORD_RESERVOIR_6	-72.73	41.80	113			
69162	WEST_HARTFORD	-72.78	41.75	84	26.8	7.9	3896
Illinois							
111166	CAIRO_3_N	-89.18	37.05	94	26.8	7.8	5055
111577	CHICAGO_MIDWAY_AP_3_SW	-87.77	41.73	189	28.8	0.9	2230
117150	RANTOUL	-88.17	40.32	226	28.2	3.0	3081
Iowa							
137167	ROCKWELL_CITY_2	-94.60	42.40	363	28.6	1.5	2179
137700	SIoux_CENTER_2_SE	-96.15	43.05	415	28.9	0.8	2400
Kansas							
141162	BURLINGAME	-95.83	38.80	311			
140443	AUBURN	-95.82	38.93	357	28.4	2.3	3693
143527	HAYS_1_S	-99.33	38.87	613	28.8	1.1	2025
Kentucky							
155389	MIDDLESBORO	-83.73	36.60	357			
408868	TAZEWELL, TN	-83.55	36.47	416	28.7	1.2	2927
Louisiana							
166664	NEW_ORLEANS_AUDUBON	-90.13	29.92	2	28.9	0.8	12220
Maine							
177827	SKOWHEGAN	-69.72	44.77	50			
174927	MADISON	-69.88	44.80	79	28.8	1.1	1345
Minnesota							
210116	ALEXANDRIA_WTR_TR_PLT	-95.37	45.90	427			
214861	LONG_PRAIRIE	-94.85	45.98	393	28.9	0.5	1396
217907	SPRINGFIELD_1_NW	-94.98	44.25	325	29.0	0.3	1651
Mississippi							
229218	VICKSBURG_WATERWAYS_EXP	-90.87	32.30	55	28.8	1.1	8510
Missouri							
237452	ST_LOUIS_SCIENCE_CTR	-90.20	38.63	165			
111160	CAHOKIE, IL	-90.20	38.57	122	26.4	9.2	2859
Nebraska							
250260	ANTIOCH	-102.58	42.07	1184			
252645	ELLSWORTH	-102.28	42.05	1190	29.0	0.3	766
255040	LYNCH	-98.47	42.83	426	28.7	1.3	1651

Table 5. (Concluded)

Station #	Station name	Longitude	Latitude	Elevation (ft)	Number of years	Percent missing	R-factor Brown-Foster (-0.72,0.082)
Nebraska (cont.)							
257685	SCRIBNER	-96.67	41.67	381			
259200	WEST_POINT_1_W	-96.72	41.83	384	28.9	0.6	2536
New Jersey							
288880	TRENTON_STATE_COLLEGE	-74.78	40.27	30			
284635	LAMBERTVILLE	-74.95	40.37	21	28.6	1.6	2979
New Mexico							
297610	ROSWELL_FAA_ARPT	-104.53	33.30	1112	27.0	7.1	1600
New York							
300049	ALBANY_4_S	-73.73	42.58	4			
309303	WEST_SAND_LAKE_2_S	-73.60	42.62	195	28.8	1.1	1702
307398	SALAMANCA	-78.73	42.17	418			
300093	ALLEGANY_STATE_PARK	-78.75	42.10	457	28.5	2.2	1719
North Carolina							
317079	RALEIGH_NC_STATE_UNIV	-78.70	35.78	122	28.9	0.8	3608
Ohio							
331905	COSHOCTON_AGR_RES_STN	-81.80	40.37	347	28.9	0.7	1991
Oklahoma							
340292	ARDMORE	-97.15	34.20	256	28.6	1.7	5191
345664	MCALESTER_FAA_AIRPORT	-95.78	34.88	232	26.4	9.2	4919
Oregon							
356749	PORTLAND_WB_CITY	-122.68	45.52	48	25.8	11.3	885
Pennsylvania							
363028	FRANKLIN	-79.82	41.38	302	29.0	0.3	2162
367322	READING_4_NNW	-75.93	40.42	110	26.8	8.0	2638
South Carolina							
381770	CLEMSON_COLLEGE	-82.82	34.68	250	29.0	0.2	4085
South Dakota							
394268	ISABEL	-101.43	45.38	732			
398307	TIMBER_LAKE	-101.07	45.43	655	29.0	0.2	936
Tennessee							
405954	MEMPHIS_WSCMO_AP	-90.00	35.05	81	29.0	0.2	7778
Texas							
412244	DALLAS_FAA_AP	-96.85	32.85	134	27.7	4.6	4698
415410	LUBBOCK_9_N	-101.83	33.70	989			
415411	LUBBOCK_WSQ_AIRPORT	-101.82	33.65	992	29.0	0.2	1464
416177	NACOGDOCHES	-94.65	31.62	133	26.2	10.0	6655
West Virginia							
464388	HUNTINGTON_FEDERAL_BLDG	-82.45	38.42	172			
464393	HUNTINGTON_FAA_AIRPORT	-82.55	38.37	252	29.0	0.2	2264

Table 6. Minimum and Maximum Values of R-factor (MJ mm ha⁻¹ h⁻¹yr⁻¹) for the Brown-Foster Equation with Coefficients (-0.72, 0.082) and the Wischmeier-Smith Values in Table 17 in Agricultural Handbook 537 (Stations in Italics Below a Station are Daily Substitutes for 15-Minute Stations)

Station #	Station name	R-factor			
		<i>Brown-Foster</i> (-0.72, 0.082)		<i>Wischmeier-Smith</i> <i>Handbook 537 (1978)</i>	
		Min	Max	Min	Max
Alabama					
10831	BIRMINGHAM_FAA_ARPT	2655	10127	3047	10229
California					
47851	SAN_LUIS_OBISPO_POLYTEC	204	3030	85	2961
Colorado					
50109	AKRON_4_E	289	1481	136	4204
Connecticut					
63449	HARTFORD_RESERVOIR_6			1106	6042
69162	WEST_HARTFORD	1532	6331		
Illinois					
111166	CAIRO_3_N	478	8476	2145	9804
111577	CHICAGO_MIDWAY_AP_3_SW	1464	3812	851	6451
117150	RANTOUL	1140	5378	1242	4868
Iowa					
137167	ROCKWELL_CITY_2	834	2523	681	6655
137700	SIoux_CENTER_2_SE	1004	4289	953	5719
Kansas					
141162	BURLINGAME			970	7608
140443	AUBURN	1583	8612		
143527	HAYS_1_S	443	4817	1123	6348
Kentucky					
155389	MIDDLESBORO			1821	5123
408868	TAZEWELL, TN	1583	4868		
Louisiana					
166664	NEW_ORLEANS_AUDUBON	4817	28645	4646	23249
Maine					
177827	SKOWHEGAN			664	2536
174927	MADISON	596	2417		
Minnesota					
210116	ALEXANDRIA_WTR_TR_PLT			562	5123
214861	LONG-PRAIRIE	477	1906		
217907	SPRINGFIELD_1_NW	511	3234	630	4936
Mississippi					
229218	VICKSBURG_WATERWAYS_EXP	4936	13650	2808	13338
Missouri					
237452	ST_LOUIS_SCIENCE_CTR			1004	12544
111160	CAHOKIE, IL	851	4561		

Table 6. (Concluded)

Station #	Station name	<i>R-factor</i>			
		<i>Brown-Foster (-0.72,0.082)</i>		<i>Wischmeier-Smith Handbook 537 (1978)</i>	
		<i>Min</i>	<i>Max</i>	<i>Min</i>	<i>Max</i>
Nebraska					
250260	ANTIOCH			306	2230
252645	ELLSWORTH	136	1515		
255040	LYNCH	494	3506	579	3693
257685	SCRIBNER			1174	5310
259200	WEST_POINT_1_W	698	5004		
New Jersey					
288880	TRENTON_STATE_COLLEGE			630	6502
284635	LAMBERTVILLE	1055	5378		
New Mexico					
297610	ROSWELL_FAA_ARPT	153	6706	85	2706
New York					
300049	ALBANY_4_S			681	2927
309303	WEST_SAND_LAKE_2_S	851	2791		
307398	SALAMANCA			528	3488
300093	ALLEGANY_STATE_PARK	817	3234		
North Carolina					
317079	RALEIGH_NC_STATE_UNIV	2093	6519	2638	9684
Ohio					
331905	COSHOCTON_AGR_RES_STN	902	3370	1225	7251
Oklahoma					
340292	ARDMORE	2110	10297	1702	11540
345664	MCALISTER_FAA_AIRPORT	1736	9208	1787	12612
Oregon					
356749	PORTLAND_WB_CITY	289	2093	272	1362
Pennsylvania					
363028	FRANKLIN	953	4374	851	3881
367322	READING_4_NNW	1208	4204	1430	5242
South Carolina					
381770	CLEMSON_COLLEGE	2281	5719	2349	10620
South Dakota					
394268	ISABEL			272	2400
398307	TIMBER_LAKE	204	2655		
Tennessee					
405954	MEMPHIS_WSCMO_AP	4357	12867	2366	10127
Texas					
412244	DALLAS_FAA_AP	2281	9378	1583	10723
415410	LUBBOCK_9_N			289	7063
415411	LUBBOCK_WSO_AIRPORT	443	2570		
416177	NACOGDOCHES	2740	12237	2604	13088
West Virginia					
464388	HUNTINGTON_FEDERAL_BLDG			953	3881
464393	HUNTINGTON_FAA_AIRPORT	1481	4085		

Table 7. Values of R-factor (MJ mm ha⁻¹ h⁻¹yr⁻¹) for the 50, 20, and 5 Percent Probability Levels with the Brown-Foster Equation Coefficients (-0.72, 0.082) and the Wischmeier-Smith Values in Table 17 in Agricultural Handbook 537 (Stations in Italics Below a Station are Daily Substitutes for 15-Minute Stations)

Station #	Station name	<i>R-factor</i>					
		<i>Brown-Foster</i>			<i>Wischmeier-Smith</i>		
		<i>(-0.72, 0.082)</i>			<i>Handbook 537 (1978)</i>		
		50	20	5	50	20	5
Alabama							
10831	BIRMINGHAM_FAA_ARPT	5685	7302	9412	6025	7846	10076
California							
47851	SAN_LUIS_OBISPO_POLYTEC	1481	2123	3149	732	1191	1923
Colorado							
50109	AKRON_4_E	732	987	1328	1225	2196	3830
Connecticut							
63449	HARTFORD_RESERVOIR_6				2264	3140	4476
69162	WEST_HARTFORD	3591	4681	6093			
Illinois							
111166	CAIRO_3_N	4919	6502	8561	3932	5940	8816
111577	CHICAGO_MIDWAY_AP_3_SW	2247	2791	3523	2383	3608	5361
117150	RANTOUL	3013	3916	5072	2621	3574	4817
Iowa							
137167	ROCKWELL_CITY_2	2025	2723	3625	2332	3676	5702
137700	SIOUX_CENTER_2_SE	2298	3030	3983	2298	3489	5242
Kansas							
141162	BURLINGAME				2996	4544	6774
140443	AUBURN	3676	4970	6655			
143527	HAYS_1_S	2145	3047	4238	1974	3098	4749
Kentucky							
155389	MIDDLESBORO				2621	2253	4221
408868	TAZEWELL, TN	3030	3812	4834			
Louisiana							
166664	NEW_ORLEANS_AUDUBON	12578	17463	23811	12271	17139	23556
Maine							
177827	SKOWHEGAN				1328	1838	2519
174927	MADISON	1427	1838	2366			
Minnesota							
210116	ALEXANDRIA_WTR_TR_PLT				1498	2502	4085
214861	LONG_PRAIRIE	1158	1515	1974			
217907	SPRINGFIELD_1_NW	1736	2349	3166	1634	2621	4136
Mississippi							
229218	VICKSBURG_WATERWAYS_EXP	8646	10757	13480	6212	8391	11199
Missouri							
237452	ST_LOUIS_SCIENCE_CTR				2859	4936	8306
111160	CAHOKIE, IL	2774	3625	4715			

Table 7. (Concluded)

Station #	Station name	<i>R-factor</i>					
		<i>Brown-Foster</i> <i>(-0.72,0.082)</i>			<i>Wischmeier-Smith</i> <i>Handbook 537 (1978)</i>		
		50	20	5	50	20	5
Nebraska							
250260	ANTIOCH				1021	1434	2042
252645	ELLSWORTH	749	1072	1498			
255040	LYNCH	1685	2315	3132	1634	2417	3489
257685	SCRIBNER				2621	3489	4578
259200	WEST_POINT_1_W	2536	3506	4749			
New Jersey							
288880	TRENTON_STATE_COLLEGE				2536	3676	5242
284635	LAMBERTVILLE	3064	3898	4987			
New Mexico							
297610	ROSWELL_FAA_ARPT	1523	2876	4578	698	1242	2179
New York							
300049	ALBANY_4_S				1379	1940	2706
309303	WEST_SAND_LAKE_2_S	1753	2196	2757			
307398	SALAMANCA				1191	1804	2672
300093	ALLEGANY_STATE_PARK	1770	2281	2944			
North Carolina							
317079	RALEIGH_NC_STATE_UNIV	3693	4629	5855	4766	6451	8612
Ohio							
331905	COSHOCTON_AGR_RES_STN	2042	2604	3336	2689	3400	5838
Oklahoma							
340292	ARDMORE	5310	7370	10025	4476	6723	9906
345664	MCALESTER_FAA_AIRPORT	4919	6417	8357	4629	6995	10365
Oregon							
356749	PORTLAND_WB_CITY	936	1259	1685	681	953	1311
Pennsylvania							
363028	FRANKLIN	2179	2893	3830	1651	2298	3132
367322	READING_4_NNW	2689	3370	4255	2451	3472	4851
South Carolina							
381770	CLEMSON_COLLEGE	4238	5038	6059	4766	6536	8833
South Dakota							
394268	ISABEL				817	1328	2128
398307	TIMBER_LAKE	970	1413	2008			
Tennessee							
405954	MEMPHIS_WSCMO_AP	8153	10110	12663	4629	6536	9123
Texas							
412244	DALLAS_FAA_AP	4936	6706	9004	4476	6740	9974
415410	LUBBOCK_9_N				1396	2689	6021
415411	LUBBOCK_WSO_AIRPORT	1430	1957	2638			
416177	NACOGDOCHES	6774	9038	11982	6825	9718	13633
West Virginia							
464388	HUNTINGTON_FEDERAL_BLDG				2162	2944	3966
464393	HUNTINGTON_FAA_AIRPORT	2383	2910	3591			

made using the R-factor computed from the daily station record and the corresponding 15-minute regression equation. Table 5 lists the stations with latitude and longitude coordinates, elevation in feet, number of years of daily data, percent of daily missing data, and R-factor values calculated in this study. Where the 15-minute and daily rain gauge stations were collocated, only one line was used to describe the modern station location. Where the daily rain gauge station was separate from the 15-minute station, the location of the daily station, its elevation, number of years of daily data, missing data information, and R-factor are provided in italics immediately below the 15-minute station information.

A total of 39 stations corresponded to the 181 stations included in the appendices of Wischmeier and Smith (1978). Four stations are located in the western states of California, Colorado, New Mexico, and Oregon. The remaining 35 stations were spread throughout the eastern United States with 19 stations located above 40° north latitude.

Computations of the R-factor values used 1971-1999 data. The total length of record for individual stations ranged from 25.8 to 29 years. Within the record length of each station, the percentage of missing or invalid data was determined. For these 39 stations, 0.2 to 11.3 percent of data were missing. Only the new R-factor was available for the 39 stations (Table 5) as number values for the R-factor were not given in Agricultural Handbook 537.

Minimum and maximum yearly R-factors (Table 5) computed using daily station data were compared to those from Table 17 (Wischmeier and Smith, 1978). New R-factor minimums for the 39 stations averaged 15 percent greater than old R-factor minimums. Differences ranged from as much as 140 percent greater in California to 78 percent less at Cairo, Illinois. Minimums for only two stations (McAlester, Oklahoma, and Clemson, South Carolina) were less than 5 percent.

New R-factor maximums (Table 6) averaged 18 percent less than the old R-factor maximums with a range of 77 percent less (Nacogdoches, Texas) to 55 percent more (Portland, Oregon). Five stations had new R-factor maximum differences of less than 5 percent than old R-factor maximums. These stations were Hartford, Connecticut; Middlesboro, Tennessee; Skowhegan, Maine; Vicksburg, Mississippi; and Albany, New York. It is interesting to note that, with the exception of Vicksburg, Mississippi, daily rain gauges of all stations with less than 5 percent differences were located at a nearby station.

Table 7 presents the 50, 20, and 5 percent probability annual R-factor values computed from daily station data. Where the daily station was not collocated with the 15-minute station, the daily station data are located on the line immediately below the 15-minute station. The median (50 percent probability) of the new R-factor values averaged 15 percent greater than the old R-factor median, similar to the minimum R-factor differences. The new R-factor median differences ranged from 40 percent less than the old (San Louis Obispo, California) to 127 percent greater (Roswell, New Mexico). Twelve stations had new medians less than the old median, and one median (Sioux Center, Iowa) was the same. The mean difference in size of the 20 percent probability R-factor value was only 4 percent. The new 20 percent probability values ranged from 55 percent less than the old (Akron, Colorado) to 132 percent greater (Roswell, New Mexico). The new mean 5 percent probability R-factor value was 5 percent less than the old, and ranged from 65 percent less than the new (Akron, Colorado) to 110 percent greater (Roswell, New Mexico).

Changes in Precipitation Climatology Since Previous R-factor Studies

Comparison of the R-factor derived in this project to Agricultural Handbook 537 (Wischmeier and Smith, 1978) indicated a potential change in the precipitation regime. Thus, storm characteristics may have changed over time, which can have significant impacts on hydrological processes such as streamflow and soil erosion. Karl and Knight (1998) found that precipitation has increased by about 10 percent across the conterminous United States, and that these changes appear to be due to an increase in the frequency and amount of heavier precipitation events. Kunkel et al. (1999) confirmed this trend, especially in the Midwest, for precipitation events of 7-day duration that exceeded the 1-year recurrence interval for 1931-1996. Therefore, it should not be surprising to find changes in the R-factor over time.

Wischmeier (1962) described the original calculations for the R-factor for the eastern two-thirds of the United States. Detailed 22-year (1936-1957) storm-intensity records were obtained from 16 USDA and 165 United States Weather Bureau sites. The R-factor then was computed for each of these 181 sites. To provide more spatial detail, Wischmeier developed regression equations based on the three-factor product of average annual rainfall times the 2-year, 1-hour intensity times the 2-year, 24-hour intensity. These factors were used because they were widely available from other United States Weather Bureau publications (1957, 1958, 1959a, 1959b, 1960). These regression equations were applied to 1,700 additional sites. The fit was better than 90 percent in all regions although the original R-factor calculations relied on 1936-1957 data, and the factors in the regression equations relied on data from approximately the same period. As a result, comparisons were made between the 1936-1957 period and the 1971-1999 period of this study.

Istok (1989) computed the R-factor for the remaining western third of the United States. Using 12 years of 15-minute data (1971-1983), he developed regression relationships between the EI calculated from 15-minute interval precipitation data and the more common 60-minute interval data. Once the relationships were in place, he calculated the R-factor based on hourly precipitation data for the period 1948-1983. Therefore, a second set of comparisons was made between the 1948-1983 period and the 1971-1999 period of this study.

To determine regions with potential changes in the R-factor, annual precipitation by climate division was obtained from the NCDC for 1895-1999. Climate divisions divide each state into sub-regions of approximately similar climate because a particular state may span several climate zones (e.g., California). Typically, states have between two and ten climate divisions. Digital records of hourly or 15-minute precipitation were not available for most of the earlier time period; therefore, annual precipitation behavior was used as a proxy for the R-factor. This approach assumes that changes in the annual precipitation also would be reflected in the annual R-factor.

Climate division data were examined for 1936-1957 and 1971-1999 (the period covering the current study). A map showing the ratio of the annual average precipitation for 1971-1999 divided by that for 1936-1957 is shown (Figure 9). Average annual precipitation increased by 5 percent or more in the central and southwestern United States. Although not as widespread nor as strong, evidence of increases also can be found in portions of the southeastern and northeastern United States. Small areas of decreased annual precipitation between periods were found in Wyoming, Oregon, and Washington. Table 8 shows the area covered by increases and decreases of 5 percent or more in annual and seasonal precipitation. For annual precipitation, 58 percent of

the United States showed a 5 percent increase in amounts while only 2 percent showed a 5 percent decrease over time. The fall increases are especially important, given their widespread coverage (85 percent).

An examination of the time series of individual climate divisions suggests that the primary factor for the large increases in the Southwest was the dry decade of the 1950s. Discussions with the former state climatologist for New Mexico (Ken Kunkel, personal communication, 2001) confirmed that the 1950s were the driest decade on record for that region. Figure 10 shows the 1895-1999 annual precipitation in the Trans Pecos region of Texas, near the center of some of the largest increases in precipitation and R-factor between the two study periods. The reduced amounts of precipitation through the late 1950s clearly can be seen. Precipitation amounts were consistently higher throughout 1971-1999. This pattern was typical throughout the Southwest.

Increases in the central United States were due to extended dry periods in the 1930s and 1950s in combination with increasingly wet conditions in the 1970s, 1980s, and 1990s. Figure 11 illustrates this for the south-central climate division of Iowa, the center of maximum increases in the Midwest. This pattern is fairly typical throughout the central United States.

Continuing with the comparison of the 1936-1957 period to the current study period, changes in seasonal precipitation were typically consistent with annual precipitation, but with more spatial variability. In winter (Figure 12), large increases were found in the Southwest and along the Gulf and Atlantic coasts, while large portions of the interior United States showed decreases over time. Of the annual and seasonal precipitation maps, winter showed the smallest area (31 percent) of increased precipitation. However, in most of the United States warm season precipitation is the key contributor to the R-factor. In spring (Figure 12), increases were found in the western third of the United States, the Great Plains, and the interior Southeast. Areas of decrease were east of the Rockies, in the Great Lakes region, and in Georgia. In summer (Figure

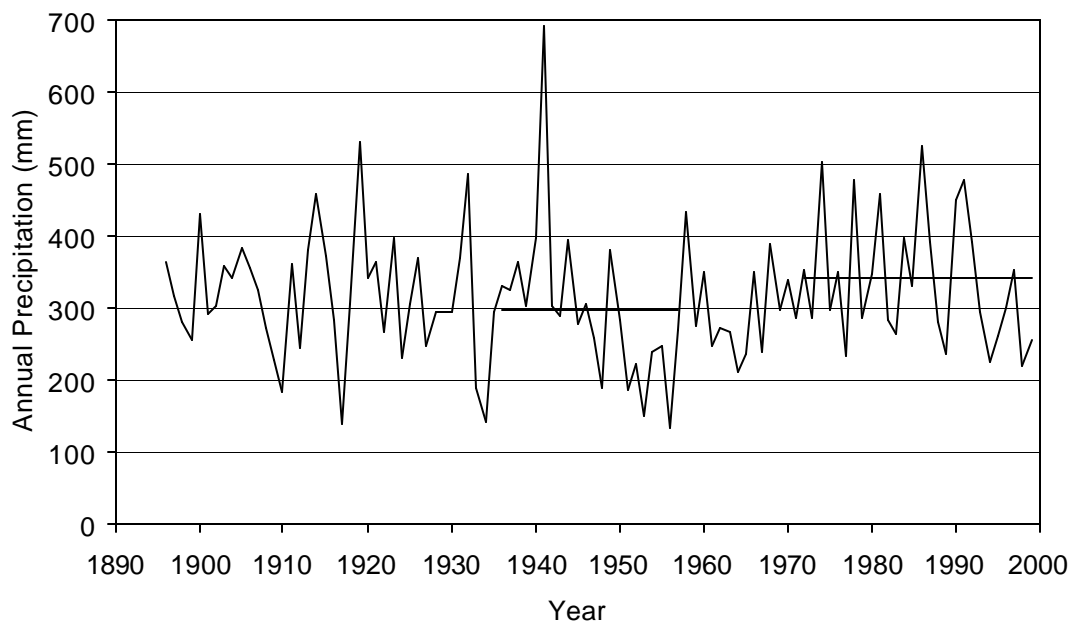


Figure 10. Annual precipitation (mm) for the Trans Pecos region of western Texas. Darker line segments represent average precipitation amounts for 1936-1957 and 1971-1999, respectively.

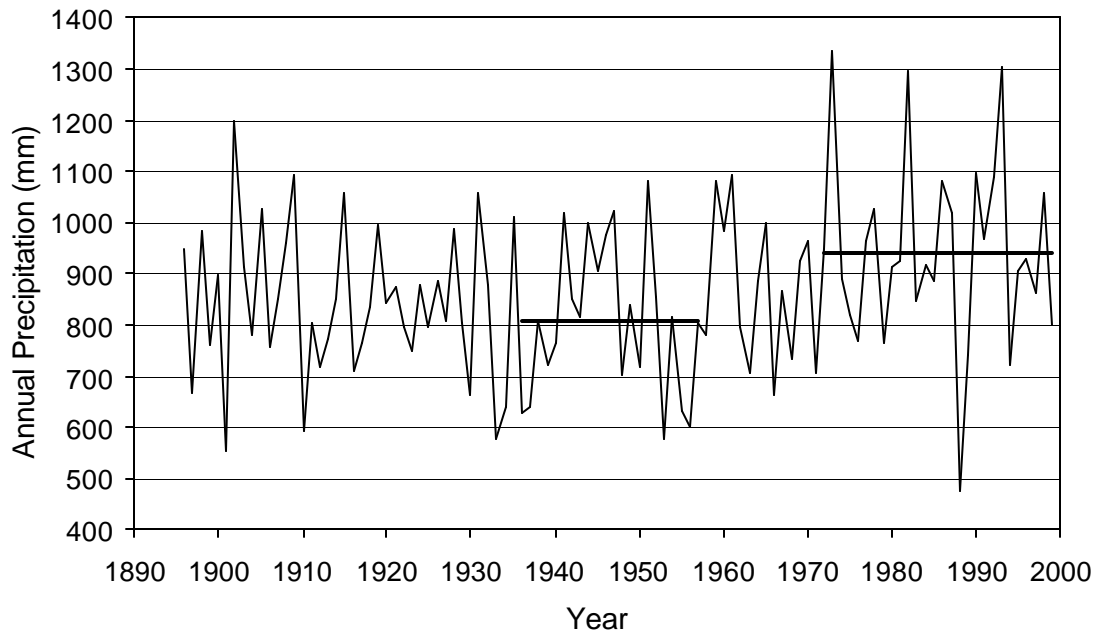


Figure 11. Annual precipitation (mm) for the south-central region of Iowa. Darker line segments represent average precipitation amounts for 1936-1957 and 1971-1999, respectively.

12), large increases were found in the western United States, the lower Plains states, and in a band from the eastern Midwest to the Northeast. Decreases in summer rainfall were seen in the southeastern United States and in a band from Arizona to Montana and North Dakota. Increased precipitation dominated the pattern for fall (Figure 12), with 85 percent of the United States showing an increase. Only Florida and the Northwest showed declines.

Comparisons between the 1948-1983 time period used by Istok (1989) and the 1971-1999 period used for this study showed that the annual precipitation (Figure 13) increase occurred in the western and central United States and in a band from Michigan to Massachusetts. Most of this pattern was probably a result of the relatively wet 1990s. Forty-eight percent of the United States showed an increase in precipitation of 5 percent or more (Table 8). In winter (Figure 13), this increase was much more pronounced in the Southwest and Gulf states, while decreases occurred in the Northwest and North-Central United States. In spring (Figure 13), the area of increased precipitation expanded from the Southwest into the Northwest and the western half of the Midwest. The Gulf states showed smaller increases, the Georgia-South Carolina region showed a substantial decrease, and the northern half of the Atlantic Coast showed increases. The pattern in summer (Figure 13) had the fewest areas of increased rainfall of the four seasons. Some increases can be seen along the Pacific Coast, the Texas-New Mexico-Colorado region, and the Great Lakes/New England region. In fall (Figure 13), 77 percent of the United States had an increase of precipitation of 5 percent or more between the two periods. Overall, there is a sound basis in the precipitation record for an expected increase in the R-factor in most areas of the country, especially in the Southwest.

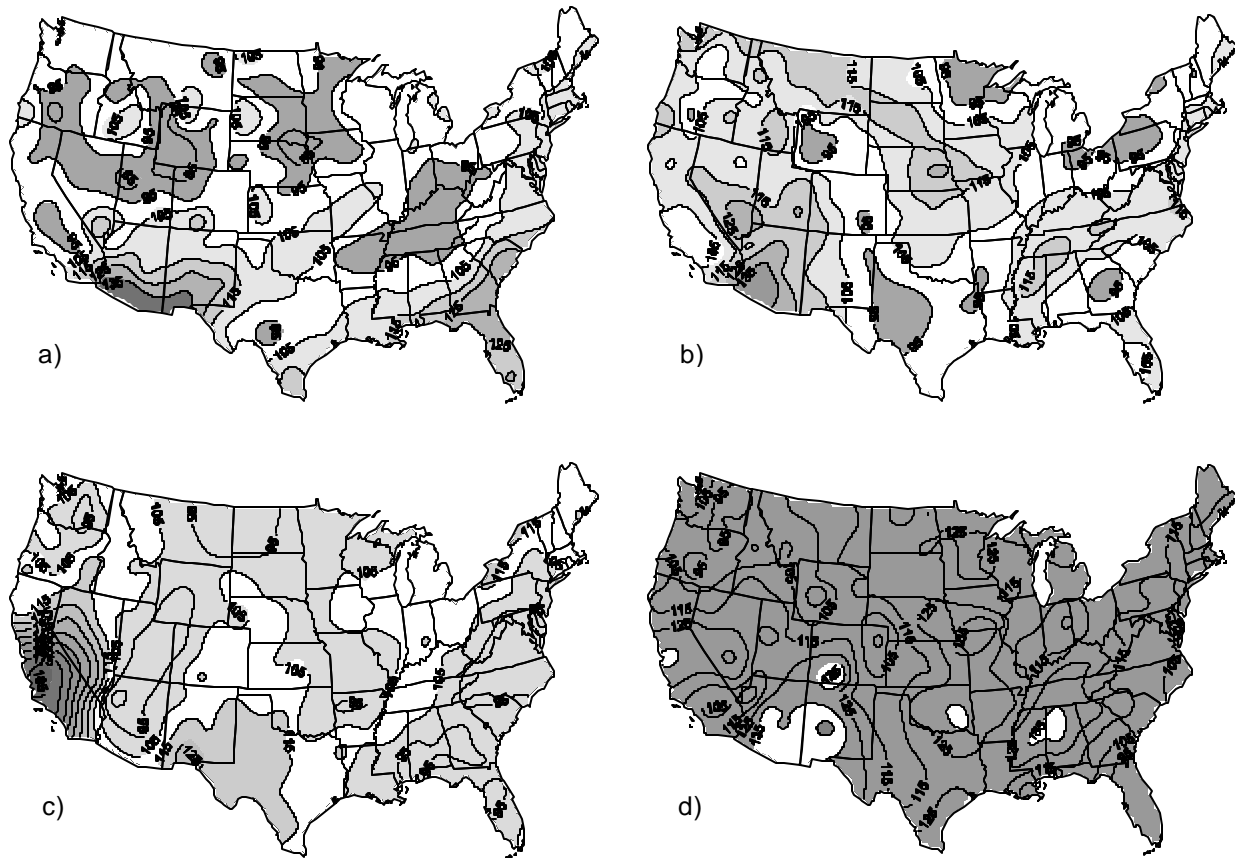


Figure 12. Ratio of climate division average a) winter, b) spring, c) summer, and d) fall precipitation for 1971-1999/1936-1957, expressed as a percentage. Values above 100 percent indicate an increase in precipitation over time.

Comparison of 1936-1957, 1971-1999, and Wischmeier and Smith Data

The original data used by Wischmeier and Smith (1978) were not available for comparison with the current data. However, daily rainfall data for 19 stations were available (Table 9) for 1936-1957. These data and the 15-minute/daily regression equations, developed from the 1971-1999 data using the Brown-Foster equation with coefficients of -0.72 and 0.082, were used to compute an R-factor for the 1936-1957 period. Using the regression equations developed from the 1971-1999 data and applying them to the 1936-1957 data makes use of the underlying assumptions that the structure and erosivity characteristics of the storms in the two periods are temporally stationary, and that the two procedures used are similar.

The 1936-1957 R-factors computed from the daily data are generally smaller than both the modern R-factor (1971-1999) and the Wischmeier and Smith R-factor (Table 9). The average median R-factor for the 19 stations was 4 percent less than the Wischmeier and Smith values, and 12 percent smaller than the modern R-factor calculated from the 1971-1999 data.

Three comparisons were made with the median R-factor values from the 19 sites with digital daily precipitation records dating back to the earlier study period. The first comparison

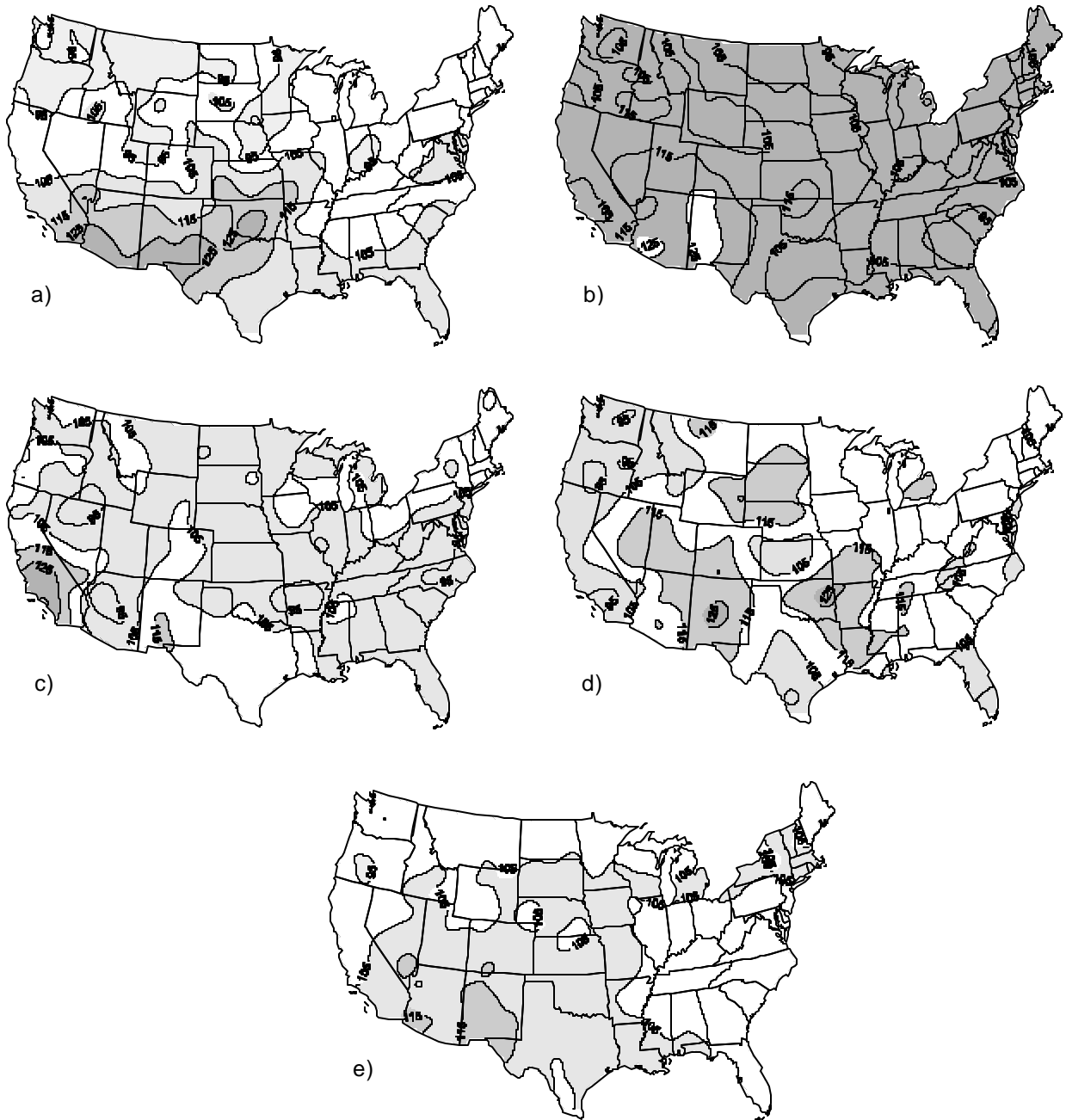


Figure 13. Ratio of climate division average a) winter, b) spring, c) summer, and d) fall, and e) annual precipitation for 1971-1999/1948-1983, expressed as a percentage. Values above 100 percent indicate an increase in precipitation over time.

Table 9. Minimum, Maximum, and Median Values of Erosion Index (EI, MJ mm ha⁻¹ h⁻¹ yr⁻¹) for the Brown-Foster Equation Coefficients (-0.72, 0.082) for 1971-1999 Data, the Brown-Foster Equation for 1936-1957 Data, and the Wischmeier-Smith Values in Table 17 in Agricultural Handbook 537 (Stations in Italics Below a Station are Daily Substitutes for 15-Minute Stations)

Station #	Station name	<i>R-factor</i>									
		<i>Brown-Foster 1971-1999</i>			<i>Brown-Foster 1936-1957</i>			<i>Wischmeier-Smith Handbook 537</i>			
		<i>(-0.72,0.082)</i>	<i>(-0.72,0.082)</i>	<i>(-0.72,0.082)</i>	<i>(-0.72,0.082)</i>	<i>(-0.72,0.082)</i>	<i>(-0.72,0.082)</i>	<i>(-0.72,0.082)</i>	<i>(-0.72,0.082)</i>	<i>(-0.72,0.082)</i>	
		Min	Max	Median	Min	Max	Median	Min	Max	Median	
Alabama											
10831	BIRMINGHAM_FAA_ARPT	2655	10127	5685	3013	7285	5242	3047	10229	6025	
California											
47851	SAN_LUIS_OBISPO_POLYTEC	204	3030	1481	153	2519	1294	85	2502	732	
Illinois											
111166	CAIRO_3_N	477	8476	4919	2110	9974	4919	2145	9804	3932	
111577	CHICAGO_MIDWAY_AP_3_SW	1464	3812	2247	562	3761	1549	851	6451	2383	
Kansas											
143527	HAYS_1_S	443	4817	2145	374	5668	1957	1123	6348	1974	
Kentucky											
155389	MIDDLESBORO				221	4442	2774	1821	5123	2621	
408868	TAZEWELL, TN	1583	4868	2774							
Maine											
177827	SKOWHEGAN				579	2434	1311	664	2536	1328	
174927	MADISON	596	2417	1311							
Minnesota											
210116	ALEXANDRIA_WTR_TR_PLT				460	2536	1225	562	5123	1498	
214861	LONG-PRAIRIE	477	1906	1157							
217907	SPRINGFIELD_1_NW	511	3234	1736	528	2927	1396	630	4936	1634	
Nebraska											
255040	LYNCH	204	3506	1685	408	2570	1430	579	3693	1634	
257685	SCRIBNER				357	3131	1566	1174	5310	2621	
259200	WEST_POINT_1_W	698	5004	2536							
New Jersey											
288880	TRENTON_STATE_COLLEGE				919	3812	2485	630	6502	2536	
284635	LAMBERTVILLE	1055	5378	3064							
New York											
307398	SALAMANCA				851	3030	1770	538	3438	1191	
300093	ALLEGANY_STATE_PARK	817	3234	1770							
North Carolina											
317079	RALEIGH_NC_STATE_UNIV	2093	6519	3693	2230	5617	3847	2638	9684	4766	
Oklahoma											
340292	ARDMORE	2110	10297	5310	323	9616	5072	1702	11540	4476	
Pennsylvania											
363028	FRANKLIN	953	4374	2179	1140	3285	1787	851	3881	1651	
South Carolina											
381770	CLEMSON_COLLEGE	2281	5719	4238	2213	6110	3795	2349	10620	4766	

Table 9 (Concluded)

Station #	Station name	<i>R-factor</i>								
		<i>Brown-Foster 1971-1999</i>			<i>Brown-Foster 1936-1957</i>			<i>Wischmeier-Smith</i>		
		<i>(-0.72,0.082)</i>			<i>(-0.72,0.082)</i>			<i>Handbook 537</i>		
		<i>Min</i>	<i>Max</i>	<i>Median</i>	<i>Min</i>	<i>Max</i>	<i>Median</i>	<i>Min</i>	<i>Max</i>	<i>Median</i>
South Dakota										
394268	ISABEL				119	1668	902	272	2400	817
398307	TIMBER_LAKE	204	2655	2008						
Texas										
415410	LUBBOCK_9_N				357	6517	1889	289	7063	1396
415411	LUBBOCK_WSO_AIRPORT	443	2570	2383						
	Average	1021	4834	2672	885	4578	2434	1157	6161	2502

featured the use of the modern regression equations to calculate the daily EI from the daily precipitation. Daily data for the period of this report (1971-1999) were contrasted with daily data from the earlier Wischmeier-Smith study period (1936-1957). Such a comparison, with a constant technique, would identify differences in the R-factor caused by significant changes in the precipitation regime between the two periods for the 19 sites. Figure 14 shows a near one-to-one relationship between R-factors of the two periods with 94 percent of the variance explained. Although the slope was less than one, the large y-intercept assures that R-factors in the later period were generally larger. The increase in the R-factor in the later period was due to a precipitation regime change as the calculation method was constant. The R-factor at 13 stations was greater in 1971-1999 than in 1936-1957, smaller at 2 stations in 1971-1999, and unchanged at 4 stations. The slope of less than one indicates that small R-factor values increased more than the larger R-factors, which resulted in drier regions with relatively greater increases in precipitation during the latter period or increased sensitivity to increases in precipitation that caused more storms to reach the 12.7 mm threshold.

The second comparison was between R-factor values of the original Wischmeier-Smith study and those from the application of modern regression equations to the 1936-1957 daily data. This comparison identified differences in the R-factor caused by significant changes in the technique used during a constant time period. In this comparison, the one-to-one relationship was extremely strong (Figure 15), and the y-intercept was small. This further confirmed that technique changes were not an issue, and precipitation changes largely were responsible for the shift in R-factor between periods.

Possible Nonclimate Causes for Differences between R-factors

It is impossible to know all the reasons for differences between Wischmeier and Smith R-factors and those calculated for 1971-1999 because there is no way to replicate the development of the Wischmeier-Smith R-factors. In addition to the more obvious effects of climate variability on rainfall intensity and amounts at a given station as described above, other factors may cause significant differences between the old and new R-factors. For example, it was not uncommon to mount rain gauges on roofs of buildings during the earlier time frame used for the old R-factor calculation. It is now known that rain gauges mounted high aboveground result in the

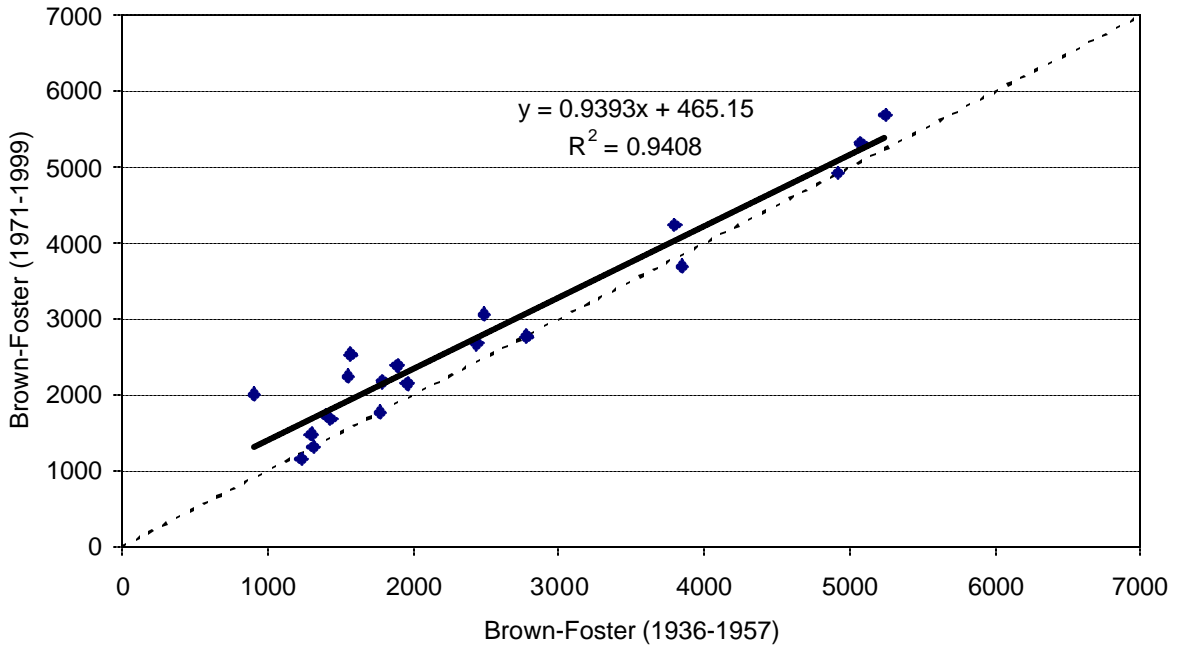


Figure 14. Relationship between R-factor calculated using the Brown-Foster equation and the 1971-1999 and 1936-1957 daily precipitation data. Dotted line indicates the 1:1 relationship.

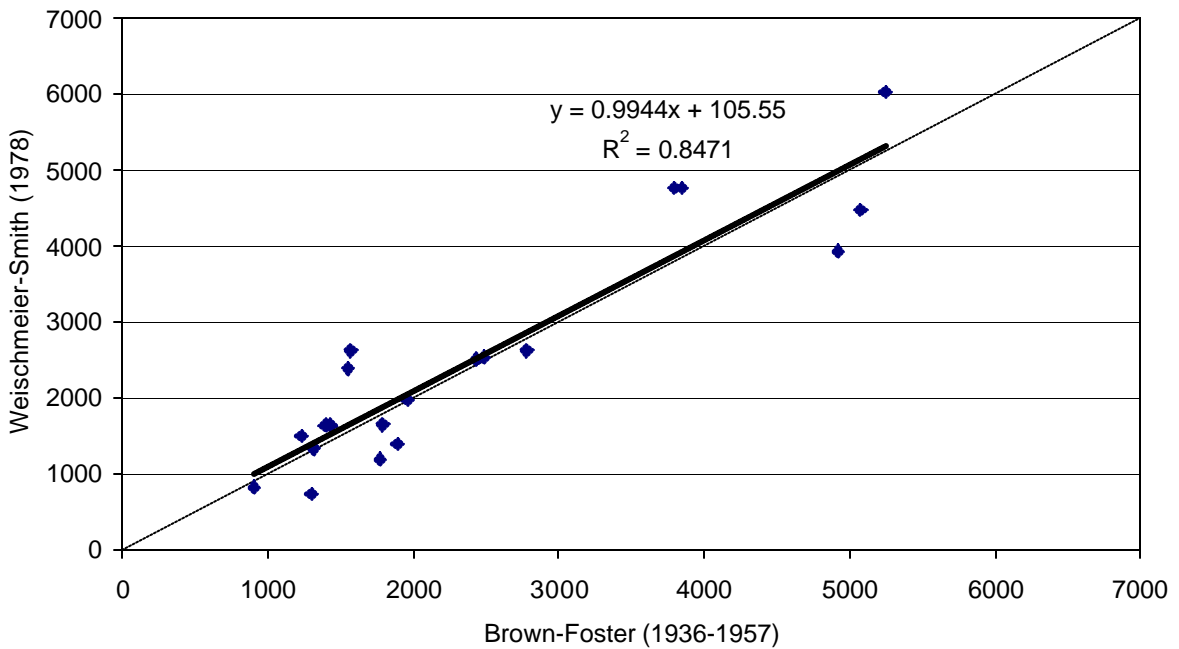


Figure 15. Relationship between R-factor computed from 1936-1957 data by Wischmeier and Smith and the Brown-Foster equation and daily regression equations. Dotted line indicates the 1:1 relationship.

undercatchment of rainfall. If early data at a particular station were collected by a rain gauge mounted on top of a building and the new data were collected by a rain gauge with the opening 1 meter (m) aboveground, the new data will show a larger catch of rain, resulting in a larger R-factor. Rainfall recorded by a rain gauge sheltered by vegetation or a building will be less than from a similar gauge without the shelter effects. In some cases where vegetation may provide a dripline over the rain gauge, the catch will be greater than from a gauge without the dripline.

Another cause of the differences may be that the original station was moved from its earlier location to a nearby location. Because documentation is unavailable on the location of the old stations, there is no guarantee that the new station is the same as the old station, and there is no way to determine the distance between the new station and the old station with the same name. Some station moves are the result of urban sprawl. For example, new stations are located at airports rather than at the original 1936-1957 location.

Although the differences in the Wischmeier-Smith and the Brown-Foster equations appear to be small, changing the equation used introduced some differences in R-factor values. With rainfall intensities from 17 to 60 mm hr⁻¹, use of the Brown-Foster equation and its coefficients (0.72, 0.082) resulted in R-factors and erosivities 5 percent greater than from the Wischmeier-Smith equation (Figure 2). With rainfall intensities less than 9 mm hr⁻¹, the Brown-Foster equation resulted in erosivities 5 percent lower than the Wischmeier-Smith equation.

The resolution of the 15-minute rain gauges is 2.54 mm; thus, the smallest rainfall intensity that can be measured is 10.2 mm hr⁻¹. Rain gauge limitations had no effect on the computed erosivity values as all nonqualifying storms were deleted.

The greatest differences in the erosivity values occur in the 17.8 and 61.0 mm hr⁻¹ rainfall intensities. In this range, the deviations exceed 5 percent but are less than 10 percent (Figure 2). However, this range covers the majority of rainfall intensities observed in the data. As a result, storm erosivities and R-factors using the Brown-Foster equation may be greater, under the same rainfall regime, than those computed with the Wischmeier-Smith equation using the same data.

10-Year Return Interval EI Levels

The 10-year return interval single-storm EI levels are used in the RUSLE equation component accounting for erosion control practices (P-factor). These EI levels were computed for the 1,409 15-minute stations with 18 years or more data and less than 25 percent data missing. For each site, time series of the highest single-storm EI value for each year of record were constructed. The L-moments fitting technique and the Generalized Extreme Value (GEV) distribution then were used to determine the single-storm EI at the 10-year return period. The L-moments software uses linear combinations of rank-order statistics to fit the particular distributions to the data. The advantage of L-moments, in particular, and rank-order statistics, in general, is a general robustness from outliers. More information on L-moments can be found in Hosking (1990, 1991), and Hosking and Wallis (1991). In addition to the 10-year single-storm EI values, the estimates of the three parameters of the GEV distribution (location, shape, and skewness) are available for calculating the single-storm EI at other return periods.

The 10-year single-storm EI (Figure 16), shown in units of MJ mm ha⁻¹ h⁻¹, results in a pattern that is generally similar to the R-factor map (Figure 8). Highest values of the single-storm EI are found along the Gulf Coast and the southern half of the East Coast. However, unlike the general R-factor pattern, the ridge of relatively high values extending north from the Gulf breaks down in Missouri, Iowa, and Illinois. In addition, the values in the Appalachians drop more



Figure 16. Value of erosivity index for a single-storm 10-year return frequency ($\text{MJ mm ha}^{-1} \text{hr}^{-1}$).

rapidly relative to surrounding areas than they do for the R-factor. Finally, the pattern from the Rocky Mountains westward is much flatter than the pattern for the R-factor. Even local gradients along the West Coast are weaker than for the R-factor. One explanation for the differences is that the R-factor pattern is built on the cumulative effect of many storms, while Figure 16 was constructed from larger and rarer events. Although many of the basic precipitation controls (orography, moisture sources, etc.) operate in both cases, and therefore lead to the same general pattern, the 10-year single-storm EI may be more heavily influenced by smaller scale features, such as tropical storms or meso-scale convective systems.

A comparison of the new map with the maps in Agricultural Handbook No. 703 (Renard et al., 1997) shows that the new map portrays a more coherent and physically plausible pattern in the eastern two-thirds of the United States (Renard et al., 1997, Figure 2-9). In general, the 10-year single-storm EI values are now higher along the Gulf Coast and lower along the East Coast from Florida to Chesapeake Bay. The numbers are generally comparable between the old and new studies for the rest of the northeastern United States. Due to the unorthodox contouring in the Renard et al. (1997) figure, it is hard to make comparisons in the central portion of the United States. New values for the western states are in general agreement with the old values in Figure 2-10 (Renard et al., 1997). However, the new numbers are lower in eastern Colorado and southern Arizona. Many of the very high local single-storm EI values in their figure are not evident in the new map. Of course, features at this scale usually are supported only by a single station and are hard to verify by independent means. The same general relationship with the new map persists in Figure 2-11 and Figure 2-12 (Renard et al., 1997) for California, Oregon, and Washington, with fewer local maxima in the new map.

Geographical Distribution and Temporal Variability of Storm Characteristics

The 15-minute precipitation data were used to evaluate the temporal precipitation structure of individual storms. The set of 1,409 stations chosen had a record longer than 18 years with less than 25 percent data missing. A storm was defined as any period of precipitation separated from preceding and succeeding precipitation by 6 hours (Huff, 1967). Separate statistics also were developed for R-factor-eligible storms with precipitation totals greater than 12.7 mm or a maximum intensity greater than 25.4 mm hr⁻¹ (Wischmeier and Smith, 1978). Each station was evaluated independently from neighboring stations. Storm characteristics included: 1) storm total precipitation, 2) storm duration, 3) storm precipitation intensity, 4) storm precipitation kinetic energy (E), 5) storm maximum 30-minute precipitation intensity (I_{30}), 6) total storm erosivity (EI_{30}), 7) storm maximum 15-minute precipitation intensity, 8) ratio of maximum 15-minute intensity to whole-storm intensity, and 9) maximum shower precipitation where a shower was defined as a continuous precipitation period during a storm. The total number of storms and the number of R-factor eligible storms also were examined.

Mean storm characteristics were computed using all storms at each 15-minute precipitation station of high quality. Storm characteristic descriptions are presented for all storms in each season and for the entire year, and for just those storms with rainfall greater than 12.7 mm or a 15-minute rainfall intensity greater than 24 mm hr⁻¹ for each of the four seasons and for the entire year. The seasons were divided into climatological winter (December – February), spring (March – May), summer (June – August), and fall (September – November).

Seasonal Variations

Seasonal cycles of storm characteristics were examined by mapping seasonal mean values of the variables. The general patterns of these maps were examined with respect to potential mechanisms for seasonal variations.

Storm Total Precipitation

Mean storm total precipitation ranges from more than 16 mm to less than 5 mm when averaged over all storms throughout the year (Figure 17). Lower totals occurred in the Great Basin, and larger totals occurred along the Gulf of Mexico. During the winter, the largest storms occur in the southeast and along the East and West coasts. Minnesota, and Great Basin, Rocky Mountain, and Northern Great Plains states all showed winter mean storm total precipitation less than 5 mm. This was due to the reduced capacity of the atmosphere to sustain water vapor pressure at cold temperatures. Spring and fall showed similar mean storm total precipitation patterns. There was a stronger gradient of storm total precipitation across Texas, Oklahoma, and Kansas during the fall than during the spring. This steeper gradient continued southeasterly across Missouri, southern Illinois, Kentucky, and Tennessee, and then proceeded along the axis of the Appalachian Mountains into Maine. A steep gradient across Pacific Coast states occurred in winter, spring, and fall. Two strong gradients with a south-southwest to north-northeast axis orientation existed along the Atlantic Coast and High Plains states during the summer. Summer storm total precipitation (< 9 mm) was low in both the southwestern United States and the Pacific Coast states in the summer. All seasons, except summer, showed a region with storm total precipitation greater than 17 mm along the coast of the Gulf of Mexico, and precipitation less

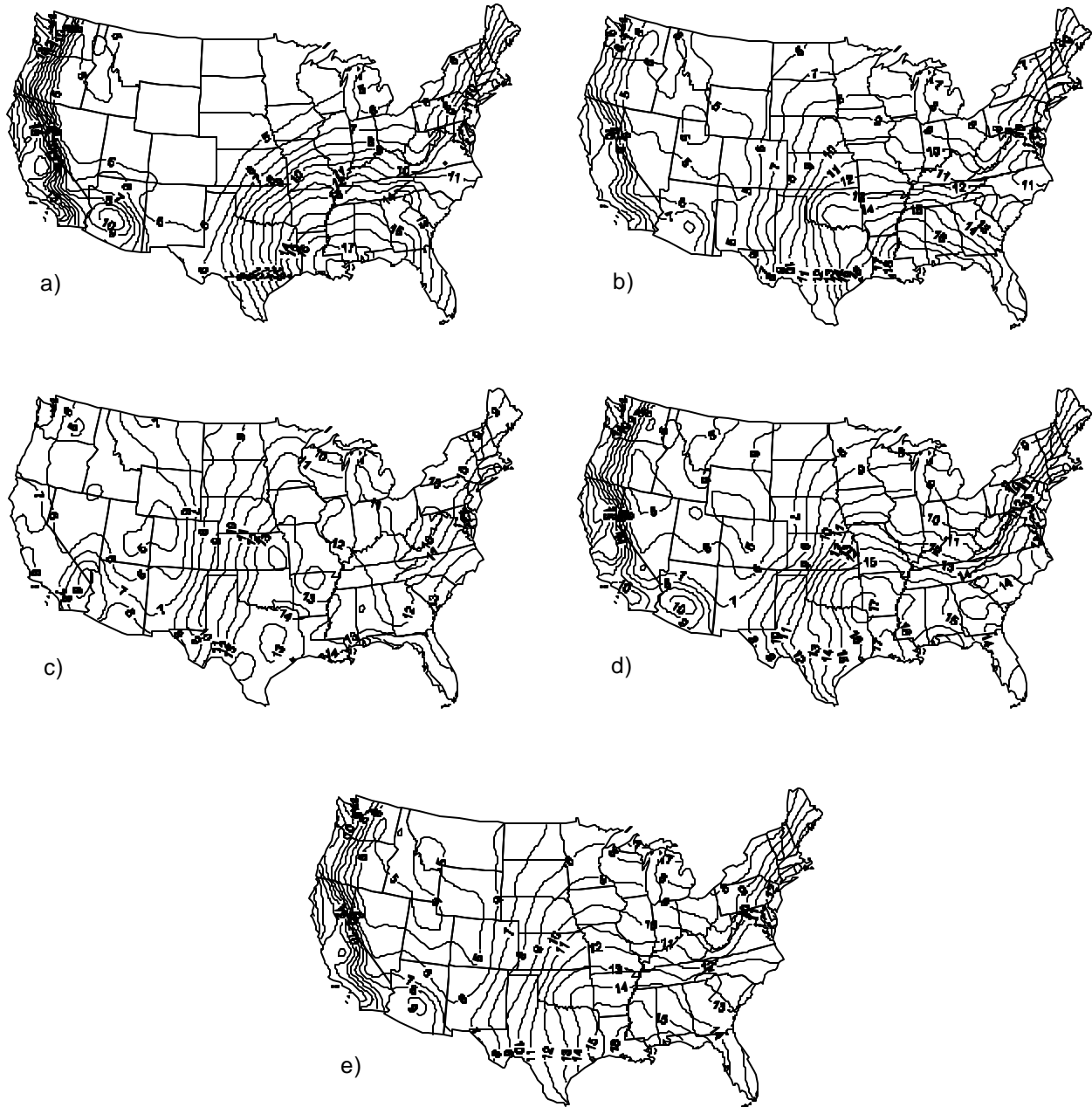


Figure 17. Mean total storm precipitation (mm) for all storms during a) winter, b) spring, c) summer, d) fall, and e) the entire year.

than 6 mm in the intermountain region of the West. In the North Central Plains and Montana, summer storm total precipitation was the largest of all seasons.

Mean storm total precipitation for storms large enough to be included in the R-factor computation range from 18 to 36 mm and were a factor of 2 greater than the mean storm total precipitation for all storms. Storm total precipitation patterns for these larger storms (Figure 18) were not as distinct as those for all storms. However, gradients of storm total precipitation did occur in approximately the same seasons and same areas of the country.

Storm Duration

Storm duration was defined as the time from the start of the first 15-minute period with rainfall to the end of the 15-minute period with rainfall that was separated from the start of the next shower by 6 hours or more. On an annual basis, the average storm duration for all storms ranges from 2 to 5 hours (Figure 19), with the longest storm durations along the Northwest Coast ranging from 3 hours in summer to 6 hours in winter.

Winter storm durations ranged from less than 1 hour to approximately 6 hours (Figure 19) and from 4 to 4.5 hours in southeastern states. The area of storms with a duration of 4 hours or greater extended up the East Coast to Maine. In the area where the storm total precipitation was least in the winter, the storms lasted, on average, from 1 to 2 hours.

Summer mean storm durations for all storms ranged from 1 to 3 hours (Figure 19), displaying the clear dominance of convective storms over stratiform rain events. The duration of storms across the eastern two-thirds of the United States was 2 hours. The mean duration was from 1 to 2 hours in the Great Basin and southwestern states. Storm durations exceeded 2 hours in the Northwest, particularly in the state of Washington.

During the transition seasons of spring and fall, storm durations were similar. However, in the spring, the 2.5- and 3.0-hour duration isolines were shifted more westerly than in the fall (Figure 19). The storm duration gradient along the West Coast was steeper in fall than in spring. Areas of storm duration tended to be associated with orographic features such as the Ozarks in Missouri and Arkansas and to the east of the Appalachian Mountain Range in North Carolina and Virginia in fall.

Mean storm durations for all larger storms averaged over the entire year ranged from 5 to 16 hours, with shorter storm durations in southern states and longer durations in the northern and western states (Figure 20). The pattern in drier western regions of the United States was complex, especially in the winter when many isolated maxima and minima occurred in the Rocky Mountain states and extended into the Dakotas. Winter mean durations of larger storms ranged from 8 to 16 hours. Corn Belt states averaged approximately 12 hours. Large storm durations ranged from 4 hours in the southeastern United States to 12 hours in the Pacific Northwest in the summer. Spring and fall storm durations west of the High Plains were generally in the 10 to 15 hour range, while the eastern two-thirds of the country ranged from 5 to 10 hours. Mean storm durations for larger storms were generally 2 to 4 times longer than those for all storms.

Storm Precipitation Intensity

Mean storm intensity, measured by the average rainfall rate over the entire storm, ranged from 6 to 10 mm hr⁻¹ for all storms for the entire year (Figure 21). The seasonal range was least in winter, 6 to 9 mm hr⁻¹, and greatest in summer, 7.5 to 12 mm hr⁻¹. During the transition seasons, the range was similar to the mean for the entire year, with little change in the pattern of

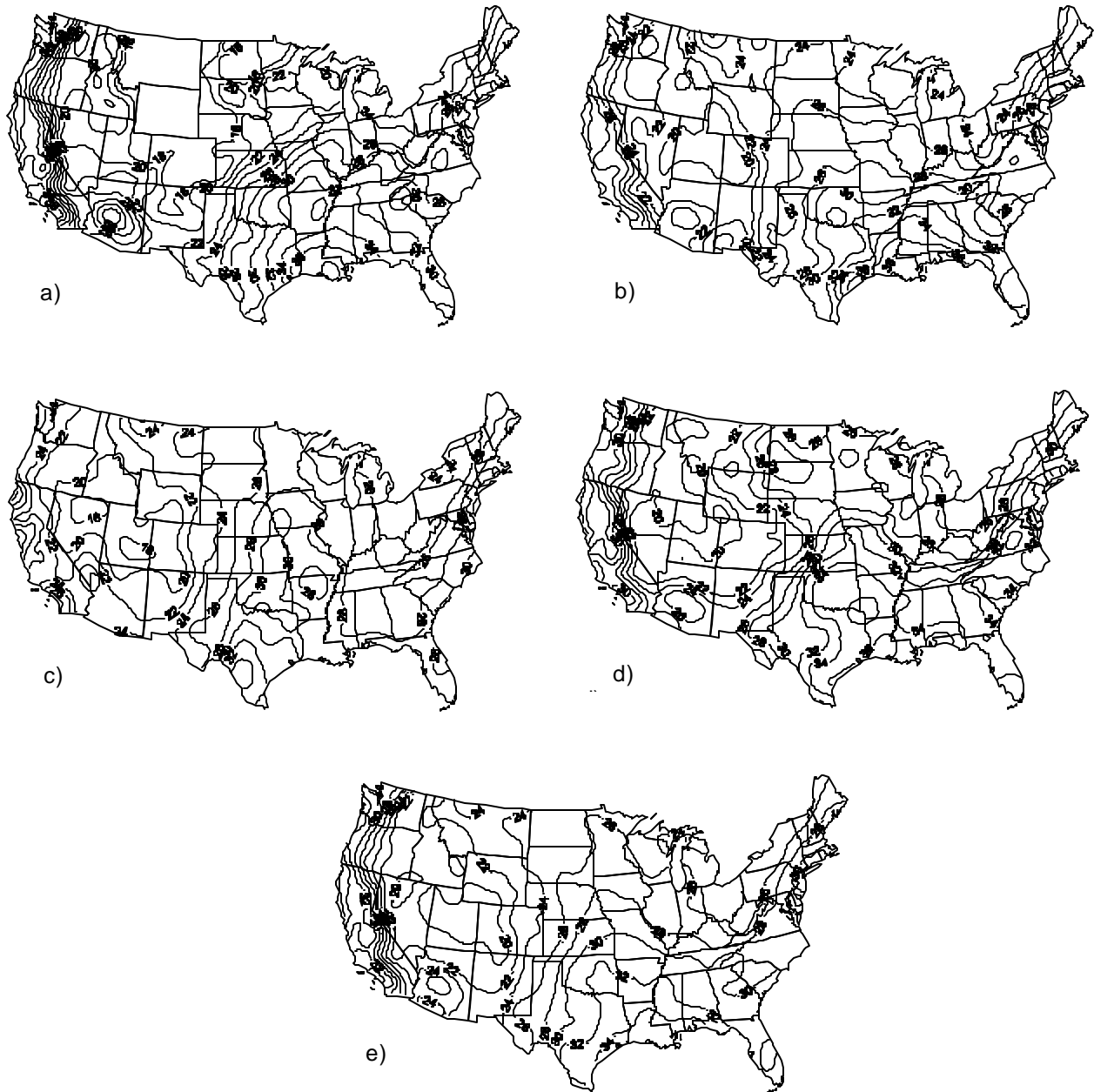


Figure 18. Mean storm total precipitation (mm) for all storms with greater than 12.7 mm of rainfall or a 15-minute rainfall intensity greater than 24 mm hr⁻¹ during a) winter, b) spring, c) summer, d) fall, and e) the entire year.

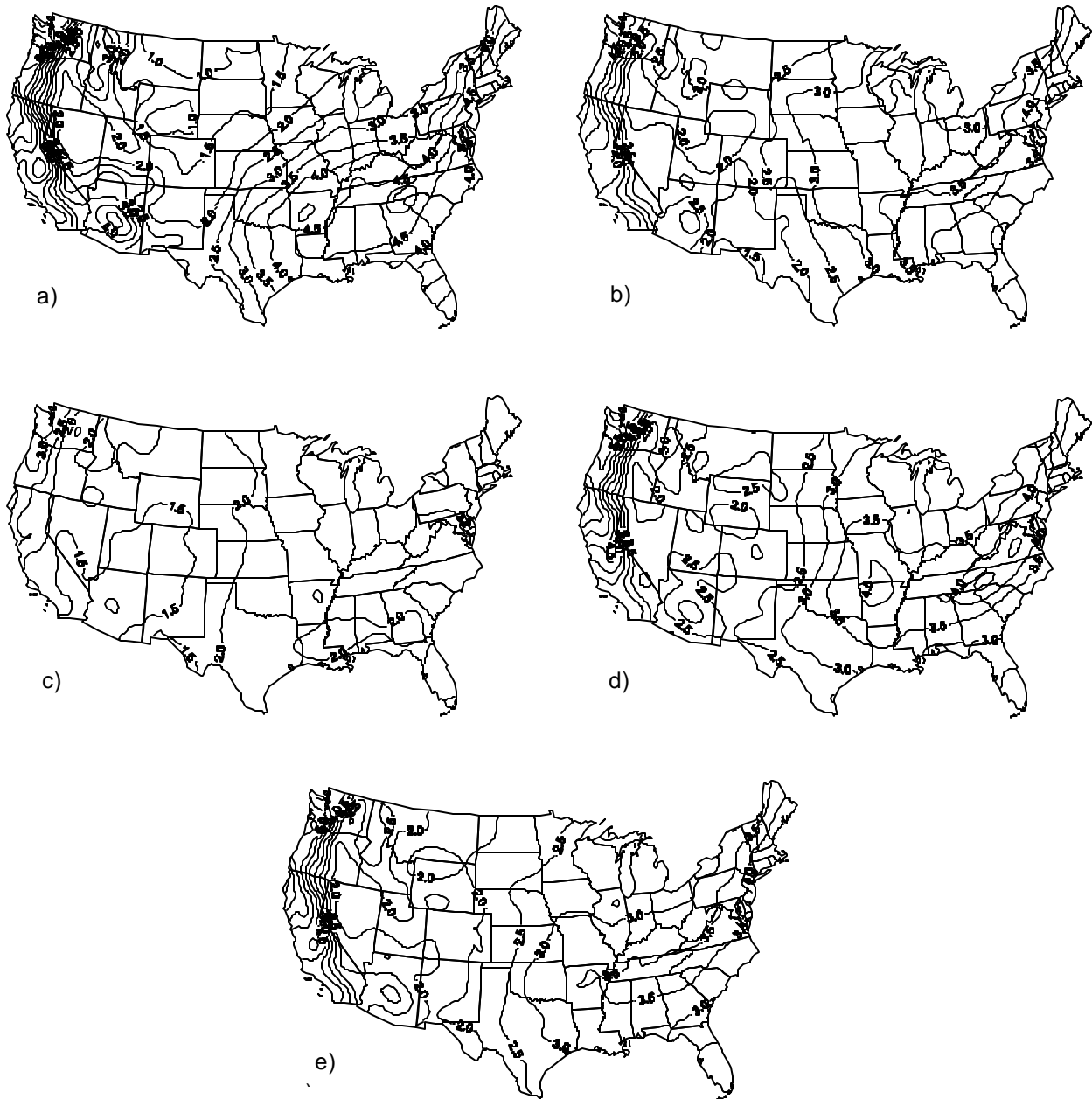


Figure 19. Mean storm duration (hr) for all storms during a) winter, b) spring, c) summer, d) fall, and e) the entire year.

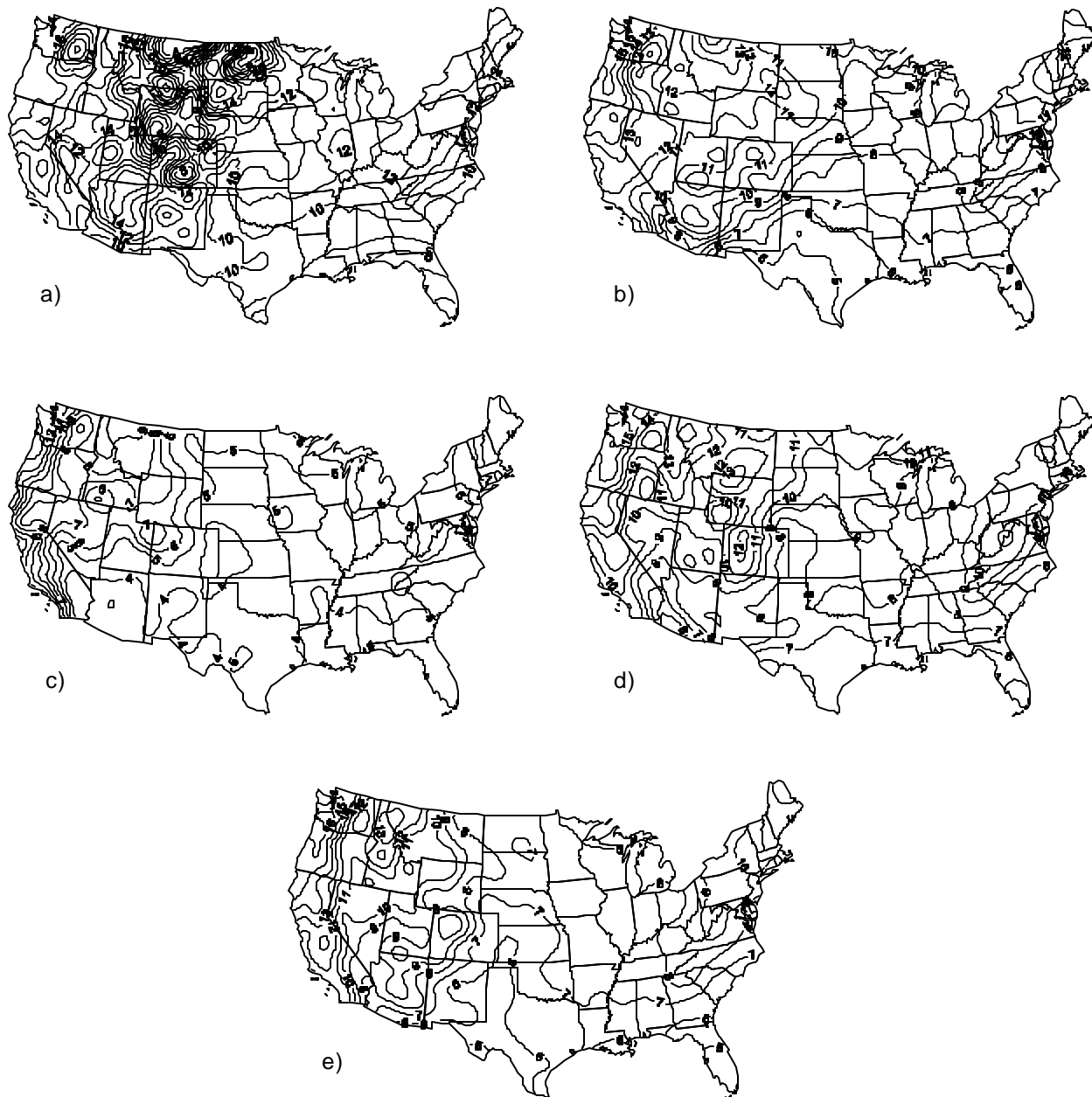


Figure 20. Mean storm duration (hr) for all storms with greater than 12.7 mm of rainfall or a 15-minute rainfall intensity greater than 24 mm hr⁻¹ during a) winter, b) spring, c) summer, d) fall, and e) the entire year.

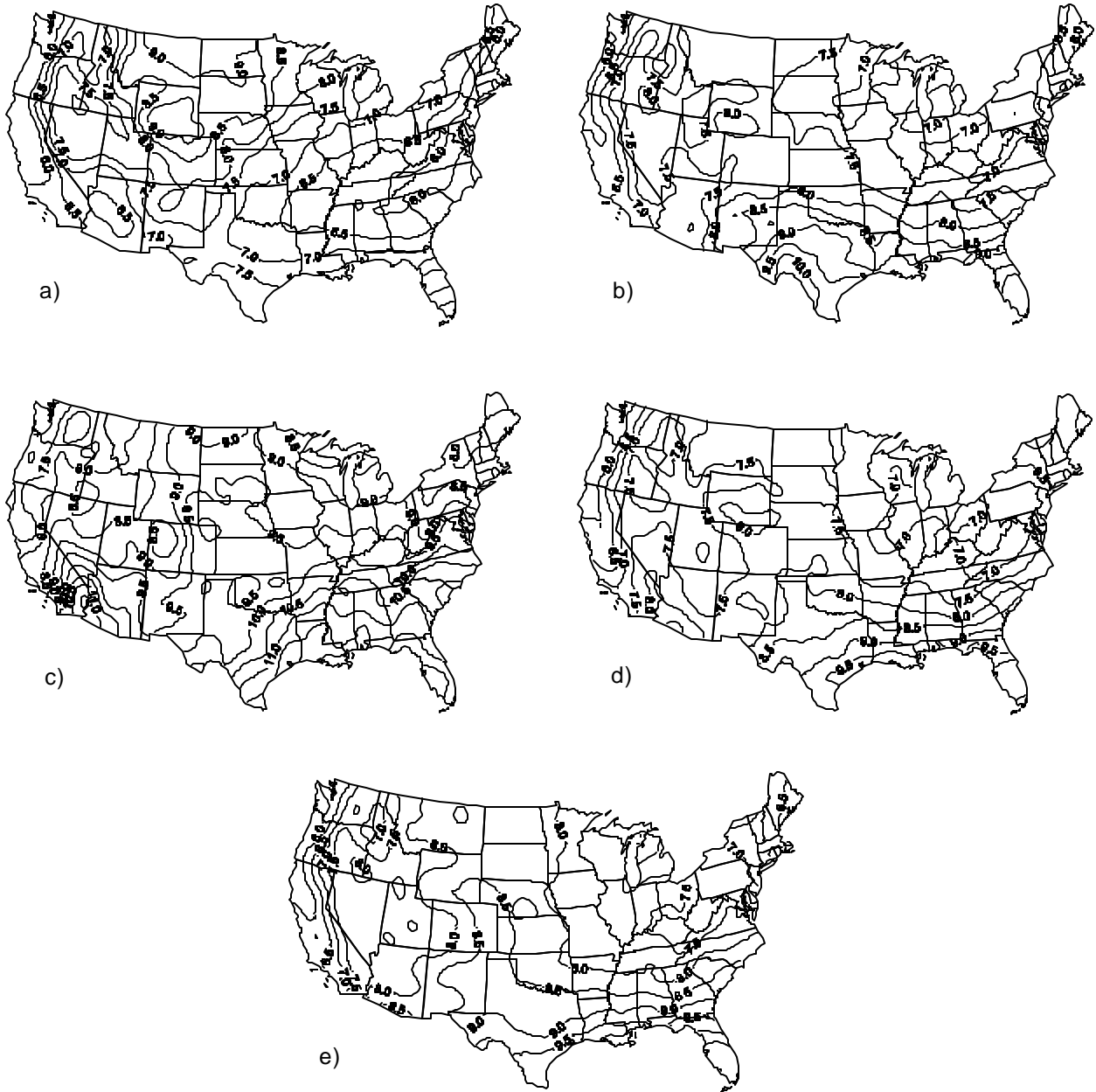


Figure 21. Mean storm intensity (mm hr⁻¹) for all storms during a) winter, b) spring, c) summer, d) fall, and e) the entire year.

storm intensity between spring and fall. The least intense storms were located along the Pacific Coast.

Surprisingly, the larger storms (Figure 22), included in the R-factor computation, tended to be less intense than the average for all the storms (Figure 21), especially in the winter, spring, and fall. Large storm intensity in winter was 1.5 to 3 times less than the mean for all storms combined. This is actually somewhat misleading as very short duration storms with little total precipitation skew the all-storm result. For instance, if 2.5 mm fell in one 15-minute increment, the storm intensity was 10 mm hr^{-1} . Storms with larger precipitation totals usually were spread over longer periods and included periods without rainfall, further reducing storm intensity. Mean intensity of larger storms in summer tended to be greater than the mean for all storms combined. Thus, smaller storms in summer were less intense than larger storms.

Storm Kinetic Energy (E)

Total storm kinetic energy in MJ ha^{-1} was computed using Equation (2) and averaged for all storms throughout each season and for the year. The mean kinetic energy for all storms during the year ranged from 1.0 to 3.5 MJ ha^{-1} (Figure 23). Storms with the greatest kinetic energy occurred in the southeastern United States, the region where the mean storm total precipitation was greatest, and those with the least kinetic energy occurred in the West. The general patterns (Figure 23) of the mean storm kinetic energy were similar to storm total precipitation patterns (Figure 17), indicating that the amount of rainfall in a storm had a greater impact on the kinetic energy than the rainfall intensity. In Pacific Coast states, the storm kinetic energy was greatest in the winter and fall, and least in the summer (Figure 23). East of the Rocky Mountain states, the storm kinetic energy was approximately the same in all seasons, with summer storms exhibiting only slightly more energy and winter storms slightly less energy.

For larger storms (Figure 24), the mean storm kinetic energy was two to three times greater during all seasons and for the entire year than the mean for all storms in the same time periods. The mean kinetic energy range for larger storms was from 4 to 8 MJ ha^{-1} for all storms in the year. Kinetic energy patterns for these larger storms did not change greatly over the seasons. The kinetic energy of storms in western states was least in winter and greatest in summer. East of the Rocky Mountain states, the kinetic energy was approximately the same for all seasons. Only the winter season showed a north to south gradient, with the storms of less energy located in the north. This pattern was consistent with reduced total precipitation in qualifying storms due to cold conditions in the northern tier of states.

Storm Maximum 30-Minute Precipitation Intensity (I_{30})

The 30-minute maximum intensity of a storm was a more useful indicator of the storm's intensity at its peak. Storm erosivity was calculated by multiplying the storm kinetic energy by the 30-minute maximum precipitation intensity (I_{30}). This had the effect of weighting each storm by the period of greatest rainfall intensity and increasing storm erosivity over what would have occurred if only the mean rainfall intensity were used. The range of the annual mean storm I_{30} was 6 to 15 mm hr^{-1} (Figure 25). The highest rainfall intensity occurred in all seasons in the southeastern United States, the lowest in the Great Basin and Pacific Northwest. The lowest I_{30} occurred in winter, the highest in summer.

The summer I_{30} ranged from 6 to 17 mm hr^{-1} (Figure 25). An east to west gradient existed along the front range of the Rocky Mountains in New Mexico, Colorado, and Wyoming. A north



Figure 22. Mean storm intensity (mm hr^{-1}) for all storms with greater than 12.7 mm of rainfall or a 15-minute rainfall intensity greater than 24 mm hr^{-1} during a) winter, b) spring, c) summer, d) fall, and e) the entire year.



Figure 24. Mean storm kinetic energy (E , MJ ha^{-1}) for all storms with greater than 12.7 mm of rainfall or a 15-minute rainfall intensity greater than 24 mm hr^{-1} during a) winter, b) spring, c) summer, d) fall, and e) the entire year.



Figure 25. Mean maximum 30-minute rainfall intensity (mm hr⁻¹) for all storms during a) winter, b) spring, c) summer, d) fall, and e) the entire year.

to south gradient also occurred in southern California, Arizona, New Mexico, southern Nevada, and Utah. The gradient along the front range of the Rocky Mountains was an orographic effect, while the gradient in the Southwest was due to the southwestern monsoon. A second orographic gradient existed east of the Appalachians in the Carolinas and Virginia.

Unlike mean storm rainfall intensity, mean I_{30} for larger storms (Figure 26) exceeded the mean for all storms. This supports the need to include the I_{30} in the calculation of storm erosivity. The I_{30} for the larger storms ranged from 8 to 30 mm hr⁻¹ (Figure 26). The general patterns of the larger storm I_{30} was similar to the mean for all storms. East of the Rocky Mountain states, the larger storm I_{30} was approximately two times larger than the mean for all storms. The summer I_{30} of the larger storms (Figure 26) ranged from 8 to 34 mm hr⁻¹. The I_{30} was smallest along the coast of Oregon and largest in Florida. Summer I_{30} values were also the largest of the four seasons, while winter I_{30} values were the smallest.

Storm Erosivity (EI_{30})

The mean storm erosivity (EI_{30}) and the number of storms during a year determined the mean annual R-factor. Maps of the mean storm EI_{30} showed a range of 10 to 120 MJ mm ha⁻¹ hr⁻¹ for all storms during the year (Figure 27), 10 to 160 MJ mm ha⁻¹ hr⁻¹ for all storms during the spring, and 10 to 140 MJ mm ha⁻¹ hr⁻¹ for all storms in both summer and fall. Along the Gulf Coast, the EI_{30} was the largest and relatively constant across all seasons. The summer mean EI_{30} increased to a maximum of 60 to 90 MJ mm ha⁻¹ hr⁻¹ in the Midwest, and was as high as 30 to 40 MJ mm ha⁻¹ hr⁻¹ along the front range of the Rocky Mountains. These values apply to a mean that included all large and small storms.

The EI_{30} for larger storms ranged from 60 to 330 MJ mm ha⁻¹ hr⁻¹ for all storms during the year, from 30 to 240 MJ mm ha⁻¹ hr⁻¹ in winter, from 60 to 420 MJ mm ha⁻¹ hr⁻¹ in spring, and from 60 to 330 MJ mm ha⁻¹ hr⁻¹ in summer and fall (Figure 28). This represented a two- to three-fold increase of the mean EI_{30} of large storms over the means for all storms during each season. This increase was consistent with the increase of the larger storm mean over the mean for all storms for both the I_{30} and storm total precipitation.

Number of Storms

The total number of storms in a year across the United States ranged from 40 to more than 130 storms (Figure 29). Arizona and southern California had the fewest storms, and the Pacific Northwest the most. Across the Intermountain West and the High Plains states, the number of storms each year ranged from 60 to 70. East of the High Plains states, the number ranged from 80 to 120 storms. The largest number of storms in the East occurred south and east of the Great Lakes. Along the East Coast, the number of storms was approximately 90. The number of storms in the eastern United States was rather constant with a total of 25 storms in winter, spring and summer, and 20 storms in fall. The fewest storms in the West were recorded during the summer, followed by fall, spring, and winter.

Storms large enough to be included in the R-factor calculation ranged from 35 in the Southeast to less than 10 in the Intermountain West for the entire year (Figure 30). In the winter approximately 12 storms occurred in the coastal regions of Washington state, 6-10 storms in the Southeast, and less than 6 storms over the rest of the United States. Spring and summer seasons in the eastern United States had approximately eight storms, while the West had fewer than four,

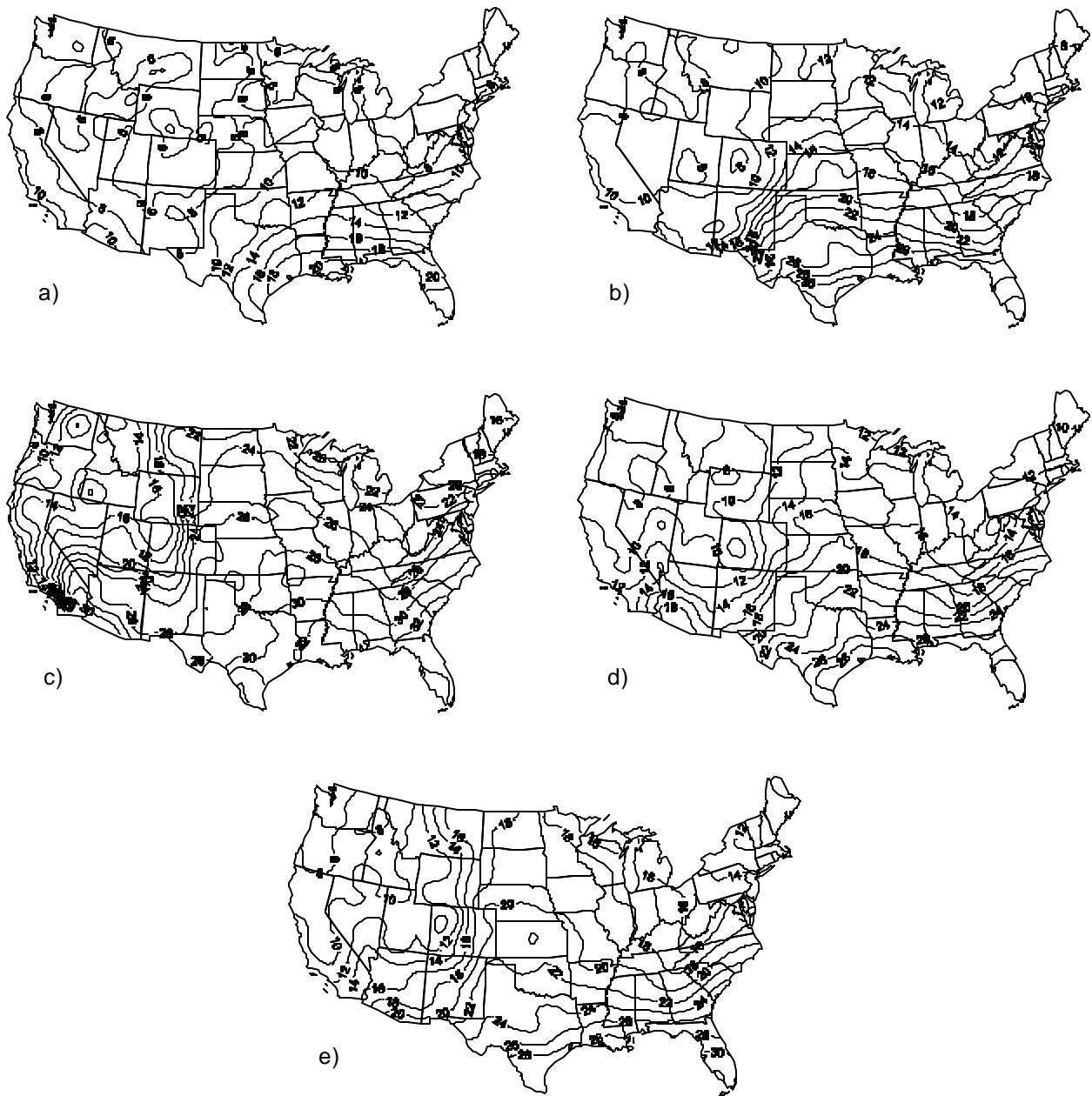


Figure 26. Mean maximum 30-minute rainfall intensity (mm hr^{-1}) for all storms with rainfall greater than 12.7 mm or a 15-minute intensity greater than 24 mm hr^{-1} during a) winter, b) spring, c) summer, d) fall, and e) the entire year.

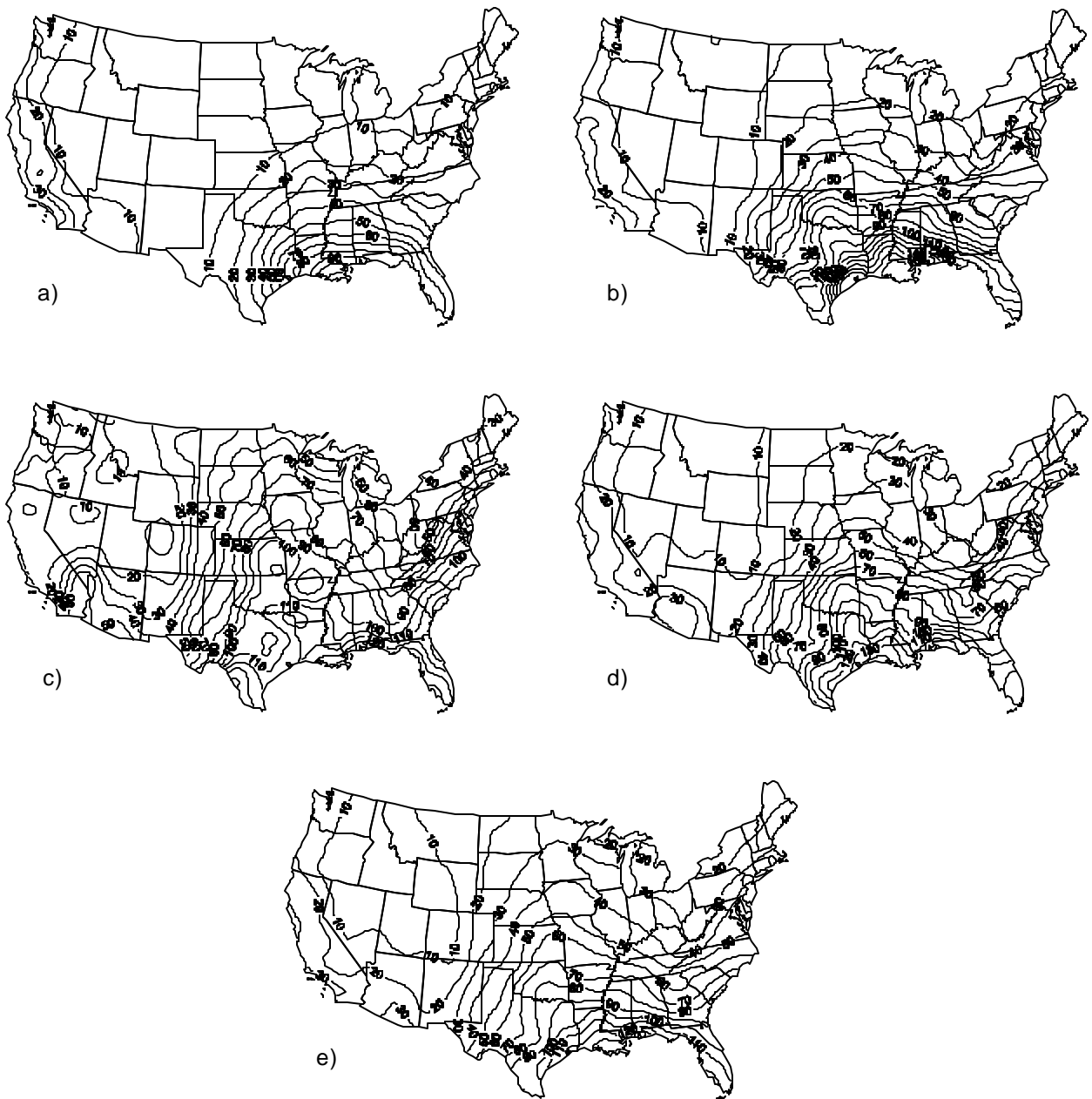


Figure 27. Mean storm erosivity (EI_{30} , $MJ\ mm\ ha^{-1}\ hr^{-1}$) value for all storms during a) winter, b) spring, c) summer, d) fall, and e) the entire year.

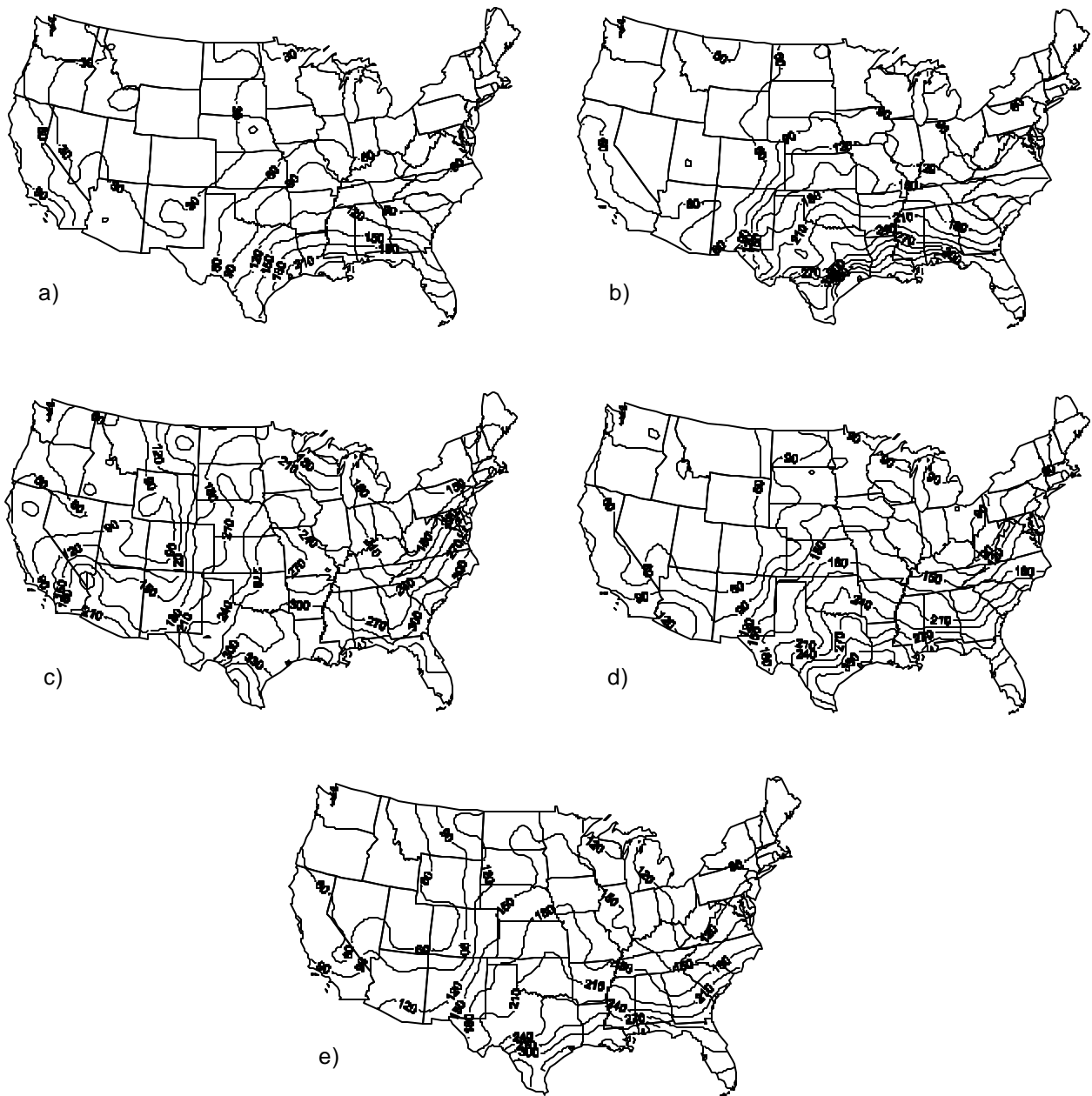


Figure 28. Mean storm erosivity (EI_{30} , $\text{MJ mm ha}^{-1} \text{hr}^{-1}$) value for all storms with rainfall greater than 12.7 mm or a 15-minute intensity greater than 24 mm hr^{-1} during a) winter, b) spring, c) summer, d) fall, and e) the entire year.

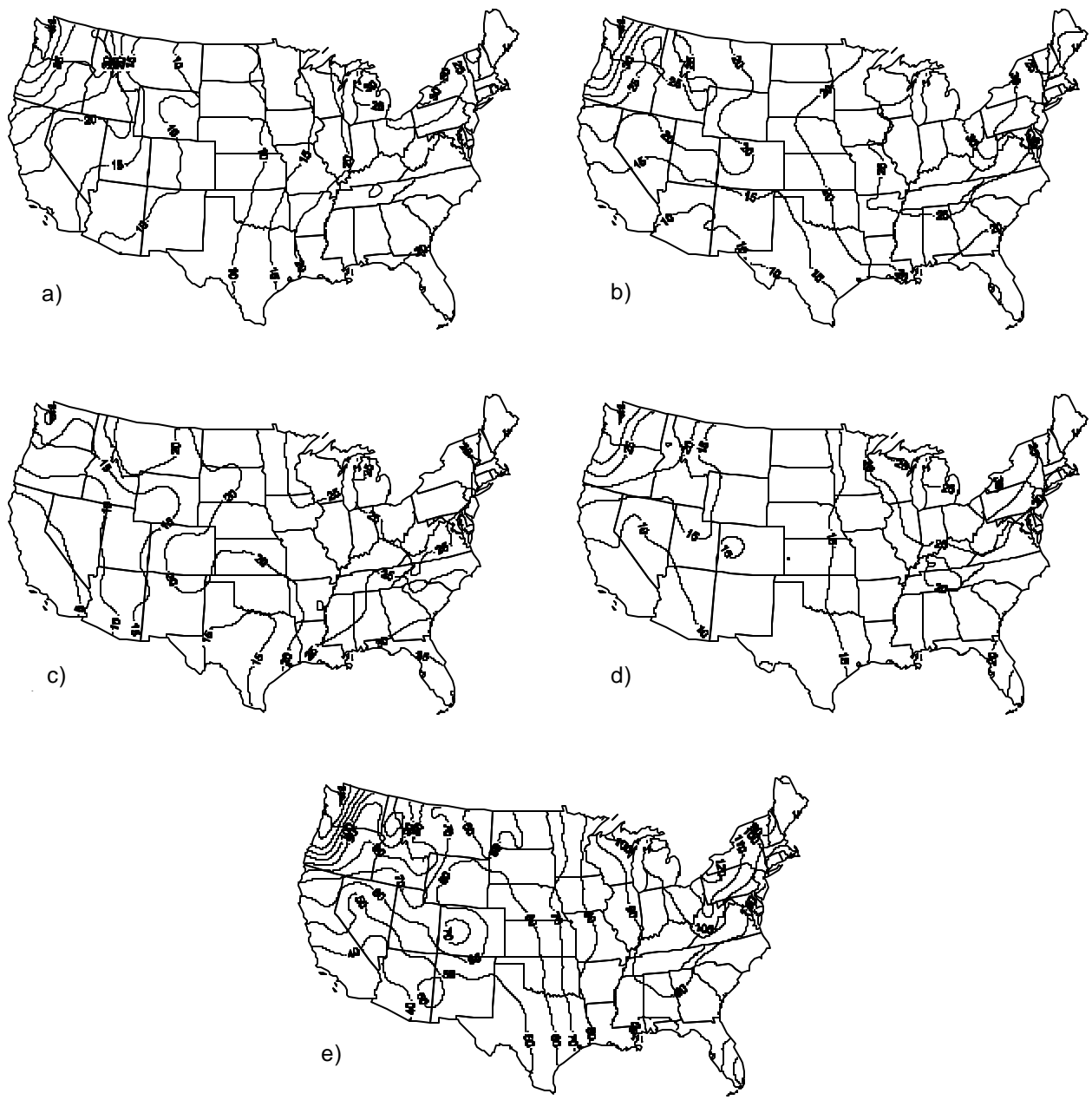


Figure 29. Mean number of storms during a) winter, b) spring, c) summer, d) fall, and e) the entire year.



Figure 30. Mean number of storms for all storms with rainfall greater than 12.7 mm or a 15-minute intensity greater than 24 mm hr⁻¹ during a) winter, b) spring, c) summer, d) fall, and e) the entire year.

except for the coastal regions of Washington and Oregon during the spring where approximately six storms were normally recorded. In the fall, the Pacific Northwest and the southeastern United States each normally recorded eight large storms, while the majority of the country recorded less than six.

Storm Maximum 15-Minute Precipitation Intensity

The mean maximum 15-minute rainfall intensity ranged from 10 to 18 mm hr⁻¹ in winter and from 10 to 24 mm hr⁻¹ in summer (Figure 31). Because the rain gauges only recorded rainfall in 2.54 mm increments, the minimum recordable 15-minute rainfall intensity was 10 mm hr⁻¹. Thus, the area lacking any isolines in the western United States in winter, spring, and fall, and on the annual map included rates between 10 mm hr⁻¹ and the first labeled contour value. The largest 15-minute maximum rainfall rates occurred in summer, the smallest in winter.

The mean for larger storm maximum 15-minute rainfall intensity ranged from 28 to 30 mm hr⁻¹ in winter, and from 16 to 44 mm hr⁻¹ in summer (Figure 32). The annual range was from 16 to 42 mm hr⁻¹, a 150 to 200 percent increase over the mean for all storms. Unlike many of the other storm characteristic variables, strong gradients across the country do not exist except over the Southwest during summer.

Maximum 15-Minute Precipitation Intensity and Storm Intensity Ratio

The 15-minute maximum intensity was from two to four times greater than the average total storm intensity in winter (Figure 33), which represented the widest range of this ratio. The other three seasons and ratio for the total year averaged between 2.2 and 4.0. Generally, east of the Rocky Mountain states, the ratio was greater than 3.0. Within the Great Basin and the Rocky Mountain states, the ratio ranged from 2.0 to 3.0. Along the Pacific Coast, the ratio was greater than 4.0, especially in the Pacific Northwest.

For the larger storms, the ratio of the 15-minute maximum precipitation intensity to the average intensity storm ranged from 6.0 to 8.0 in winter, 5.2 to 8.0 in spring, 4.0 to 6.8 in summer, and 5.2 to 6.4 in fall (Figure 34). The mean of the ratio for all large storms throughout the year ranged from 5.2 to 6.8. The ratio for only large storms was approximately two times greater than the ratio for all storms.

Trends in Storm Characteristics

Time trends in storm characteristics during 1971-1999 were examined, and 15-minute precipitation data were used to construct statistics on storm totals, duration, intensity, maximum 30-minute rainfall, and storm erosion index (EI). Storms were defined as rain events separated by six or more hours. This analysis focuses on large storms qualifying for inclusion in the R-factor calculation, with storm totals greater than 12.7 mm or rainfall rates greater than 24 mm hr⁻¹. Linear regression was applied to annual and seasonal measures of these statistics to determine trends over the 29 years. The criteria for including stations in the annual and seasonal analyses were one storm per valid year and at least 15 valid years in total. In addition, there must have been less than 25 percent missing data in the decades of the 1970s and 1990s. All trends are expressed as a percentage change per decade. In this section, cross-hatching indicates negative trends less than -2 percent, gray tones represent areas of positive trends greater than +2 percent, and blank areas represent trends between -2 to +2 percent.



Figure 31. Mean maximum 15-minute intensity (mm hr⁻¹) for all storms during a) winter, b) spring, c) summer, d) fall, and e) the entire year.

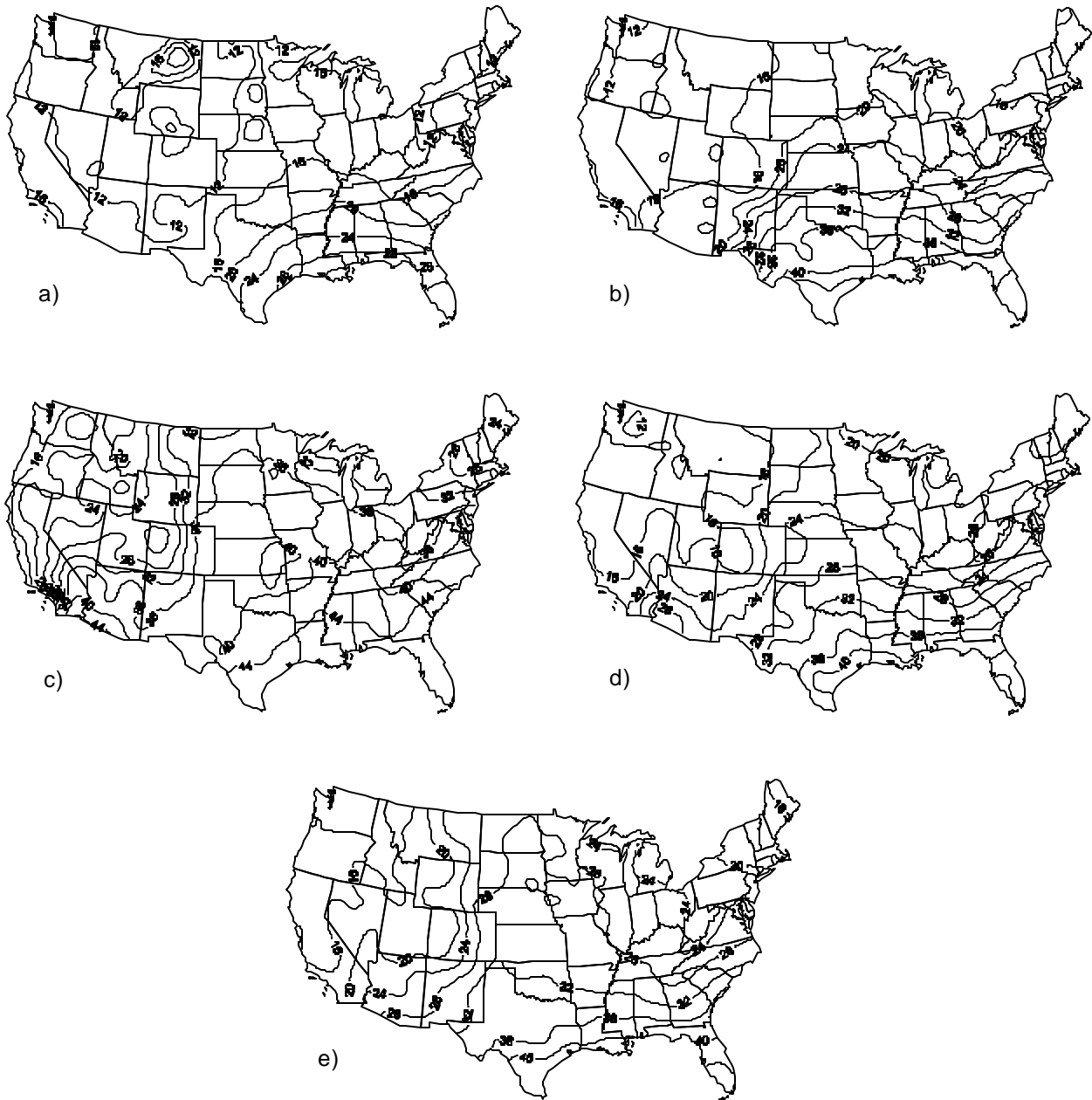


Figure 32. Mean maximum 15-minute intensity (mm hr^{-1}) for all storms with rainfall greater than 12.7 mm or a 15-minute intensity greater than 24 mm hr^{-1} during a) winter, b) spring, c) summer, d) fall, and e) the entire year.

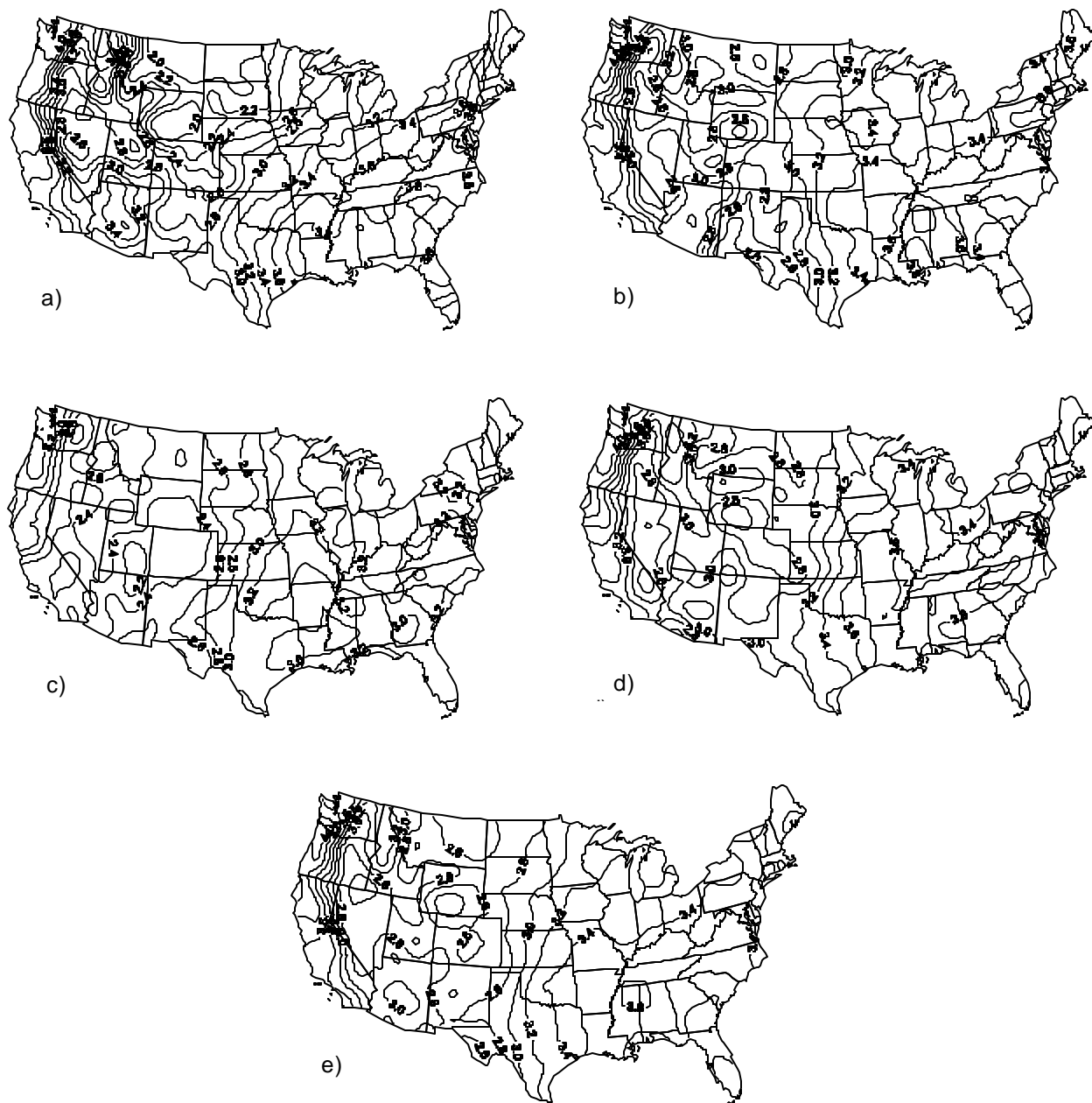


Figure 33. Mean ratio of 15-minute maximum intensity to total storm intensity for all storms during a) winter, b) spring, c) summer, d) fall, and e) the entire year.

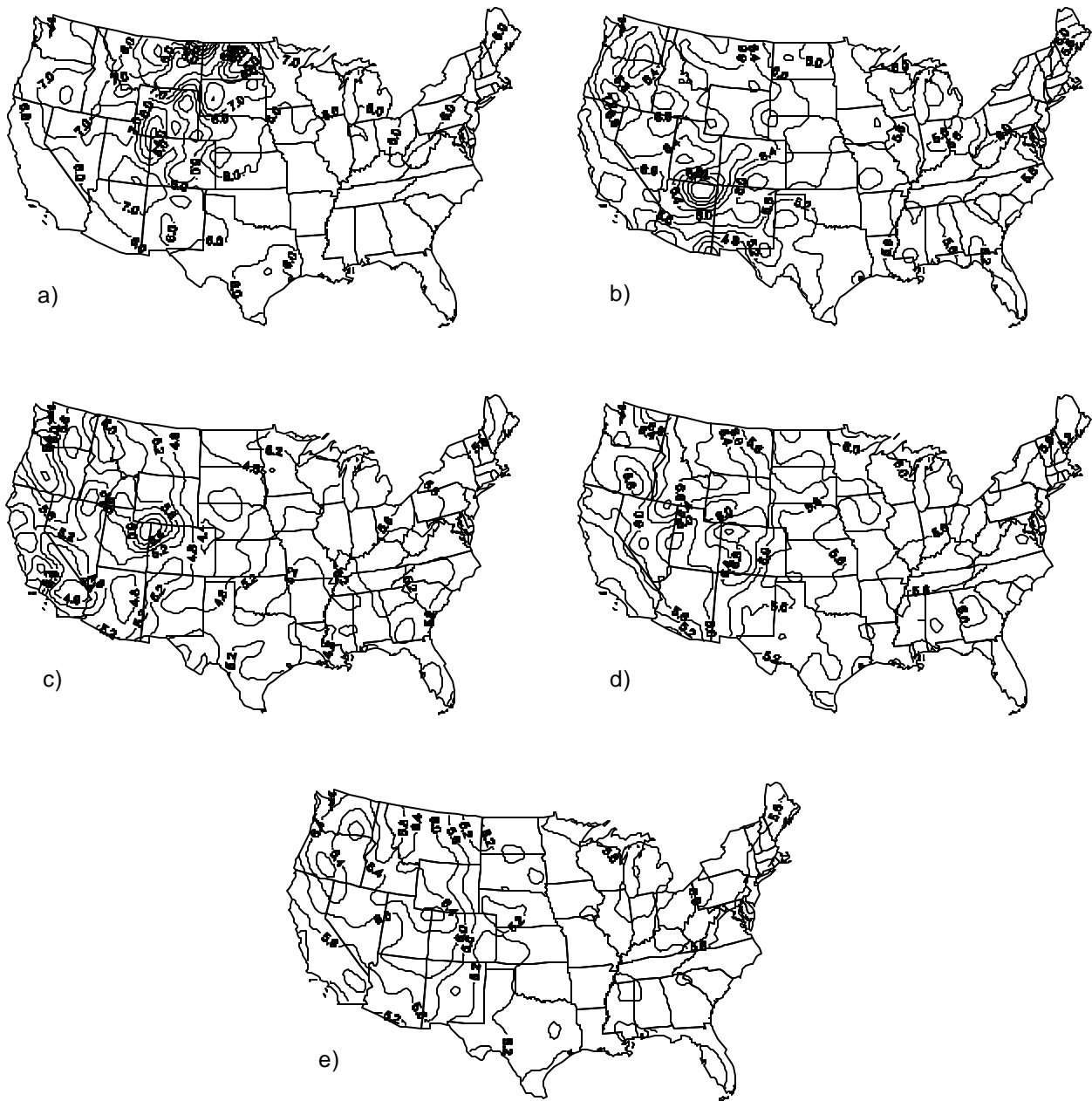


Figure 34. Mean ratio of 15-minute maximum intensity to total storm intensity for all storms with rainfall greater than 12.7 mm or a 15-minute intensity greater than 24 mm hr^{-1} during a) winter, b) spring, c) summer, d) fall, and e) the entire year.

Annual Trend Maps

No large-scale patterns were found in the annual storm total trend map (Figure 35a). An area of increase was evident in the Southeast, as well as maxima centered over South Dakota and Indiana. The annual storm duration trend map (Figure 35b) had increases of 2 percent or more per decade in a large portion of the eastern half of the United States. Smaller segments of positive trends were found in the Southwest and north-central states. Areas of decreasing duration were found in southern and western Texas, and in an area centered on Colorado. Storm intensity was based on the ratio of storm totals and storm duration. In this context, trends in intensity could have been caused by changes in either the amount of rainfall or storm duration or both. In some instances, changes in amount and duration could cancel each other out. For example, a trend of higher amounts and longer durations may leave intensity unchanged. The annual storm intensity trend map (Figure 35c) showed large areas with decreasing intensity. Examination of the annual storm total and duration trend maps suggested that the decreasing intensity was being driven primarily by trends of increased duration rather than decreased storm totals. The annual 30-minute maximum precipitation trends map (Figure 35d) showed decreasing trends in a large portion of the western and east-central United States. Increases were shown in many Plains states. Like storm intensity, storm EI was a combination of two factors: storm totals and 30-minute maximum precipitation. However, the two terms are multiplicative so the relationship is direct, rather than inverse, as was the case with intensity. Of the annual patterns of the five storm characteristics, the map of trends in storm EI (Figure 35e) was one of the most active and complex. The West was dominated by decreases in storm EI, which appeared to be driven mainly by decreases in the maximum 30-minute amounts. A band of increased EI occurred from Colorado to Kansas and then northward into North Dakota/Minnesota, primarily driven by increased maximum 30-minute precipitation amounts. Another band of increased EI from eastern Texas to South Carolina was driven primarily by increased storm totals. The annual storm count trend map (Figure 35f) showed a large area of increasing numbers of large storms west of the Mississippi River. The Southeast and East showed slightly decreased numbers of storms over time. Annual trends were weaker than the seasonal trends due to the patterns of change varying with season.

Winter Trend Maps

Because far fewer storms exceeded 12.7 mm in winter, the patterns depicted (Figure 36) were not as robust as their counterparts in other seasons. Winter storm totals trends (Figure 36a) increased in the Southwest, in western Gulf Coast states, on the southern East Coast, and in the eastern Midwest. Decreases were seen in the Northeast and Northwest. The map of storm duration trends (Figure 36b) showed a band of increasing durations from Texas to the upper Midwest and then on to several eastern states. Decreased durations were found along the southern border and in scattered regions of the West. Storm intensity trends (Figure 36c) revealed an area of increasing intensity in the Interior West and decreased intensity in the Northwest. These changes were driven primarily by changes in storm duration. Decreasing intensities in the central and eastern United States were mainly the result of increased storm amounts. Maximum 30-minute precipitation trends (Figure 36d) showed an increase in the Southwest and along the Gulf Coast. Decreases were evident in the Plains, the Northwest, and the Northeast. Storm EI trends (Figure 36e) reflect decreasing EI values in the Northwest, portions of western California, the central United States and most of the Northeast. Decreased EI values occurred in the Southwest, Gulf

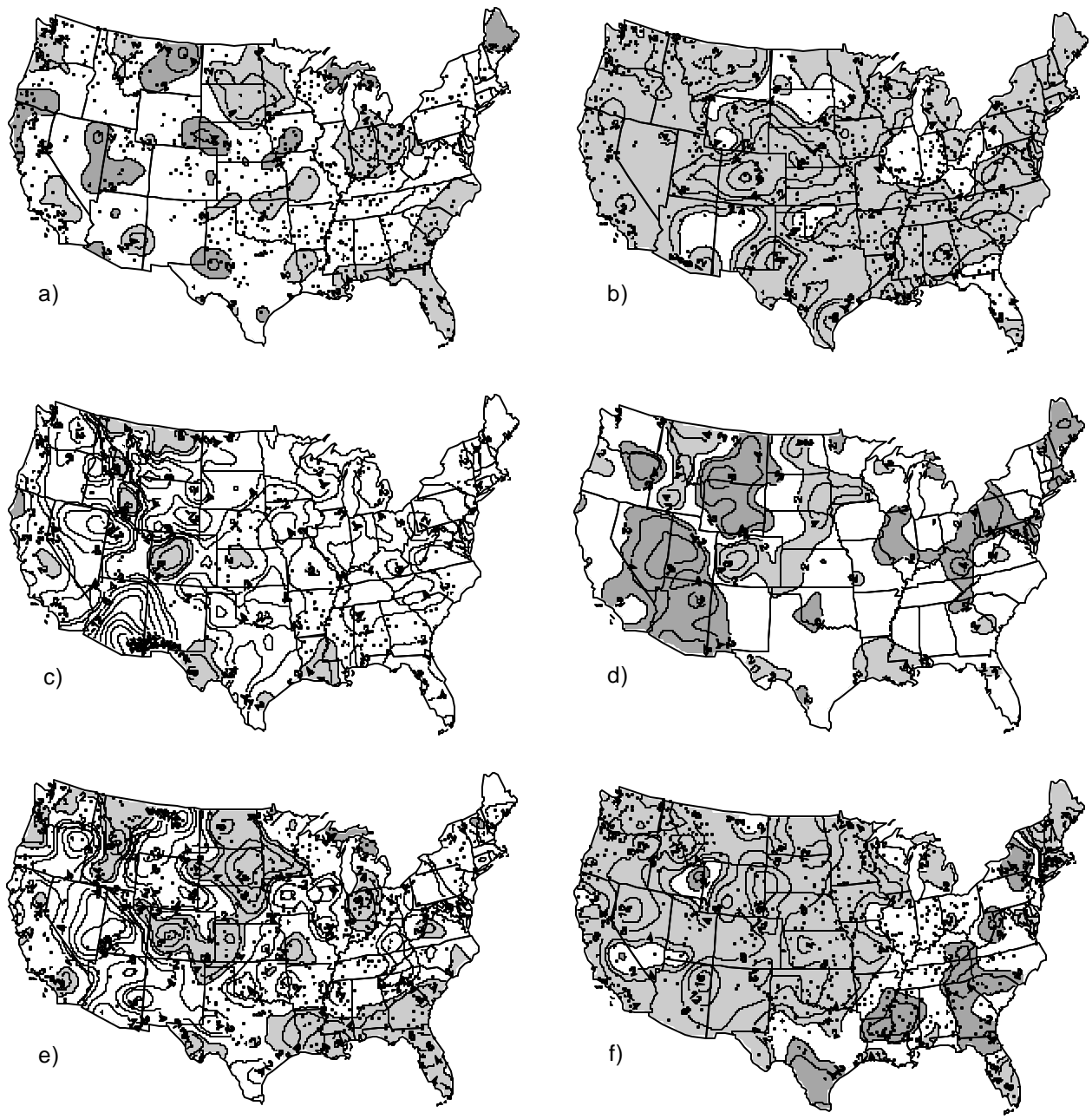


Figure 35. Annual 1971-1999 trends in storm characteristics for a) storm totals, b) storm duration, c) storm intensity, d) maximum 30-minute precipitation, e) storm EI, and f) number of storms. Trends are expressed as percent change per decade where negative trends are cross-hatched, positive trends are gray, and no trend is white. Black dots represent stations.

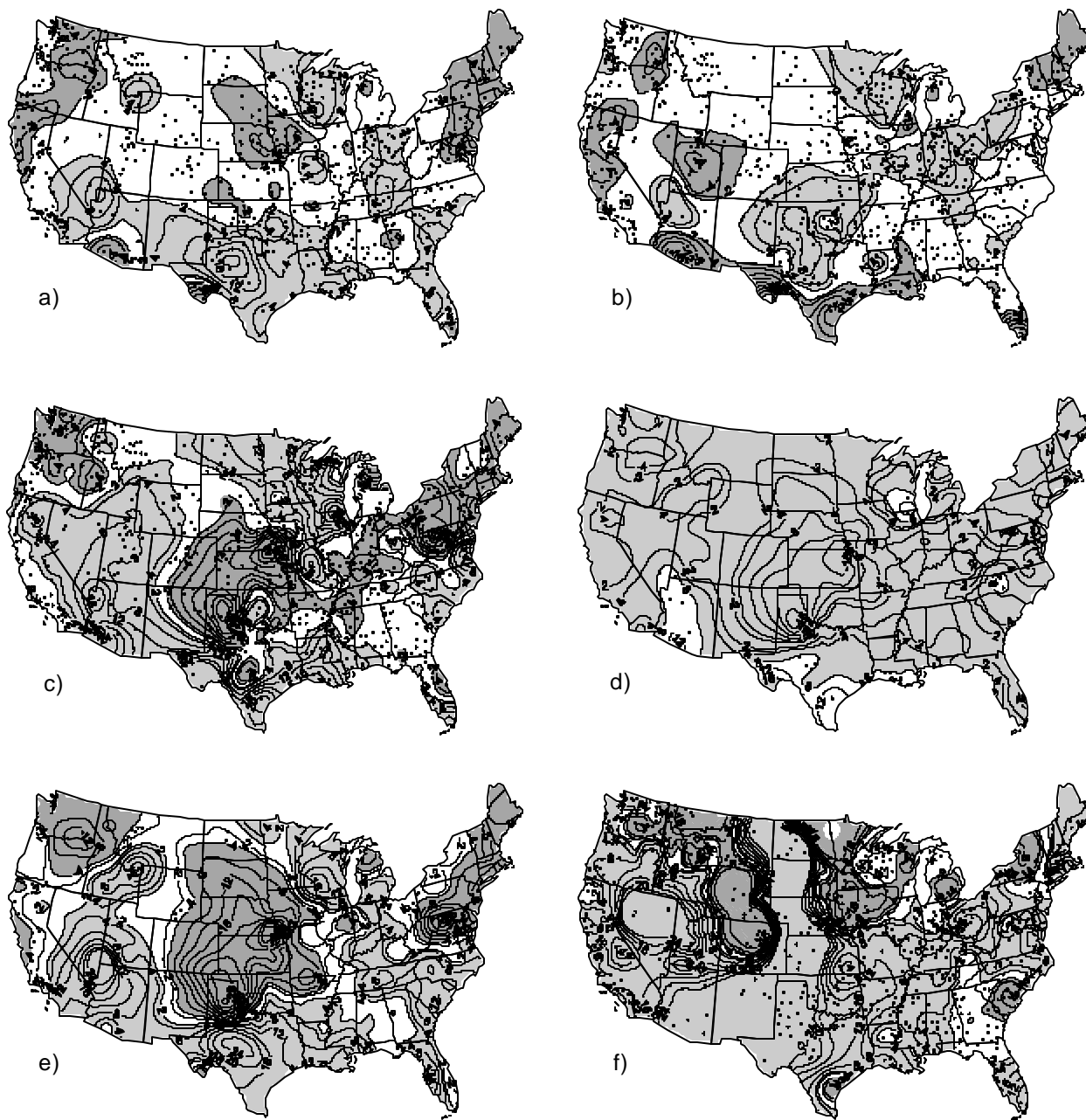


Figure 36. Winter 1971-1999 trends in storm characteristics for a) storm totals, b) storm duration, c) storm intensity, d) maximum 30-minute precipitation, e) storm EI, and f) number of storms. Trends are expressed as percent change per decade where negative trends are cross-hatched, positive trends are gray, and no trend is white. Black dots represent stations.

Coast states, the Southeast, and portions of the Appalachians and the eastern Midwest. Winter storm frequency (Figure 36f) increased over large portions of the United States. Decreases were seen in a band from Washington to Colorado, and in the Iowa/Minnesota region. Increases in the number of storms would tend to offset the decreases in EI per storm in the Great Plains.

Spring Trend Maps

Storm total trends in spring (Figure 37a) showed areas of increases in the Southwest, east-central United States, and parts of the Northwest. Areas of decreasing storm totals were found in the Southeast and the Rocky Mountain states. Storm duration trends (Figure 37b) increased in the Southwest and eastern portion of the Midwest. A large band of decreasing duration was found from Montana to Arizona and on to the central Plains. This pattern roughly matched the one for storm totals in spring. Smaller areas of increases were found in parts of California, Oregon, Washington, and the Minnesota/Dakotas region. Smaller areas of decreasing duration were found in Louisiana, Mississippi, Georgia, and the Northeast. The map of storm intensity trends (Figure 37c) showed a decrease in a large portion of the United States, while small regions, usually limited to one or two states, showed an increase. This pattern was more complex in terms of the interactions of storm total and duration trends. Northern Rocky Mountain states had both decreasing totals and decreasing durations, but the latter trend was stronger and resulted in increasing intensities. The decreasing intensity in the central United States was dominated by relatively large increases in duration. The decrease in intensity in the Southeast was due to large decreases in storm totals. Maximum 30-minute precipitation trends (Figure 37d) increased in many western states. Decreases were found in the Southwest. The remainder of the United States showed smaller pockets of weaker trends. Storm EI trends (Figure 37e) showed a complex spatial pattern of regional increases and decreases. Storm frequency trends (Figure 37f) showed an increase in the number of storms to the west of the 100° west meridian and in portions of the Midwest and Northeast. There was a large area of decreasing frequency in the Southeast, with other small regions of decreases scattered across the country.

Summer Trend Maps

Summer storm amounts (Figure 38a) revealed no large-scale pattern except for areas of decrease along the West Coast and the Central Plains, reflecting the more convective nature of summer precipitation in most areas. Summer storm durations (Figure 38b) were more coherent. Decreases were found in California/Oregon, Colorado/Wyoming, and southern Texas. Increases were found in the Southwest and in a U-shaped band from North Dakota to Louisiana to Michigan that included much of the Southeast. Storm intensities (Figure 38c) increased in New Mexico/Texas/Louisiana with decreases elsewhere. Storm amounts and durations suggested that the decreasing intensity was driven primarily by increasing duration in most areas. The only large-scale pattern for maximum 30-minute intensities (Figure 38d) was the region of decreased intensity in the West. Smaller areas of decreasing intensity were found in a band from Texas to Nebraska and in the Southeast. Areas of decreased storm EI (Figure 38e) were found in many western, southwestern, and central Plains states, while areas of increasing EI were found in the upper Plains states and the eastern half of the United States. Most areas showing an increase were fragmented. Summer storm frequencies (Figure 38f) decreased in a band from Texas to Maine and some areas in the Northwest. A large portion of the rest of the country experienced increased storm frequency.

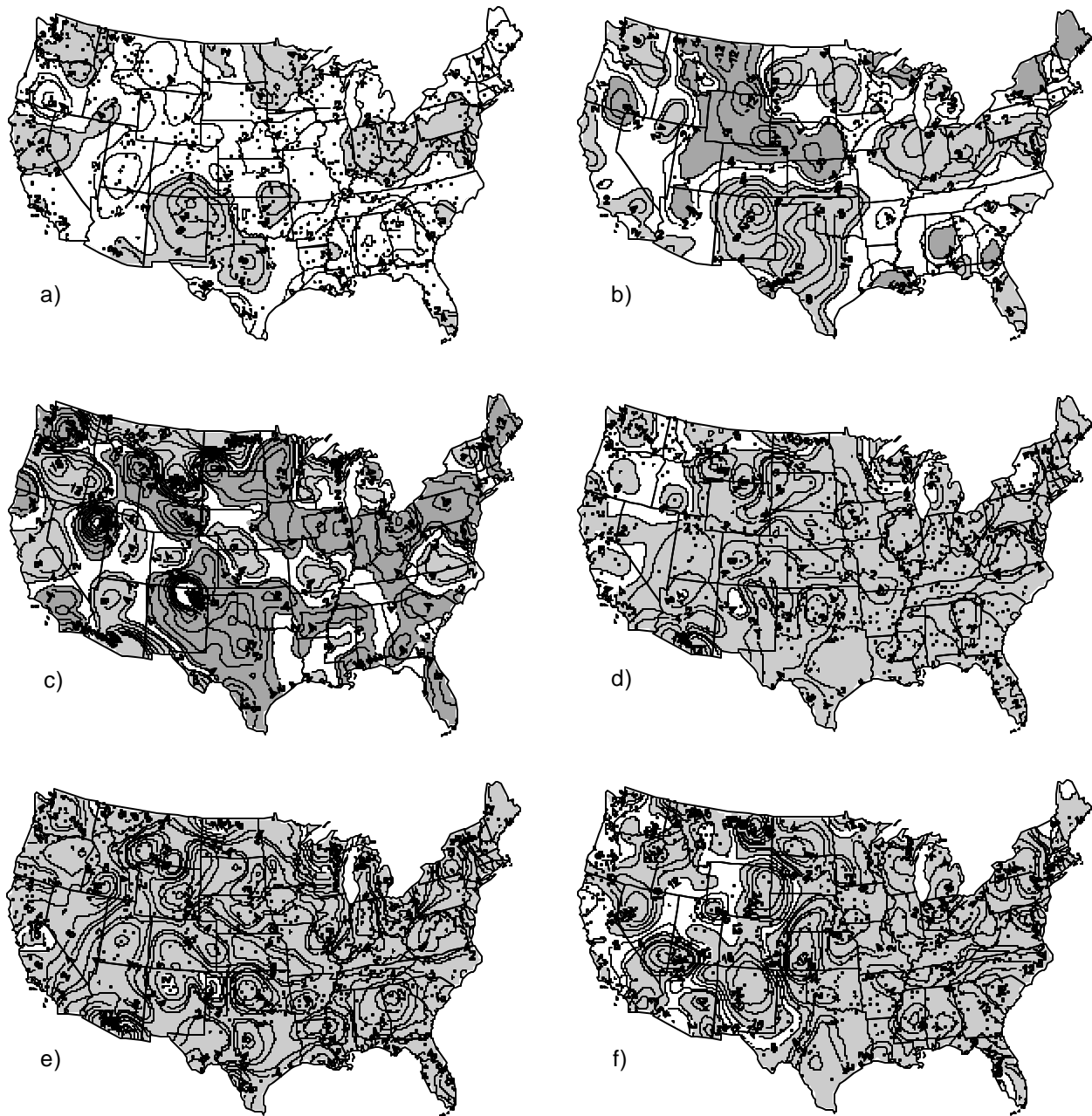


Figure 37. Spring 1971-1999 trends in storm characteristics for a) storm totals, b) storm duration, c) storm intensity, d) maximum 30-minute precipitation, e) storm EI, and f) number of storms. Trends are expressed as percent change per decade where negative trends are cross-hatched, positive trends are gray, and no trend is white. Black dots represent stations.

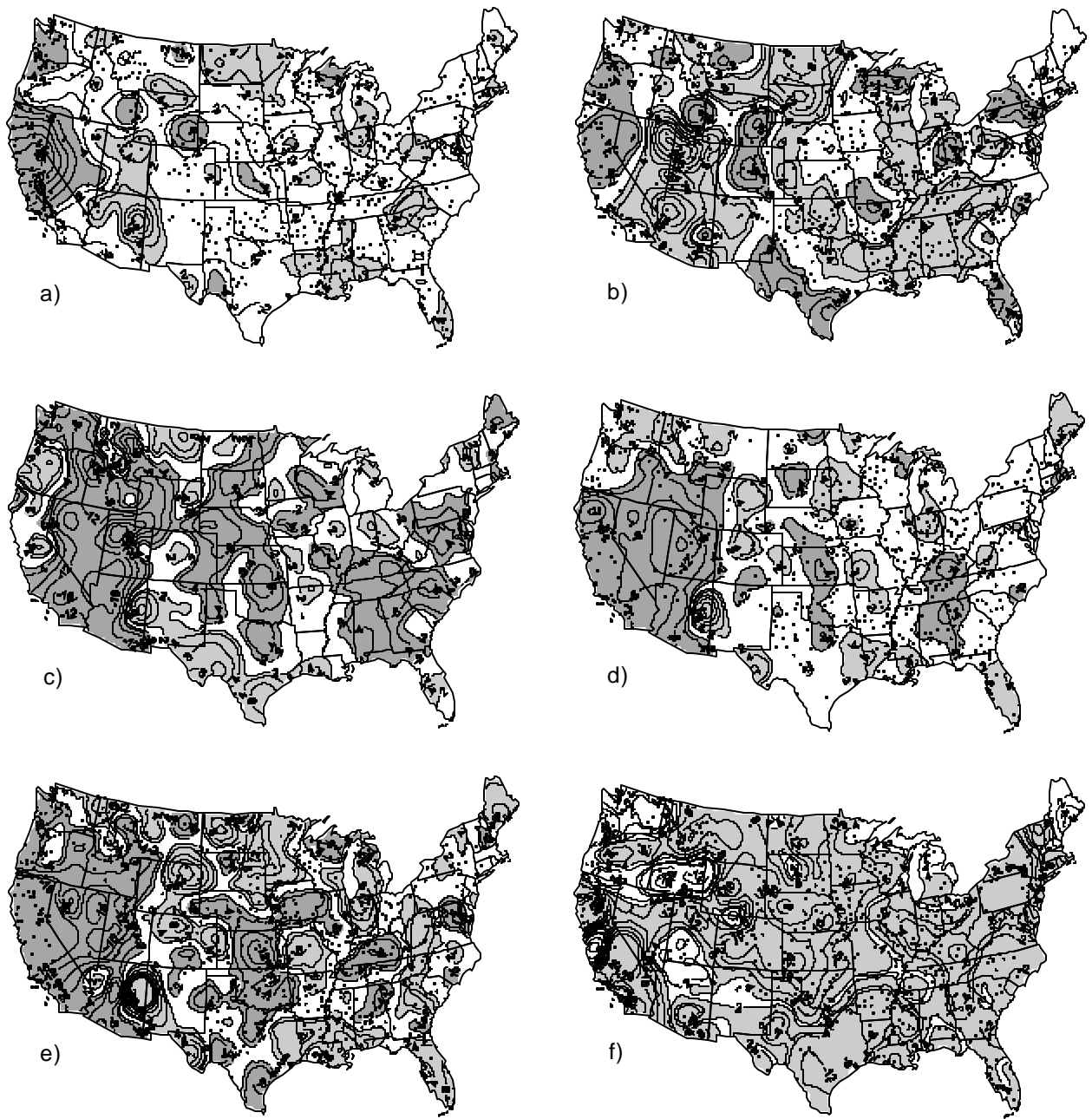


Figure 38. Summer 1971-1999 trends in storm characteristics for a) storm totals, b) storm duration, c) storm intensity, d) maximum 30-minute precipitation, e) storm EI, and f) number of storms. Trends are expressed as percent change per decade where negative trends are cross-hatched, positive trends are gray, and no trend is white. Black dots represent stations.

Fall Trend Maps

The trend for fall storm amounts (Figure 39a) became more coherent than in summer, with a large band of increasing storm amounts from the Texas Panhandle to Maine, in the Southeast, and in the Northwest. Decreases were found in southern Texas and in a number of the Rocky Mountain states. Storm durations (Figure 39b) showed that the United States was roughly divided in half, with decreases in the western half and increases in the eastern half. Storm intensities (Figure 39c) were more complex with bands of alternating trends. Starting along the West Coast, increased intensities were followed by decreased intensities in the Interior West, increased intensities in the eastern Rockies and Plains, and decreased intensities in the eastern half of the United States. While the patterns for storm totals and duration did not alternate, their complex interaction led to this banded pattern. Maximum 30-minute precipitation trends (Figure 39d) showed a large area of increased intensity in the region from Arizona to Florida, a pattern that continued into the central Plains and ended in western Montana. There was a complex pattern of increased EI amounts (Figure 39e) across the Southwest, the Southeast, and the Northeast, and in portions of the Midwest and Plains. Intense regions of decreased EI amounts extended from Idaho to California, the northern Plains, the western Corn Belt, and the central Appalachians. The strongest gradient was between large increases in eastern Nebraska and large decreases in neighboring Iowa and western Nebraska. The general pattern had contributions from trends in storm amounts and the maximum 30-minute precipitation. In particular, eastern Nebraska showed increases in both variables while Iowa showed decreases in both variables, leading to the strong differences over short distances. Storm number (Figure 39f) increased substantially over the Northwest, northern Great Plains, and East, while decreases were evident in the Ohio Valley, southern Great Plains, and the West.

Conclusion

This analysis showed many substantial trends in storm characteristics, especially in the seasonal maps. In many cases, a particular region may have experienced an upward trend in spring and a downward trend in fall, which leads to no change on the annual map. The second important point was that many trends in storm characteristics do not behave the same way across the United States. Some features were on a relatively small scale, spanning a few states. This was not surprising, given the current understanding of climate change and variability, which points toward very few atmospheric variables changing uniformly over the United States. The disrupted nature of some patterns also could be reflecting differing station start dates, to which a trend analysis would be very sensitive. In general, storm duration trends drove storm precipitation trends. Storm 30-minute maximum intensity trends generally drove the storm erosivity trends. All seasons, except fall, had increases in storm frequency in the western two-thirds of the United States.

Interannual and Interdecadal Variations

The temporal stability of storm characteristics underlying the R-factor depends largely on hemispheric and global teleconnections that influence atmospheric circulation patterns. Mid-tropospheric teleconnections, such as the Pacific/North American Pattern (PNA) and North Atlantic Oscillation (NAO) change the locations of storm tracks and their resulting precipitation on time scales of weeks to seasons (Leathers et al., 1991; Hurrell, 1995). Their effects are

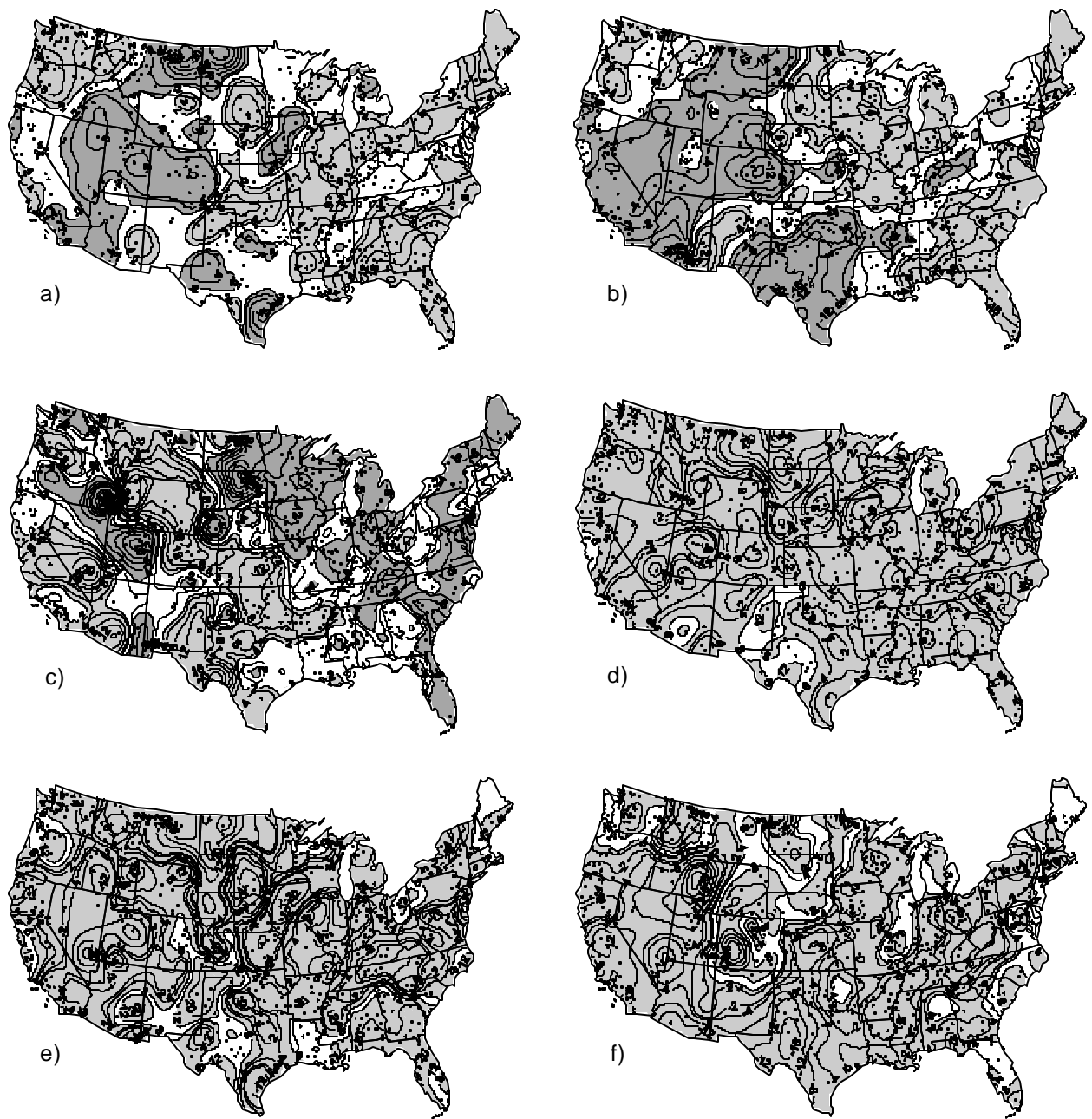


Figure 39. Fall 1971-1999 trends in storm characteristics for a) storm totals, b) storm duration, c) storm intensity, d) maximum 30-minute precipitation, e) storm EI, and f) number of storms. Trends are expressed as percent change per decade where negative trends are cross-hatched, positive trends are gray, and no trend is white. Black dots represent stations.

especially pronounced in the winter, when the polar front jet stream dominates precipitation over the conterminous United States. Global atmospheric-oceanic modes referred to as El Niño and La Niña events of the Southern Oscillation (ENSO) originate in the tropical Pacific Ocean and can alter storm tracks, subtropical ridge locations, and precipitation patterns in all seasons over periods of a year or longer (Ropelewski and Halpert, 1987, 1989). Finally, the Pacific/Decadal Oscillation (PDO) establishes new epochs every 15-25 years, altering both tropical and extratropical sea surface temperatures (SSTs) in the Pacific Ocean, and thus changing the pattern of SST forcing of atmospheric circulation over North America (Mantua et al., 1997).

The degree of temporal variability in storm characteristics can depend on all intraannual, interannual, and interdecadal time scales working simultaneously. However, in order to concentrate on the roles of specific generators of interannual variability in storm structures, each teleconnection was examined individually. Relationship patterns in each season and for each mode of variation were derived from composite differences between the five years with the most positive extreme atmospheric mode in a season and the five years with the most negative extreme atmospheric mode in the same season. Six seasonal storm statistics were examined: number of storms, storm total, storm duration, storm intensity, 30-minute maximum storm intensity, and storm erosivity. Only large storms used in the R-factor calculation were considered. Qualifying stations had less than 25 percent of their records missing during the 1970s and 1990s, and at least one valid season with one storm or more for each atmospheric circulation mode. For each storm characteristic statistic, the difference between the positive and negative modes was divided by the 1971-1999 average for that season to yield a percentage difference, which was mapped and compared spatially. While all modes of atmospheric circulation variation mentioned above have been shown to influence total precipitation in some regions and locations, actual effects on individual storm characteristics have not yet been ascertained, and may reveal nonlinear impacts on storm erosivity not expected from seasonal precipitation totals.

Winter Teleconnections

Teleconnections were identified by principal component analysis (PCA) of 50 hPa (hectopascals) geopotential heights over the months or seasons in question, with the PCA score time series representing the temporal strength of each mode over time (Barnston and Livezey, 1987). Two of the most important atmospheric circulation modes with impacts on the conterminous United States storm tracks during winter are the PNA and the NAO. The PNA represents changes in the amplitude of mid-tropospheric long waves over the eastern Pacific Ocean and North America (Wallace and Gutzler, 1981). A season with a positive PNA index is associated with north-south amplification of the climatological western ridge and eastern trough, and a negative PNA index season has a more zonal (less amplified) flow. The NAO forms over the North Atlantic Ocean and represents a low pressure/high pressure dipole oriented north-south across the polar front jet stream (Marshall et al., 2001). When both pressure centers are stronger than normal, the NAO index is positive and the jet stream is strong and zonal; when both pressure centers are weak, the NAO index is negative and the jet stream meanders. Even though the NAO is located downwind of North America, the wave pattern of the jet stream over the Atlantic propagates wave energy upwind that influences the position and amplitude of long waves over North America. Although interannual variations of most atmospheric teleconnections are normal and should not influence the long-term R-factor, both the PNA and NAO have, in fact, shown

substantial interdecadal variability at times, which may change the frequency and magnitude of their impacts on storm characteristics.

The difference in the number of storms between positive (1976-1977, 1980-1981, 1982-1983, 1985-1986, and 1997-1998) and negative (1971-1972, 1978-1979, 1981-1982, and 1988-1989) PNA winters resulted in a spatially coherent pattern. Only four strong negative cases were available in the 1971-1999 period. The positive PNA mode tended to have 20-40 percent fewer storms than the negative mode in the Ohio Valley/Tennessee Valley region and the Front Range of the Rockies, and 20 percent more in the Great Plains and northern Midwest (Figure 40a). Storm total precipitation was also larger in the Great Plains and smaller in the Ohio Valley (Figure 40b), due mostly to larger storm durations in the Great Plains (Figure 40c), and less storm intensity in the Ohio Valley (Figure 40d). The storm 30-minute maximum intensity difference pattern was somewhat weak (Figure 40e), indicating that the most important factor in determining differences in storm erosivity (Figure 40f) was storm total precipitation. Interestingly, the storm erosivity differences are quite substantial, indicating that storms were both less frequent and less erosive in the Ohio Valley/Tennessee Valley area, and more frequent and more erosive in the northern Great Plains and Midwest. However, in the latter case, many precipitation events still would arrive as snow, and their erosivity would depend on the speed and magnitude of spring snow melt.

The NAO case displayed some very interesting patterns when the differences between the positive (1980-1981, 1983-1984, 1988-1989, 1994-1995, and 1998-1999) and negative mode winters (1976-1977, 1977-1978, 1978-1979, 1995-1996, and 1997-1998) were examined. The northern tier and the central United States experienced more storms in a positive NAO condition (Figure 41a), while the southern tier of the United States had a reduction in storms, especially in the Southeast and Southwest. This pattern corresponded to the lower amplitude, west-east flow that kept the storm track to the north during positive NAO periods, while a higher amplitude negative NAO winter brought more storms to the southern latitudes. Although there may have been more storms, individual storm total precipitation displayed negative differences in the north and some weakly positive differences in the south (Figure 41b). With zonal flow, storms may be more frequent, but the duration was reduced in the north-central United States (Figure 41c) and increased in the cyclogenetic regions of the northern Rockies. The southern United States increase in storm totals was due to increased storm intensity (Figure 41d) and/or 30-minute maximum intensity (Figure 41e). A substantially nonlinear additive effect results in the storm erosivity in the south-central and southeastern United States showing a broad pattern of positive differences (Figure 41f). This was especially important in the south-central region, where there was only a minor decrease in numbers of storms, while the erosivity of each storm increased substantially in areas where most of the winter precipitation fell as rain. An increasing frequency of the positive NAO over time or a positive NAO mode preference during a multi-decadal epoch would be reflected as an increase in the R-factor in the southern Great Plains.

El Niño and La Niña Events of the Southern Oscillation

Warm and cold extremes of ENSO are well known in the climatological literature [for a recent review, see Diaz et al., 2001], and will not be discussed in detail here. In this examination of ENSO impacts on storm structure variables, the five strongest El Niño events were compared to the five strongest La Niña events in each of the four seasons. The Multi-variate ENSO Index

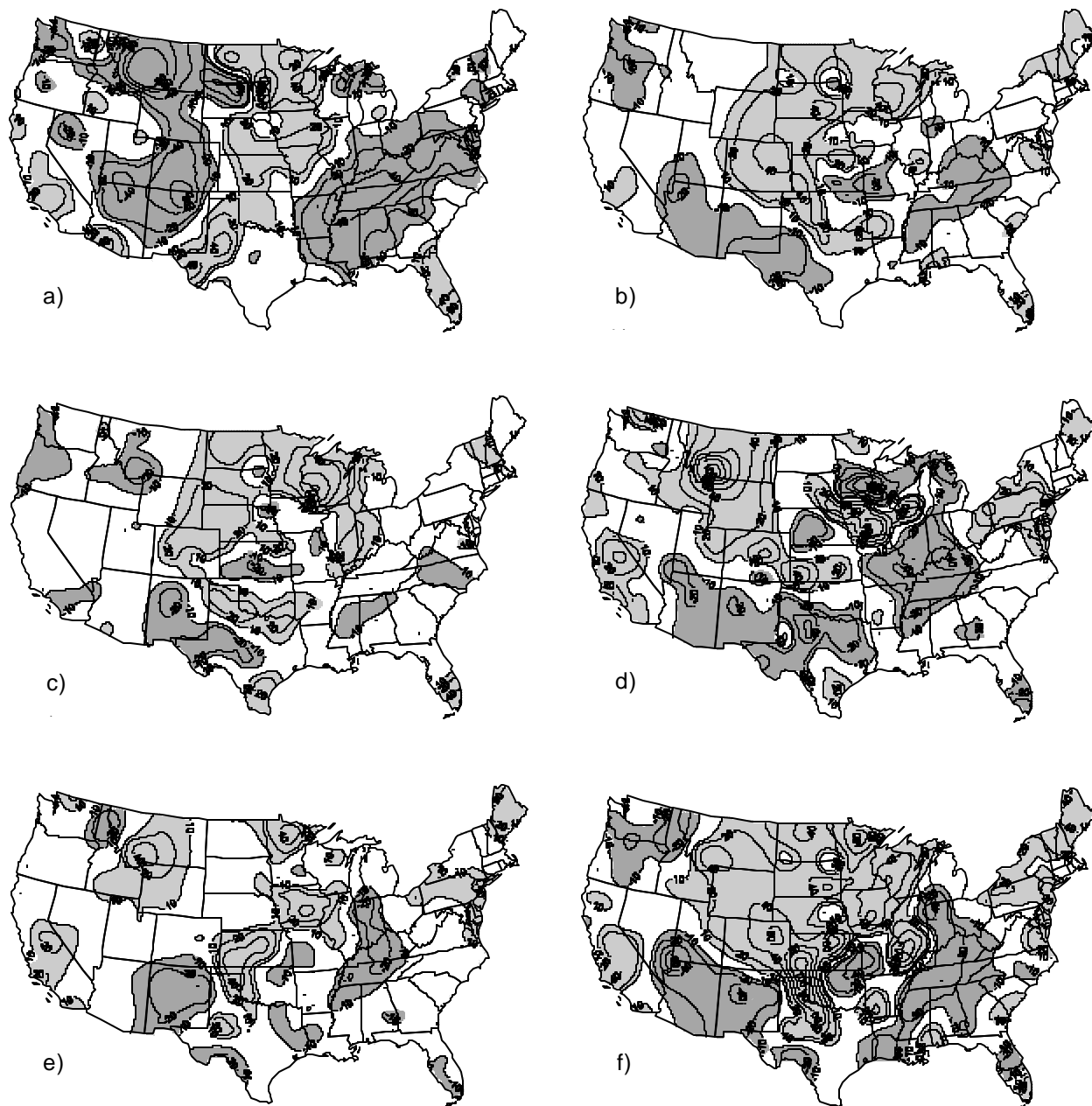


Figure 40. Percentage differences between storm statistics for positive PNA and negative PNA winter seasons for the period 1971-1999: a) number of storms, b) storm precipitation total, c) storm duration, d) storm precipitation intensity, e) storm 30-minute maximum precipitation intensity, and f) storm erosivity. Positive differences are gray, negative differences are cross-hatched. Dots represent stations that have at least one valid storm for each event mode. A valid storm must have a precipitation total greater than 12.7 mm or a precipitation maximum intensity greater than 25.4 mm hr⁻¹.

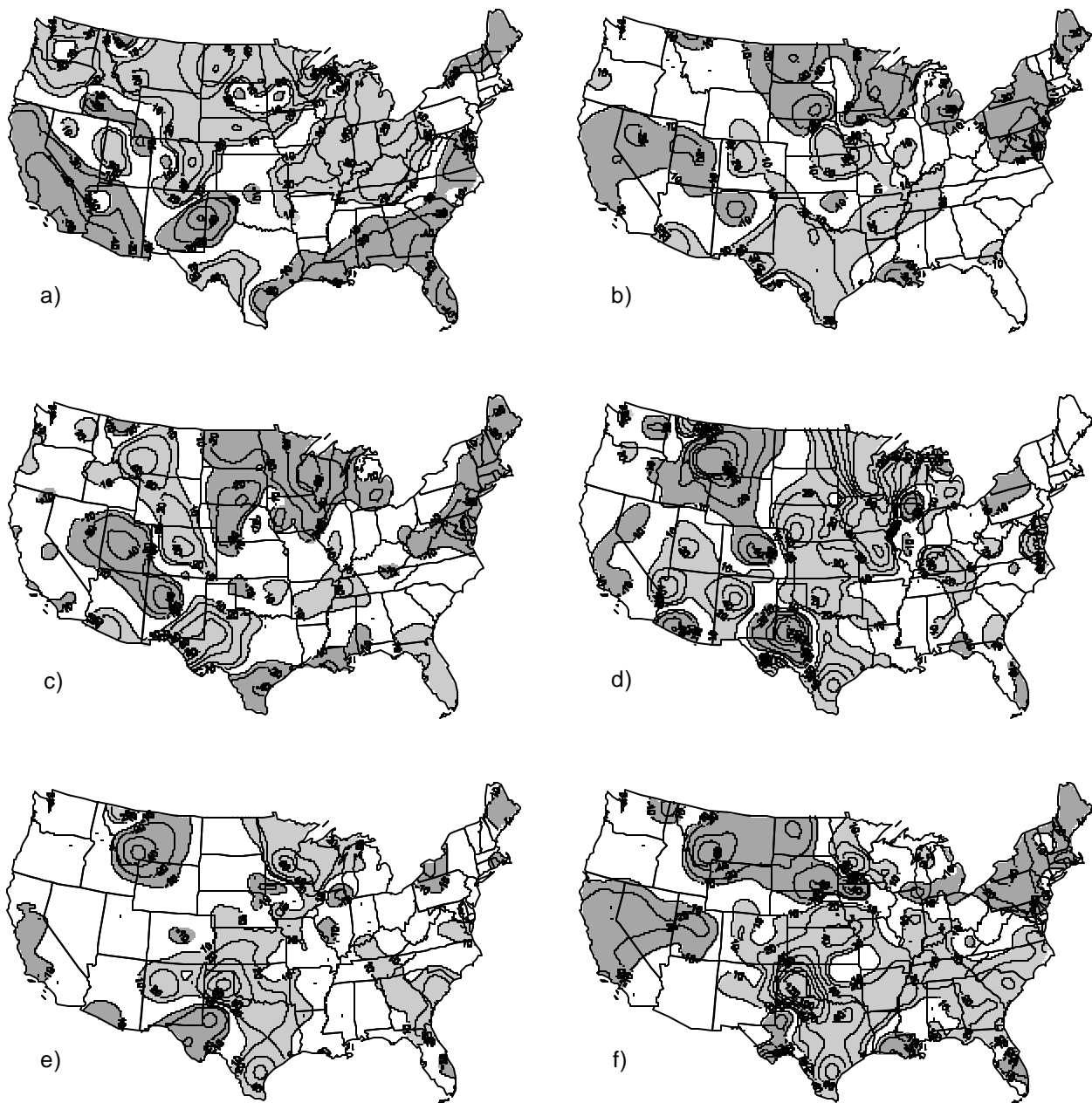


Figure 41. Percentage differences between storm statistics for positive NAO and negative NAO winter seasons for the period 1971-1999: a) number of storms, b) storm precipitation total, c) storm duration, d) storm precipitation intensity, e) storm 30-minute maximum precipitation intensity, and f) storm erosivity. Positive differences are gray, negative differences are cross-hatched. Dots represent stations that have at least one valid storm for each event mode. A valid storm must have a precipitation total greater than 12.7 mm or a precipitation maximum intensity greater than 25.4 mm hr⁻¹.

(MEI) of Wolter and Timlin (1998) was used to indicate the overall strength of the ENSO events. This index is most commonly available as a 2-month average, so seasonal values were generated by averaging the pair of relevant 2-month averages, such as December-January and January-February for a winter value. This procedure tends to weight the core of the season most heavily, as the central month receives twice the weight of the end months. The MEI has a great advantage over simple sea level pressure or sea surface temperature indices of ENSO in that it includes entire fields of variables for the Pacific Ocean: sea level pressure, sea surface temperature, air temperatures above the surface, north-south and east-west winds, and cloudiness. A large positive MEI corresponds to an El Niño event, and a large negative MEI corresponds to a La Niña event.

The winter season differences in storm structure variables between the El Niño (1972-1973, 1982-1983, 1986-1987, 1991-1992, and 1997-1998) and La Niña (1973-1974, 1975-1976, 1988-1989, and 1998-1999) events (only four strong La Niña cases were available in the 1971-1999 period) displayed some classic response patterns. The number of storms was larger during El Niño in the southern tier of the United States and smaller in the Pacific Northwest and Ohio Valley (Figure 42a). This matched well with the shift of the storm track into California and the Southwest. Interestingly, both the number of storms and the storm precipitation total (Figure 42b) were greater in the northern Great Plains, as a trough on the West Coast tended to steer storms into the Great Plains and western Midwest. Both numbers of storms and storm precipitation totals diminished during El Niño in the eastern Midwest, as storms passed by to the west or moved further south and east in an amplified East Coast trough. Storm duration differences (Figure 42c) were larger in the Great Plains than storm total differences, causing storm intensity (Figure 42d) in the central United States to be substantially less during El Niño events. Because 30-minute maximum intensity also was lowered (Figure 42e), this left a large part of the Midwest and south central United States with decreased storm erosivity (Figure 42f) and decreased storm numbers. These factors lead to a decline in the winter R-factor component over this area during El Niño events. In California, on the other hand, increased numbers of storms of larger total precipitation and higher 30-minute maximum intensity lead to a well established image of high individual storm erosivity and large total erosion effects during El Niño events.

Spring differences between El Niño (1983, 1987, 1992, 1993, and 1998) and La Niña (1971, 1974, 1975, 1976, and 1999) responses of storm structure variables substantially shifted geographically compared to the winter response. The number of storms (Figure 43a) was 20-40 percent larger during El Niño along the whole West Coast and the northeast coast of the United States, with a large region of diminished numbers of storms in the central United States. Split jet flow in the spring could take storms into southern or northern portions of the West Coast, then around the Great Plains and Midwest, which were sometimes dry during El Niño springs and wet during La Niña springs. Storm total precipitation was also higher in parts of the far western and Mid-Atlantic states (Figure 43b). The High Plains states, Midwest, and Northeast had increased storm duration during El Niño events (Figure 43c), which led to a decrease in storm intensity (Figure 43d). The 30-minute maximum intensity was also less in the central United States during El Niño (Figure 43e), which coincided with higher observed frequencies of severe weather during La Niña events. The storm erosivity difference pattern (Figure 43f) largely followed the 30-minute maximum intensity difference pattern, with predominantly higher erosivity in the far west and lower erosivity in the Midwest during El Niño events. Because the West also had increased numbers of storms during El Niño, the combination could lead to substantially increased erosion during El Niño springs.

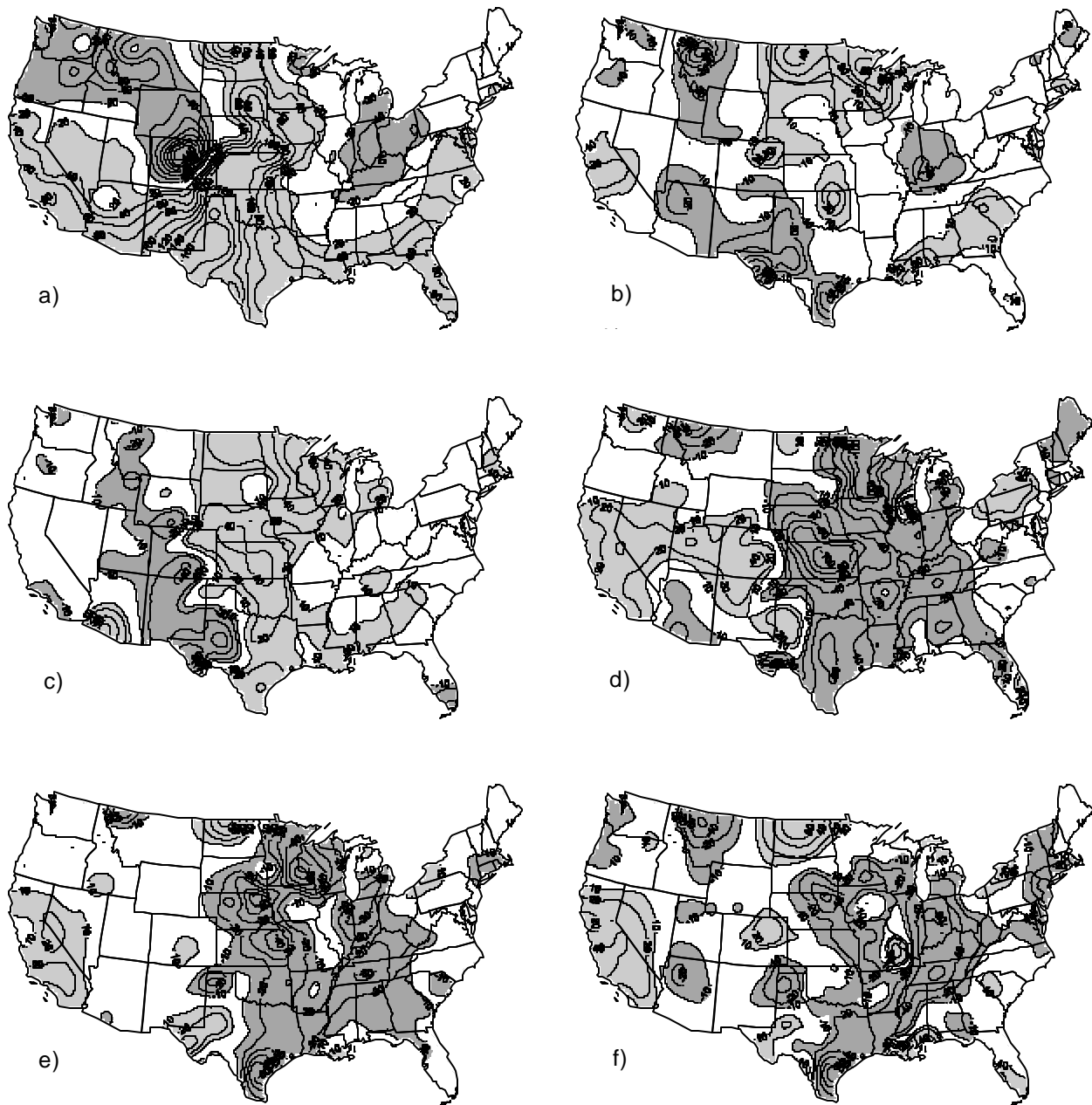


Figure 42. Percentage differences between storm statistics for El Niño and La Niña events during winter months for the period 1971-1999: a) number of storms, b) storm precipitation total, c) storm duration, d) storm precipitation intensity, e) storm 30-minute maximum precipitation intensity, and f) storm erosivity. Positive differences are gray, negative differences are cross-hatched. Dots represent stations that have at least one valid storm for each event mode. A valid storm must have a precipitation total greater than 12.7 mm or a precipitation maximum intensity greater than 25.4 mm hr⁻¹.

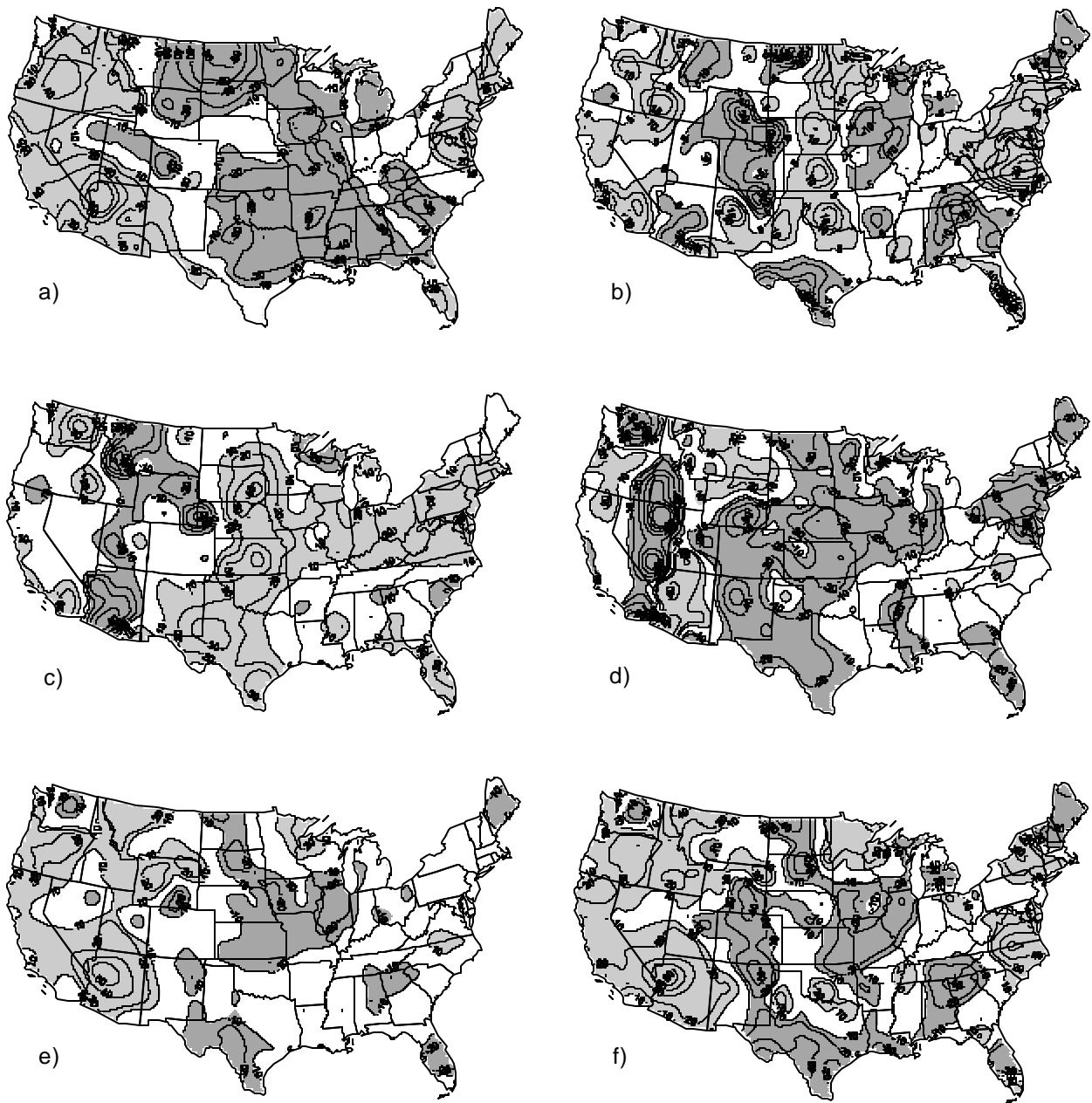


Figure 43. Percentage differences between storm statistics for El Niño and La Niña events during spring months for the period 1971-1999: a) number of storms, b) storm precipitation total, c) storm duration, d) storm precipitation intensity, e) storm 30-minute maximum precipitation intensity, and f) storm erosivity. Positive differences are gray, negative differences are cross-hatched. Dots represent stations that have at least one valid storm for each event mode. A valid storm must have a precipitation total greater than 12.7 mm or a precipitation maximum intensity greater than 25.4 mm hr⁻¹.

Summer storm characteristic differences display some surprisingly coherent features, even though El Niño (1972, 1982, 1983, 1987, and 1997) and La Niña (1971, 1973, 1974, 1975, and 1988) influences were not considered to be as strong in these months. The number of storms was higher during El Niño, not only along the West Coast, but also in the north-central United States (Figure 44a). This North-Central U.S. pattern likely was related to the tendency for La Niña events to have droughts during summer in this region, resulting in fewer storms. Storms were less common in the South and eastern United States during El Niño. Storm precipitation totals displayed a very weak difference pattern (Figure 44b), with only a few noteworthy centers of reduced totals during El Niño events in the West and Great Plains. Interestingly, storm duration differences (Figure 44c) and storm intensity differences (Figure 44d) almost were reversed in the western third of the United States, with increased duration and lowered intensity in the Southwest during El Niño and vice versa in the Northwest. Thirty-minute intensity differences also matched this pattern (Figure 44e). The final storm erosivity difference map had more noise (Figure 44f), but still showed increased erosivity in the northern tier of states during an El Niño event relative to a La Niña event, and a relative decrease in the southern tier of states. These areas corresponded in a cumulative way with the pattern of storm number difference. El Niño summers had increased numbers of storms and storm erosivity in the northern Plains, for instance, while La Niña summers had more storms and stronger storm erosivity in the Southeast.

In fall, some of the difference patterns between El Niño (1972, 1982, 1987, 1994, and 1997) and La Niña (1971, 1973, 1974, 1975, 1988, 1998, and 1999) events, observed during the winter season, again became prominent. A total of seven La Niña cases were used because the differences among the last three were too small to differentiate. A dipole structure of enhanced California and reduced Northwest storm numbers during El Niño event becomes apparent once again (Figure 45a). However, unlike the winter, the storm numbers were not larger in the south-central United States, and were only slightly more common in the Southeast. Storm precipitation totals tended to be less during El Niño falls throughout much of the eastern half of the United States (Figure 45b), but the difference pattern was somewhat heterogenous. The Rocky Mountains seem to have had longer storm durations during El Niño (Figure 45c), resulting in negative storm intensity differences over the region (Figure 45d). The eastern United States, on the other hand, had virtually no difference in storm duration between El Niño and La Niña events, but did show decreased storm intensity during El Niño events that corresponded to an area of decreased storm total precipitation. The reduction in intensity in the eastern United States during El Niño events carried over to 30-minute maximum intensity (Figure 45e), resulting in a large area with 20-40 percent reductions in storm erosivity (Figure 45f). In fact, much of the United States showed negative differences in storm erosivity in fall.

Some of the El Niño minus La Niña difference patterns presented above seem to represent large continuous areas, even though some areas contained stations lacking a difference signal. Although efforts were made to identify and use the highest quality stations, some did indeed produce differing results due to small numbers of valid cases. Some patterns may have been made clearer with additional quality control of stations, or by pooling stations over small regional grids. Comparisons of El Niño and La Niña storm precipitation characteristics indicated a potential for all seasons to have impacts from these modes of global atmospheric-oceanic teleconnections. If a change in the frequency or magnitude of either mode occurs over time, as a secular trend or a multidecadal oscillation, there may be considerable impacts on R-factor calculations.

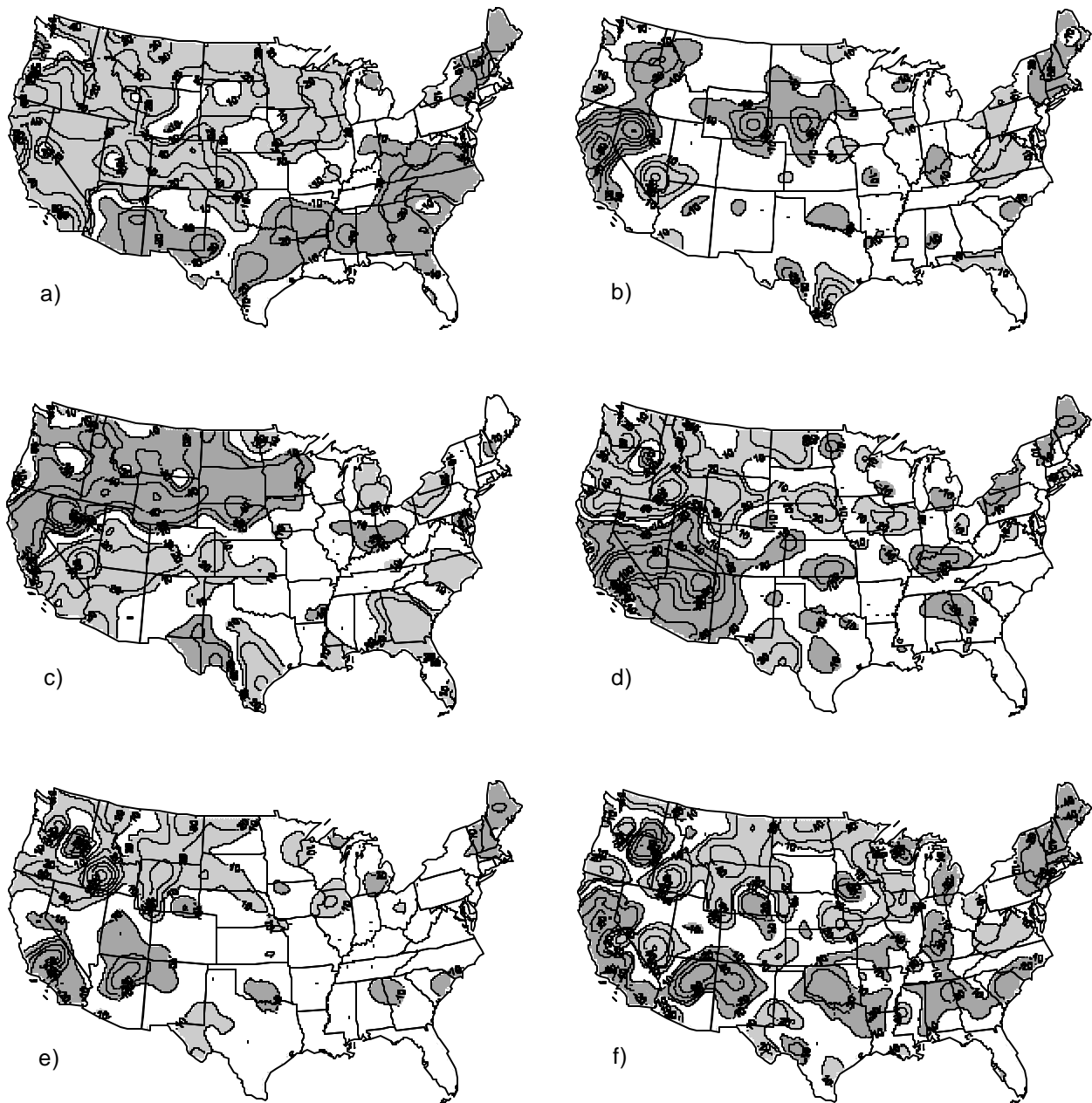


Figure 44. Percentage differences between storm statistics for El Niño and La Niña events during summer months for the period 1971-1999: a) number of storms, b) storm precipitation total, c) storm duration, d) storm precipitation intensity, e) storm 30-minute maximum precipitation intensity, and f) storm erosivity. Positive differences are gray, negative differences are cross-hatched. Dots represent stations that have at least one valid storm for each event mode. A valid storm must have a precipitation total greater than 12.7 mm or a precipitation maximum intensity greater than 25.4 mm hr⁻¹.

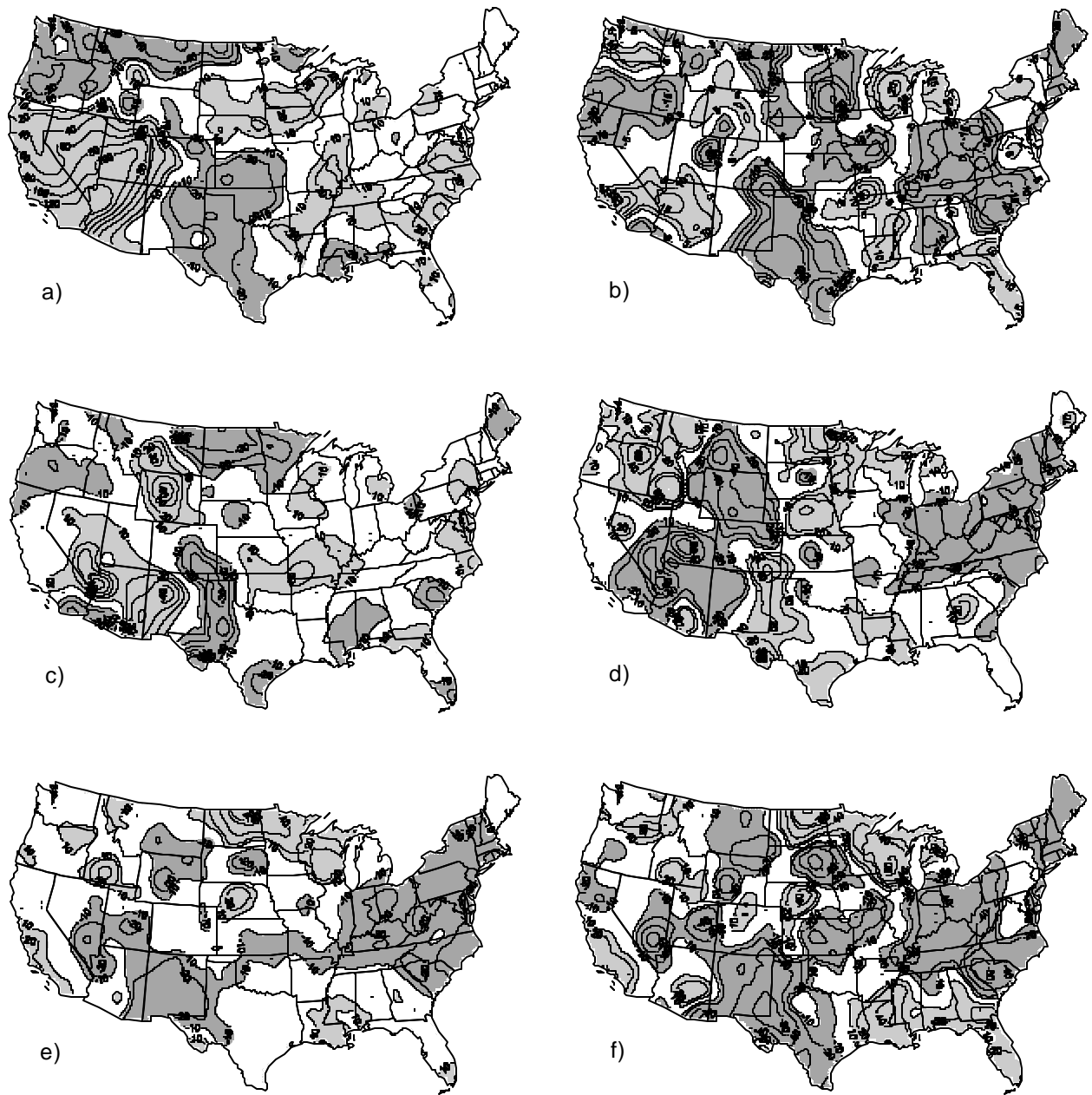


Figure 45. Percentage differences between storm statistics for El Niño and La Niña events during fall months for the period 1971-1999: a) number of storms, b) storm precipitation total, c) storm duration, d) storm precipitation intensity, e) storm 30-minute maximum precipitation intensity, and f) storm erosivity. Positive differences are gray, negative differences are cross-hatched. Dots represent stations that have at least one valid storm for each event mode. A valid storm must have a precipitation total greater than 12.7 mm or a precipitation maximum intensity greater than 25.4 mm hr⁻¹.

The Pacific Decadal Oscillation

The slow frequency changes in the Pacific Basin north of 20°N were formed into a PDO index by using PCA to identify the chief mode of variation in monthly SST anomalies (Mantua et al., 1997). Monthly mean regional SSTs were removed from these SST anomalies and thus any potential trends were removed from the data. The final PDO index represents one of the most clearly defined records of interdecadal change in climatology. Located upstream of North America, the PDO also has connections to ENSO cycles and may be related to changes in the frequency and/or magnitude of El Niño or La Niña events. In addition, slow SST changes in the North Pacific can have direct impacts on atmospheric circulations over North America through a variety of atmospheric-oceanic feedbacks. Therefore, it was useful to examine the differences of storm characteristics between the positive and negative modes of the PDO, as this is one of the more likely ways in which the storm structures underlying the R-factor may change over decadal time scales.

During the 1971-1999 period of record of this study, the PDO changed sign twice. Prior to June 1976, the PDO was in a negative mode, maintained a positive mode thereafter until June 1998, and then again switched to a negative mode. Therefore, there were many more positive PDO cases than negative PDO cases during this study period. There were enough seasons with negative PDO to justify this examination. However, it should be noted that the amplitudes of the storm characteristic differences were more strongly determined by the negative sign periods, as the amplitude of a composite usually declines with the number of members, as in the case of the positive PDO composites.

Winter composite difference between positive and negative PDO numbers of storms had a very high amplitude (Figure 46a). Most of the northern half of the United States experienced 20-80 percent fewer storms during positive PDO winters, while the southwestern United States had 20-60 percent more storms during positive PDO winters. Storm precipitation totals, on the other hand, did not display a substantial difference (Figure 46b). Only the Great Plains and part of the West showed positive differences between positive and negative PDO states. Storm duration seemed to be associated with the Great Plains increase in precipitation totals during positive PDO years (Figure 46c). Both the storm intensity (Figure 46d) and the 30-minute maximum intensity (Figure 46e) displayed an east-west dipole, where the intensity differences were negative in the East and positive in the West. This resulted in a robust pattern of positive storm erosivity differences in the western United States and negative differences in the eastern United States (Figure 46f). Because the Pacific Ocean recently entered the negative mode of the PDO, storm erosivity should increase in the Southeast in the coming decade.

The spring PDO difference in numbers of storms again displayed a large pattern of positive differences in the West and negative differences between the Rockies and the East Coast (Figure 47a). This would imply a greater number of storms in the eastern two-thirds of the United States during the present negative PDO regime. Although there were very few areas of the country with storm precipitation total differences of any magnitude (Figure 47b), the Southwest displayed a coherent region of positive differences in storm duration (Figure 47c) and negative differences in storm intensity (Figure 47d). Thus, the pattern of storm 30-minute maximum intensity differences (Figure 47e) were largely coincident with storm erosivity differences (Figure 47f), especially in the southwestern United States.



Figure 46. Percentage differences between storm statistics for positive PDO and negative PDO time periods during winter months for the period 1971-1999: a) number of storms, b) storm precipitation total, c) storm duration, d) storm precipitation intensity, e) storm 30-minute maximum precipitation intensity, and f) storm erosivity. Positive differences are gray, negative differences are cross-hatched. Dots represent stations that have at least one valid storm for each event mode. A valid storm must have a precipitation total greater than 12.7 mm or a precipitation maximum intensity greater than 25.4 mm hr⁻¹.

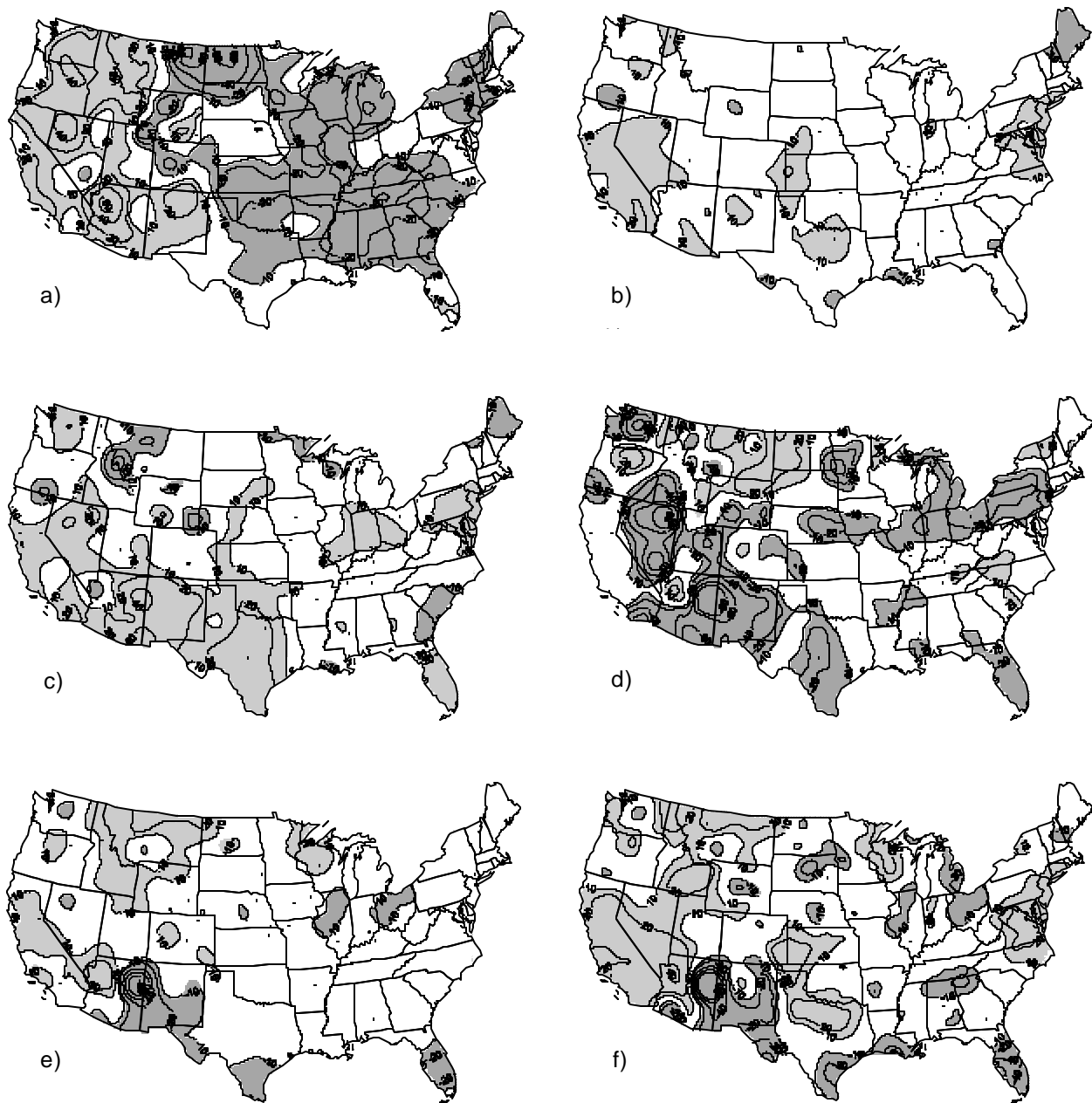


Figure 47. Percentage differences between storm statistics for positive PDO and negative PDO time periods during spring months for the period 1971-1999: a) number of storms, b) storm precipitation total, c) storm duration, d) storm precipitation intensity, e) storm 30-minute maximum precipitation intensity, and f) storm erosivity. Positive differences are gray, negative differences are cross-hatched. Dots represent stations that have at least one valid storm for each event mode. A valid storm must have a precipitation total greater than 12.7 mm or a precipitation maximum intensity greater than 25.4 mm hr⁻¹.

Summer PDO differences continued to follow a warm season pattern: only the Pacific Ocean had pronounced influences west of the Front Range of the Rocky Mountains. In all the difference maps, the signal in the eastern two-thirds of the United States was rather scattered. Both the storm number differences (Figure 48a) and storm total precipitation (Figure 48b) displayed weak difference patterns. The West showed a broad pattern of positive differences in storm duration in the Southwest and negative differences in the northern High Plains (Figure 48c), with the opposing pattern occurring with storm intensity (Figure 48d). There was a substantial strip through California, Nevada, and Oregon that showed negative differences in 30-minute maximum intensities (Figure 48e) which resulted in a similar pattern of storm erosivity differences (Figure 48f). This would indicate an increase in storm erosivity during the present negative PDO mode.

Fall PDO difference maps indicated a large area of negative differences in the number of storms in the Great Plains and northern Rocky Mountains (Figure 49a). The intermountain region, on the other hand, showed a substantially positive number difference, before the negative differences dominated on the West Coast. In the present negative regime, this would indicate increased numbers of storms on the West Coast and Great Plains, with an area of decreased numbers of storms in between. The northern Plains also showed a weak negative difference signal in both storm precipitation total (Figure 49b) and storm duration (Figure 49c). In the negative PDO regime, this would indicate increased erosivity of storms in the northern Plains. There were widespread negative differences in storm intensity in the western mountains (Figure 49d), but very little signal in 30-minute storm intensity differences (Figure 49e). The pattern of storm erosivities (Figure 49f) most closely follows that of the storm intensity.

Overall, the PDO differences seemed to have more importance in the western United States year round, but the signal extended to the East during the colder seasons of winter and spring with active jet streams crossing the Midwest and East. The most interesting finding was that large areas effectively were undergoing change as the climate system entered a negative PDO regime, and some changes in storm characteristics may be predictable. In any event, these findings indicated that the R-factor dependent on these storm characteristics may need to be recalculated on a regular basis, possibly every 10 years as is done with the official climatic normals.

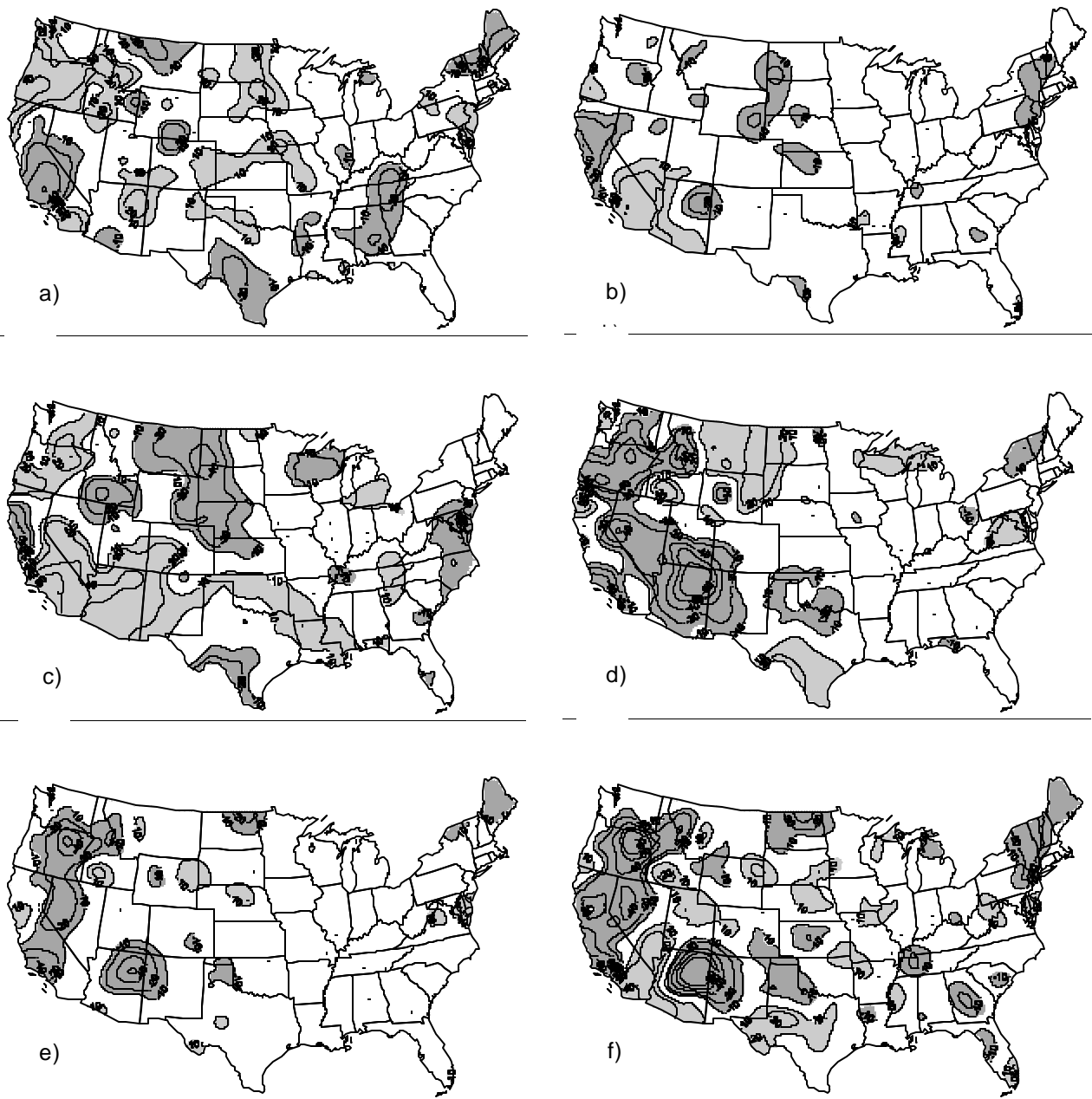


Figure 48. Percentage differences between storm statistics for positive PDO and negative PDO time periods during summer months for the period 1971-1999: a) number of storms, b) storm precipitation total, c) storm duration, d) storm precipitation intensity, e) storm 30-minute maximum precipitation intensity, and f) storm erosivity. Positive differences are gray, negative differences are cross-hatched. Dots represent stations that have at least one valid storm for each event mode. A valid storm must have a precipitation total greater than 12.7 mm or a precipitation maximum intensity greater than 25.4 mm hr⁻¹.

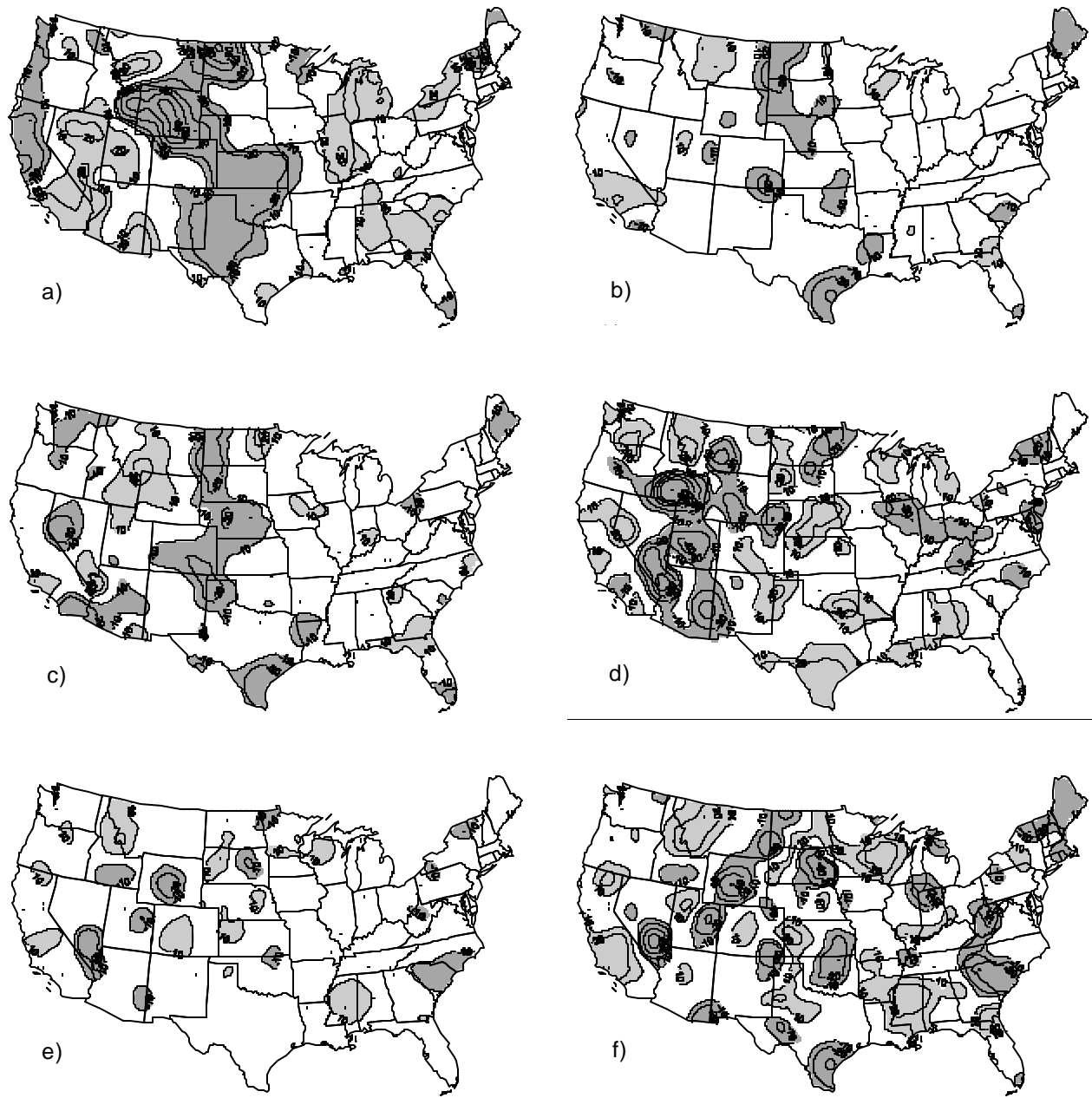


Figure 49. Percentage differences between storm statistics for positive PDO and negative PDO time periods during fall months for the period 1971-1999: a) number of storms, b) storm precipitation total, c) storm duration, d) storm precipitation intensity, e) storm 30-minute maximum precipitation intensity, and f) storm erosivity. Positive differences are gray, negative differences are cross-hatched. Dots represent stations that have at least one valid storm for each event mode. A valid storm must have a precipitation total greater than 12.7 mm or a precipitation maximum intensity greater than 25.4 mm hr⁻¹.

Summary

Soil erosion and nonpoint source pollution runoff rates are estimated using output from the Revised Universal Soil Loss Equation (RUSLE). The underlying influence of climate on surface transport processes as represented in the RUSLE is carried within one constant, the R-factor. The R-factors used vary only with location and not with time, and have been based on climate data from more than 40 years ago in most farming regions of the United States. Using an R-factor that does not change with time is appropriate if rainstorm amounts and intensities are temporally stationary. However, recently climatology has gone from the compilation of long-term statistics, assumed to be stable over time, to a more dynamic view with variability and change occurring on various temporal and spatial scales. A good example is the increased understanding of how Pacific sea surface temperatures change on a time scale of every few years (El Niño and La Niña), leading to significant changes in the climate over North America.

The purpose of this study was to process climate information from the most recent decades to update the R-factor, and to examine the nature of precipitation variation and change, its impact on the R-factor over space and time, and specifically, to test the hypothesis that storm erosivity is constant with time, i.e., temporally stationary. This was specifically addressed by developing a database of precipitation data and related information needed to calculate single-storm erosivity and cumulative R-factor for each half month of the year. In addition, the 10-year, single-storm erosivity index for each station was provided. A variety of storm characteristics were examined to see how they changed across the United States by season, how they changed over time by season, and their relationship to selected climatic forcing such as the Pacific sea surface temperatures and North American atmospheric circulation patterns.

The R-factor is a nonlinear, cumulative measure of the erosive energy contained in storm precipitation over the course of an average year. Ideally, this variable is calculated directly from the highest temporal resolution precipitation data available. Precipitation data collected every 15 minutes are the best data available with national coverage and a considerable time series available. Some undocumented quality difficulties with these data were discovered, however. A number of prorating and gap filling methodologies tested to overcome these difficulties proved satisfactory in solving all data quality problems except for one. Incorrect assignment of a flag that indicates a rain gauge was actively gathering precipitation data resulted in some records for some stations signaling zero precipitation levels rather than missing values. This problem, while not affecting daily or storm-by-storm calculations of erosivity (EI) with the 15-minute precipitation data, prevented the EIs from being properly combined over time into the R-factor. Therefore, instead of using the 15-minute data directly, EI statistics for accumulation into R-factors were calculated from more reliable daily data through the use of transfer functions. Daily precipitation totals were regressed using a power law relationship against the individual daily erosivity (EI) values calculated using 15-minute precipitation data from days when there were no data reliability problems. Because of the superior temporal coverage of the daily data, the EI values could be accumulated dependably into half-month EI values, and annual and long-term R-factors. These new R-factors were tested for spatial covariation, which was found to be minimal in even terrain, and related to the limited amount of station R-factor data from the past studies. The comparison with past R-factor studies indicated strongly that the methodologies used here adequately replicate old R-factors based on data from the 1930s to 1950s period. The observed general increases in R-factors in this study are related to increasing amounts of precipitation and qualifying (12.7

mm) storms, especially in the western United States. This agrees with recent studies showing increasing numbers of heavy precipitation events. Storms of less than 12.7 mm were excluded to be consistent with previous R-factor studies, while storms exceeding the 100-year amount were removed to address problems associated with outliers in the average calculations. In addition, the maximum single-storm EI for each year was used to compute the 10-year, single-storm EI for each site, using L-moments software.

To further explore the nature of storm precipitation variations and changes over time, individual storm statistics were examined to determine their annual cycle, long-term trends, and interannual and interdecadal variability in response to atmospheric-oceanic modes of climate system variation. Mean seasonal patterns of storm precipitation total, duration, intensity, 30-minute and 15-minute maximum intensity, kinetic energy, erosivity, and storm numbers were mapped for the conterminous United States. These analyses showed distinct patterns of precipitation change with the seasons and identified regions of strong gradients where climate change may first be noticed.

Trend analyses of storm precipitation variables over the 1971-1999 period directly indicated the lack of temporal stationarity of storm characteristics. Storm duration changes were especially important in determining the observed changes in storm precipitation totals. However, trends in storm 30-minute maximum intensity seemed to be more important in determining the patterns of storm erosivity change. In combination with trends in the frequency of 12.7 mm storms qualifying for the R-factor calculation, it is now very clear that the R-factor is undergoing trends that differ in sign and magnitude across the conterminous United States.

The examination of storm characteristic response to interannual and interdecadal variations also indicates that storm characteristics are responding at these time scales to large-scale climate system forcings. In the winter season, atmospheric teleconnections such as the Pacific/North American Pattern and the North Atlantic Oscillation were shown to influence not only storm tracks position and the number of storms at a location, but also the characteristics of individual storms. El Niño and La Niña events of the Southern Oscillation (ENSO events) had distinctive impacts on storm variables in every season of the year. Even the Pacific Decadal Oscillation (PDO), a slowly evolving pattern of sea surface temperature change in the North Pacific Ocean, has a clear effect on storm characteristics, especially in the western United States. Since the PDO switched to its negative mode in 1998, it is likely that the R-factor increasingly will be influenced to change in ways that correspond to its effects. Changes in the frequency and magnitude of the modes of ENSO events also are expected with this PDO shift. This study of storm characteristic variability clearly supports the need to understand the impacts of these changes on soil erosion and nonpoint source pollution runoff in the United States. Perhaps it is time to develop a new method of determining these impacts probabilistically, with a new R-factor that explicitly incorporates the distribution of possible R-factor states for a given year, instead of a single static number.

The results of R-factors derived from modern data compared to previous R-factors indicate conclusively that storm precipitation characteristics change sufficiently over time to warrant an evaluation of the necessity to recalculate R-factors on a regular basis. Because soil erosion by water practices is designed for long periods of time, great difficulty will be encountered if the R-factor is recalculated on a frequent basis, i.e., every 10 years. Perhaps a more reasonable approach would be to identify a period when the erosivity of storms was the greatest and develop the R-factor using that period and leave it stationary. This method, however, would not address the issue of future climate change, particularly if it resulted in more erosive storms.

Acknowledgments

This work was supported by cooperative agreement AG 68-7482-7-306 between the Water and Climate Center (WCC) of the United State Department of Agriculture Natural Resources Conservation Service (USDA-NRCS), and the Midwestern Regional Climate Center (MRCC) and the Illinois State Water Survey (ISWS). The views expressed herein are those of the authors and do not necessarily reflect those the USDA-NRCS WCC, the MRCC, or the ISWS. The authors gratefully acknowledge the discussions and direction provided by George Foster, Greg Johnson, James Marron, and Ken Renard, and the editing and graphics work of Eva Kingston and Linda Hascall.

References

- Barnston, A.G., and R.E. Livezey. 1987. Classification, Seasonality and Persistence of Low-Frequency Atmospheric Circulation Patterns. *Monthly Weather Review* **115**:1083-1126.
- Brown L.C., and G.R. Foster. 1987. Storm Erosivity Using Idealized Intensity Distributions. *Transactions of American Society of Agricultural Engineers* **30**:379-386.
- Diaz, H.F., M.P. Hoerling, and J.K. Eischeid. 2001. ENSO Variability, Teleconnections, and Climate Change. *International Journal of Climatology* **21**:1845-1862.
- Hammer, G. 1998. *Data Documentation for 15-Minute Precipitation Data TD-3260*. National Climatic Data Center, United States Department of Commerce, Ashville, NC, p. 21.
- Hosking, J.R.M. 1990. L-moments: Analysis and Estimation of Distributions Using Linear Combinations of Order Statistics. *Journal of the Royal Statistical Society B* **51**(1): 105-124.
- Hosking, J.R.M. 1991. *Fortran Routines for Using the Method of L-moments, Version 2*. IBM Research Report RC17097, IBM Research Division, T. J. Watson Research Center, Yorktown Heights, NY.
- Hosking, J.R.M., and J. R. Wallis. 1991. *Some Statistics Useful in Regional Frequency Analysis*. IBM Research Report RC17096, IBM Research Division, T. J. Watson Research Center, Yorktown Heights, NY.
- Huff, F.A. 1967. Time Distribution of Rainfall in Heavy Storms. *Water Resources Research* **3**:1007-1019.
- Huff, F.A., and J.R. Angel. 1992. *Rainfall Frequency Atlas of the Midwest*. Midwestern Climate Center and Illinois State Water Survey, Bulletin 71, Champaign, IL, p. 141.
- Hurrell, J.W. 1995. Decadal Trends in the North Atlantic Oscillation: Regional Temperatures and Precipitation. *Science* **269**:676-679.

- Istok, J.D. 1989. *Improved Erosivity Values for the Western United States*. Final completion report, Oregon State University, Corvallis, OR, p. 23.
- Karl, T.R., and R.W. Knight. 1998. Secular Trends in Precipitation Amount, Frequency, and Intensity in the United States. *Bulletin of the American Meteorology Society* **79**:231-241.
- Kunkel, K.E., K. Andsager, G. Conner, W.L. Decker, H.J. Kilaker, P. Naber Knox, F.V. Nurnberger, J.C. Rogers, K. Scheeringa, W.M. Wendland, J. Zandlo, and J.R. Angel. 1998. An Expanded Digital Database for the Climatic Resources Applications in the Midwestern United States. *Bulletin of the American Meteorology Society* **79**:1357-1366.
- Kunkel, K.E., K. Andsager, and D.R. Easterling. 1999. Long-term Trends in Extreme Precipitation Events over the Conterminous United States and Canada. *Journal of Climate* **12**:2515-2527.
- Leathers, D.J., B. Yarnal, and M.A. Palecki. 1991. The Pacific/North American Teleconnection Pattern and United States Climate. Part I: Regional Temperature and Precipitation Associations. *Journal of Climate* **4**:517-528.
- Mantua, N.J., S.R. Hare, Y. Zhang, J.M. Wallace, and R.C. Francis. 1997. A Pacific Interdecadal Climate Oscillation with Impacts on Salmon Production. *Bulletin of the American Meteorological Society* **78**:1069-1079.
- Marshall, J., Y. Kushnir, D. Battisti, P. Chang, A. Czaja, R. Dickson, J. Hurrell, M. McCartney, B. Saravanan, and M. Visbeck. 2001. North Atlantic Climate Variability: Phenomena, Impacts, and Mechanisms. *International Journal of Climatology* **21**:1863-1898.
- McGregor, K.C., R.L. Binger, A.J. Bowie, and G.R. Foster, 1995. Erosivity Index Values for Northern Mississippi. *Transactions of American Society of Agricultural Engineers* **38**:1039-1047.
- McGregor, K.C., and C.K. Mutchler. 1976. Status of the R factor in Northern Mississippi. In *Soil Erosion: Prediction and Control*, SCSA, Ankey, IA, pp. 135-142.
- Renard, K.G., and V.A. Ferreira. 1993. RUSLE Model Description and Database Sensitivity. *Journal of Environmental Quality* **22**:458-466.
- Renard, K.G., G.R. Foster, G.A. Weesies, D.K. McCool, and D.C. Yoder (coordinators). 1997. *Predicting Soil Erosion by Water: A Guide to Conservation Planning with the Revised Soil Loss Equation (RUSLE)*. United States Department of Agriculture, Agriculture Handbook No. 703, Washington, DC, p. 404.
- Renard, K.G., and J.R. Freimund. 1994. Using Monthly Precipitation Data to Estimate the R-factor in the Revised USLE. *Journal of Hydrology* **157**:287-306.

- Richardson, C.W., G.R. Foster, and D.A. Wright. 1983. Estimation of Erosion Index from Daily Rainfall Amount. *Transactions of American Society of Agricultural Engineers* **26**:153-160.
- Ropelewski, C.F., and M.C. Halpert. 1987. Global and Regional Scale Precipitation Patterns Associated with the El Niño/Southern Oscillation. *Monthly Weather Review* **115**:1606-1626.
- Ropelewski, C.F., and M.C. Halpert. 1989. Precipitation Patterns Associated with the High Index Phase of the Southern Oscillation. *Journal of Climate* **2**:268-284.
- United States Weather Bureau. 1957a. *Climatic Summary of the United States - Supplement for 1931 through 1952*. United States Weather Bureau, Washington, DC.
- United States Weather Bureau. 1957b. *Mean Temperature and Precipitation*. United States Weather Bureau, Washington, DC.
- United States Weather Bureau. 1957c. *Rainfall Intensity-Frequency Regime. Part 1 - Ohio Valley*. Technical Paper No. 29, United States Weather Bureau, Washington, DC, p. 44.
- United States Weather Bureau. 1958a. *Rainfall Intensity-Frequency Regime. Part 2 - Southeastern United States*. Technical Paper No. 29, United States Weather Bureau, Washington, DC p. 51.
- United States Weather Bureau. 1958b. *Rainfall Intensity-Frequency Regime. Part 3 - Middle Atlantic Region*. Technical Paper No. 29, United States Weather Bureau, Washington, DC, p. 38.
- United States Weather Bureau. 1959a. *Local Climatological Data*. United States Weather Bureau, Washington, DC.
- United States Weather Bureau. 1959b. *Rainfall Intensity-Frequency Regime. Part 4 - Northeastern United States*. Technical Paper No. 29, United States Weather Bureau, Washington, DC, p. 35.
- United States Weather Bureau. 1960. *Rainfall Intensity-Frequency Regime. Part 5 - Great Lakes Region*. Technical Paper No. 29, United States Weather Bureau, Washington, DC, p. 31.
- Wallace, J.M., and D.S. Gutzler. 1981. Teleconnections in the Geopotential Height Field during the Northern Hemisphere Winter. *Monthly Weather Review* **109**:84-812.
- Weiss, L.L. 1964. Ratio of True to Fixed-interval Maximum Rainfall. *Journal Hydraulics Division, ASCE* **90**:7-82.
- Wischmeier, W.H., and D.D. Smith. 1958. Rainfall Energy and Its Relationship to Soil Loss. *Transaction of American Geophysical Union* **39**:85-291.

Wischmeier, W.H. 1962. Rainfall Erosion Potential. *Agricultural Engineering* **43**:212-215.

Wischmeier, W.H., and D.D. Smith. 1978. *Predicting Rainfall Erosion Losses—a Guide to Conservation Planning*. United States Department of Agriculture, Agriculture Handbook 537, Washington, DC.

Wolter, K., and M.S. Timlin. 1998. Measuring the Strength of ENSO - How Does 1997/98 Rank? *Weather* **53**:315-324.

Illinois State

WATER SURVEY

ILLINOIS



DEPARTMENT OF
NATURAL
RESOURCES



ILLINOIS

Illinois State

WATER SURVEY

ILLINOIS



DEPARTMENT OF
NATURAL
RESOURCES



ILLINOIS